Optimized Scheduling and Sizing of an Energy Storage System into a UFCS

Jasper Meyboom

Optimized Scheduling and Sizing of an Energy Storage System into a UFCS

by

Jasper Meyboom

to obtain the degree of Master of Science
at the Delft University of Technology,
to be defended publicly on Tuesday November 27, 2023 at 1:00 PM.

Student number:	4552652	
Project duration:	March 1, 2023 – November 1, 2023	
Thesis committee:	Prof. dr. ir. P. Bauer,	TU Delft
	Dr. Z. Qin,	TU Delft, supervisor
	Dr. P. V. Barrios,	TU Delft
	Ir. A. Ahmad,	TU Delft, , daily supervisor

This thesis is confidential and cannot be made public until November 28, 2023.

TU Delft

Acknowledgment

During my M.Sc. graduation project, I experienced an enlightening journey that significantly deepened my passion for the subject. This endeavor was more than an academic task; it was a path of immense learning and personal growth. The more I delved into the research, the more my curiosity grew, fueling my dedication and enthusiasm. This project not only honed my analytical and critical thinking skills but also affirmed my commitment to the field. As I move forward, I carry a deep-seated passion and a wealth of knowledge that will undoubtedly influence my future pursuits.

I would like to extend my heartfelt gratitude to my supervising student, Adnan Ahmad, for his invaluable assistance and support throughout the course of this project. His expertise, insightful feedback, and unwavering dedication have been pivotal in the successful completion of this work. Adnan's guidance and mentorship have not only helped me navigate the complexities of the project but have also contributed significantly to my personal and professional growth.

I would also like to express my sincere appreciation to my professor, Dr. Zian Qin, for his academic guidance and profound insights. Dr. Qin's expertise in the field and his constructive criticism have been instrumental in refining my research and broadening my understanding. His encouragement and wisdom have been a constant source of inspiration and motivation.

Their combined support has been a cornerstone of my journey, and I am immensely grateful for their contributions to my academic endeavors.

Abstract

In the evolving energy landscape marked by a surge in electric vehicle (EV) adoption, efficient and rapid charging infrastructure becomes imperative. Ultra-Fast Charging Stations (UFCS) employing Direct Current (DC) have arisen as a pivotal solution to this challenge, primarily due to their ability to deliver high power and reduce charging times substantially compared to traditional Alternating Current (AC) charging methods. Moreover, the DC bus system allows for greater compatibility with renewable energy sources and storage systems, presenting a seamless interface that bypasses the need for recurrent AC-DC conversions, thus enhancing efficiency and flexibility.

Against this backdrop, this research investigates the techno-economic feasibility of integrating Battery Energy Storage Systems (BESS) with a DC UFCS, factoring in current technological constraints and prevailing market conditions. The study was inspired by the pressing need to alleviate grid congestion, notably in areas like the Netherlands, and the prospective role of BESS in achieving significant cost and energy savings. An analytical energy model was employed alongside a physical battery model to rigorously evaluate the performance outcomes of the proposed integration. Leveraging a dual simplex algorithm, the research capitalizes on the price oscillations in the day-ahead market, optimizing the BESS's charging during low-price windows and discharging when prices escalate, enabling a substantial energy cost reduction, with savings up to 49% in certain scenarios.

Next to energy cost reduction a grid searching optimization is employed to work in a peak shaving function to alleviate peak demand on the grid while subsequently reducing network operator costs by up to 79%.

This reduction in operational costs will be compared against the large capital investment cost associated with such Battery Energy Storage Systems (BESS) to examine whether the reduction in operational costs is more significant than the upfront costs they come with

Additionally, the research examines the intricacies of battery aging vis-à-vis its operational patterns. The findings reveal that batteries engaged extensively in cost-saving operations tend to have a reduced lifespan due to increased cycling and higher average currents. However, larger battery configurations, which maintain lower average currents relative to their peak capacities, demonstrated more extended life cycles, thereby suggesting long-term economic viability. It was found that the lifetime of all examined configurations was significantly larger then the payback time of the systems.

In summary, when optimally sized and orchestrated, BESS can offer significant lifetime cost advantages for UFCS, with potential savings reaching upwards of 56% for new DC UFCS installations and 46% for existing systems. The meager performance variance (0.6%) between the analytical model and the actual battery model further accentuates the practical viability of BESS-integrated UFCS. This research highlights the profound economic and technical benefits of merging battery systems with UFCS, advocating for their adoption as a forward-looking solution in the realm of electric mobility.

Jasper Meyboom
Delft, November 2023

Contents

List of Figures

List of Tables

Acronyms

AC Alternating Current. vii, ix, 6–10, 19–21, 33

BESS Battery Energy Storage Systems. v, 2–5, 11, 18–25, 33, 36, 43, 46, 47, 54, 61–63, 68, 71, 72

BMS Battery Management System. 8

C&C Cost of Commissioning. 37, 62

CCS Combined Charging System. 8

chademo Charge de Move. 8, 9

CIC Capital Investment Costs. 61, 62

COC Cost of Capacity. 37

DC Direct Current. vii, ix, 6–11, 19–22, 33, 43, 61, 62, 64, 72

DOD Depth of Discharge. 19, 43

EMI Electromagnetic Interference. 22

EOL End of Lifetime. 43, 59–61

EU European Union. 1

EV Electric Vehicle. vii, 1–4, 6–12, 16–23, 33, 34, 36, 51, 53, 73, 74

GA Genetic Algorithm. 25

GBT Guobiao Standards. 8

GHG Green House Gasses. 1

HPCCV High Power Charging Consumer Charging. 11

IPT Inductive Power Transfer. 11

kW Kilowatt. 7–9, 11, 19

LFP Lithium Iron Phosphate. 36, 37, 40–43, 68

LFT Low Frequency Transformer. 21

LP Linear Programming. 25

MISC Miscellaneous. 61

MV Medium Voltage. 2, 3

NO Network Operator. 24, 46, 47

OM Operation and Maintenance. 37, 46, 56, 61

PAR Peak to Average Ratio. 47, 58

PCS Power Conversion System. 7, 9, 21, 54, 61

PFC Power Factor Correction. 19, 20

PSO Particle Swarm Optimization. 25

RES Renewable Energy Sources. 19

SEI Solid Electrolyte Interphase. 16, 18

SOC State of Charge. ix, 9, 11, 12, 18, 35, 40, 68

SOH State of Health. 59, 60

SST Solid State Transformer. 21, 43

UFCS Ultra Fast Charging Station. vii, ix, 2, 3, 5–14, 16–18, 20–24, 33–35, 43, 46, 47, 49, 51, 54, 57, 59, 61, 62, 64, 71, 72

UPS Uninterruptible Power Supply. 16

ZCS Zero Current Switching. 21

ZVS Zero Voltage Switching. 21

1 Introduction

The increase in global mean temperature has led to more frequent and severe weather events, highlighting the urgent need for sustainability and climate action. It's crucial to address these issues to ensure a better future for our planet and all its inhabitants. The European Union (EU) has committed to a binding target of reducing Green House Gasses (GHG) emissions by at least 55% by 2030 compared to 1990 levels. This commitment is part of the EU's efforts to align with the goals of the Paris Agreement, which aims to limit global warming to well below 2 $^{\circ}C$ above pre-industrial levels and to pursue efforts to limit the temperature increase to 1.5 $^{\circ}C$.

The EU's 55% emissions reduction target by 2030 is a significant step toward achieving these global climate goals. It is part of the EU's broader strategy to become carbon-neutral by 2050, known as the EUropean Green Deal. This ambitious target requires comprehensive changes in various sectors, including energy, transportation, industry, and agriculture, to reduce GHG emissions and transition to a more sustainable and climate-friendly economy. The EU is also working on policies and initiatives to support member states in achieving these emission reduction goals.

Achieving the ambitious GHG emission reduction goals, such as those set by the EU, requires a radical transformation of all sectors of the economy, and the transportation sector is a significant contributor to emissions. Transportation is a major source of GHG emissions worldwide, and a substantial portion of these emissions comes from vehicles powered by internal combustion engines.

Here are some key points related to the transportation sector's role in emissions:

- As mentioned, transportation is responsible for a substantial portion of energy-related GHG emissions. This includes emissions from cars, trucks, buses, ships, airplanes, and trains.
- Internal combustion engine vehicles, which run on gasoline or diesel, are a major source of emissions within the transportation sector. These vehicles emit carbon dioxide (CO_2) and other pollutants when burning fossil fuels.
- To address this issue, there is a growing emphasis on transitioning to electric vehicles (Electric Vehicle (EV)s), which produce zero tailpipe emissions. EVs are seen as a key solution to reducing emissions in the transportation sector.
- Alongside EV adoption, the development of charging infrastructure and incentives for EV purchases are crucial to encourage the shift away from internal combustion engine vehicles.
- Encouraging the use of public transportation, cycling, walking, and other sustainable modes of transportation can help reduce the reliance on personal vehicles and lower emissions.
- Governments and regions, like the EU, are implementing policies and regulations to promote cleaner transportation, such as stricter emissions standards and incentives for cleaner vehicles.

- Continued research and innovation in battery technology, alternative fuels, and sustainable transportation solutions are essential for achieving emission reduction targets.

Reducing emissions from the transportation sector is a key component of broader climate action plans, as transportation plays a significant role in the overall carbon footprint of many countries and regions. Transitioning to cleaner and more sustainable modes of transportation is vital in the global effort to combat climate change. It is evident that EVs are gaining prominence as a solution to reduce carbon-intensive transportation, and addressing the challenge of efficiently and sustainably charging these vehicles is crucial for the success of the transition to electric mobility.
The rising energy demand, coupled with a transition away from fossil fuels, has resulted in a marked increase in electricity consumption. This has placed considerable stress on the Dutch energy grid, complicating the process of drawing or supplying power. Figure 1.1 showcases the gravity of the situation: areas denoted in red are nearing their capacity for power intake, orange zones have some available capacity after a waiting period, and those in yellow have limited room left.

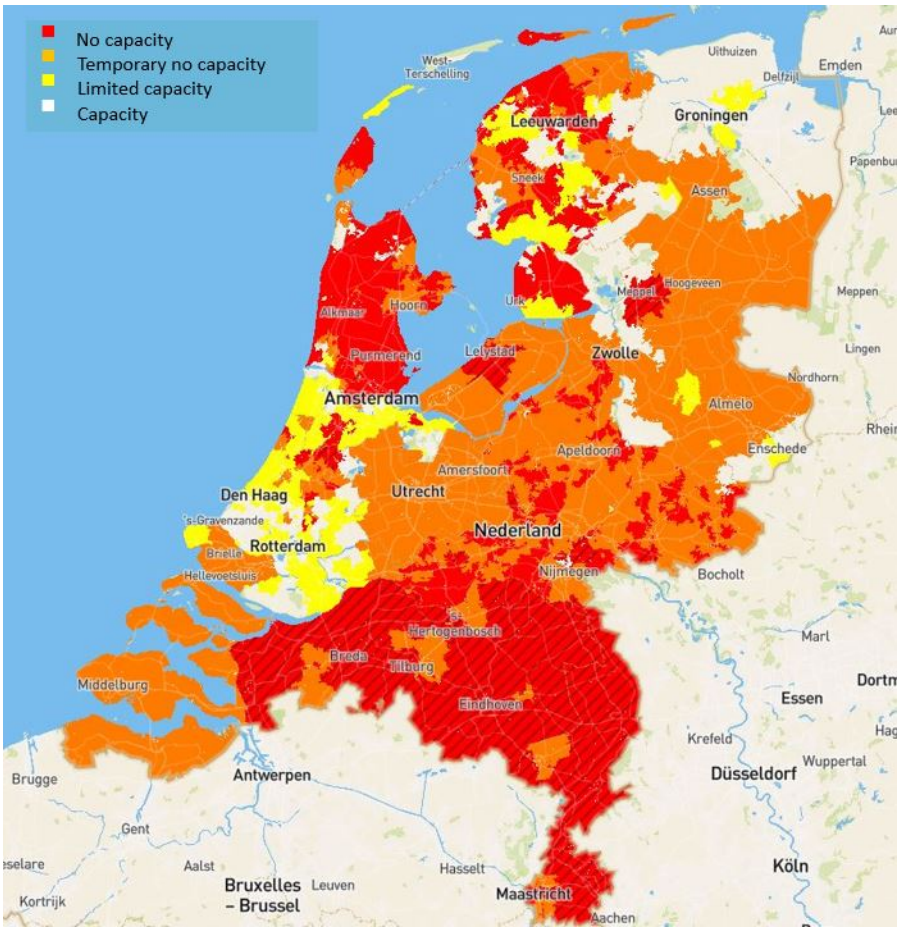

Figure 1.1: Net congestion for drawing power from the grid [1].

This congestion poses challenges for accommodating the substantial power demands of the evolving electric mobility sector in the Netherlands. Notably, while the peak power requirements for EV charging are substantial, the average consumption remains lower. A potential solution involves integrating a battery system within the charging stations. By leveraging the relatively lower average power needs of EVs, this system could alleviate peak demands on the grid. However, the introduction of large-scale battery systems comes with financial considerations.

The objective of this research, which focuses on the optimal sizing and deployment of battery energy storage systems Battery Energy Storage Systems (BESS) in conjunction with (Medium Voltage (MV) grids to power ultra-fast charging stations Ultra Fast Charging Station (UFCS), aligns with the goals of achieving practical, sustainable, and economically viable electric mobility (e-mobility) solutions. Here

are some key points and research objectives:

- BESS is a vital component of modern electric grids. It can store excess electricity when generation exceeds demand and release it when demand is high. This flexibility is especially valuable for integrating renewable energy sources like wind and solar, as they are intermittent.
- MV grids are a critical part of the electricity distribution system. They can efficiently transmit electricity over medium distances and serve as a backbone for local distribution networks. Integrating UFCS with MV grids can help distribute power effectively.
- UFCS is essential for enabling convenient and rapid charging of EVs, especially in urban areas. Proper sizing and deployment are crucial to ensure accessibility and reduce congestion in charging infrastructure.
- The deployment of BESS and UFCS is not only efficient but also sustainable. This includes considerations for the solutions' environmental impact, energy efficiency, and long-term viability.
- Economic viability is a key factor in the adoption of EV charging solutions to ensure economically feasible solutions that can attract investment and provide value to consumers.

The transition to sustainable transportation and the integration of EVs into our daily lives require innovative solutions and research efforts. Finding practical, efficient, and sustainable ways to charge EVs is a critical step in reducing carbon emissions from the transportation sector and combating climate change. The effective harnessing and managing of renewable energy resources is pivotal to addressing a highly relevant and critical aspect of the transition to a sustainable and green future. This thesis provides an in-depth analysis of an essential, yet often overlooked, facet of this expansive discourse - BESS and their intricate optimization in the context of a UFCS, thereby highlighting the crucial role of intelligent energy storage in accelerating our transition towards a green future.

The context and relevance of this study are underscored by the rapidly growing demand for fast and efficient EV charging solutions, which reflects the global shift towards electrified transportation. Various factors, including environmental concerns and advancements in EV technology, drive this demand. The transition to electrified transportation holds the potential for substantial reductions in GHG emissions. Aligns with broader efforts to combat climate change and reduce the transportation sector's environmental impact. Nevertheless, the challenges the Netherlands faces regarding slower growth in energy infrastructure compared to rising power demand are significant. This issue is common to the Netherlands and a common challenge in many regions aiming to accommodate the energy needs of emerging technologies like UFCS. When observing this problem the following question arises: How does the integration of a battery storage system influence the techno-economic performance and viability of an ultra-fast charging station connected to the grid, considering current technological constraints and market conditions? And how can this be determined?

This research navigates two interlinked facets of the BESS—deployment and sizing. Deployment pertains to the charging and discharging of the BESS, determined by evolving demand profiles and fluctuating electricity prices. Simultaneously, sizing is concerned with identifying the optimal capacities for both the grid connection and BESS. This thesis's overarching objective is to significantly reduce the operational expenses of the UFCS, composed of both energy costs and demand tariffs. As well as the peak-to-average ratio reduction which is an important aspect from a utility point of view as it flattened the peaks in the load profile and minimized the spinning reserves requirement.

Utilizing linear programming optimization—specifically the Dual Simplex algorithm—this study investigates several combinations of grid and BESS capacities, aiming to identify an optimal solution. This study incorporates real-world data about hourly electricity pricing and the power demand profile of the UFCS, ensuring this research's analysis remains grounded in practical, tangible scenarios.

The implications of this research extend far beyond monetary savings. Efficiently managed BESS could facilitate better grid stability, providing more reliable and consistent charging solutions for EVs and, ultimately, contributing to a more robust, resilient, and sustainable energy infrastructure.

The rest of the thesis provides an in-depth exploration of the research methodology, a detailed analysis of the data collected, findings of optimization models, and comprehensive conclusions drawn from this study. Through this, this research aims to provide a robust road map for harnessing the outreached potential of BESS in the rapidly evolving landscape of EV charging. In short, this work provides valuable insights into harnessing the potential of BESS in the context of EV charging infrastructure. It is essential work that can contribute to the sustainable development of e-mobility solutions and address critical challenges in adopting EVs.

2

Literature Review

This chapter defines the research problem within the electric vehicle (EV) charging context and efficient energy management. It explores EV charging modes, focusing on DC Fast Charging, its mechanics, and technology. The chapter analyzes demand dynamics of Ultra-Fast Charging Stations (UFCS), considering EV characteristics and charging pole utilization. It covers selecting appropriate battery technology for UFCS and examines battery aging impacted by operational patterns. The chapter also compares AC and DC bus systems in efficiency and compatibility with renewable energy. It concludes by examining electricity costs, including market pricing and network operator expenses.

2.1. Problem Formulation

The focus of this research is to optimize the sizing and deployment of a BESS and power grid connection to power an UFCS while minimizing energy-related operational expenses. BESS are becoming increasingly essential as the world continues to transition towards renewable energy sources and electric transportation systems. However, their use comes with its challenges, especially concerning the efficiency of charging and discharging cycles, the longevity of the battery, and the economics of system sizing and operation.

The UFCS considered in this research is powered by a medium voltage grid, which has implications for cost and efficiency. Grid electricity costs are composed of two parts: the cost of the energy consumed (kWh), and the demand tariff, which is based on the maximum power (kW) consumed in any given month. The first challenge is, therefore, to manage these costs and minimize the electricity bill for operating the UFCS.

A BESS connected to the UFCS can provide a buffer between the grid and the station, absorbing energy at times of low demand and/or low cost and releasing it when needed. However, the BESS's operation—when it charges from the grid, when it discharges to the station, how fully it should be charged or discharged—also has a significant impact on the overall system efficiency and cost.

Furthermore, the optimal size of the BESS—its total energy storage capacity and maximum power—also plays a crucial role. A larger BESS might offer more flexibility in managing demand and costs, but it also implies higher initial investment. Therefore, determining the optimal size of the BESS becomes a problem in balancing these costs and benefits.

This research's goal is to determine the optimal size (capacity and power) of a BESS for an UFCS and the optimal operational strategy (charging and discharging) to minimize the total electricity bill. To achieve this, a two-step optimization approach was developed and applied, considering real-world data on electricity costs and the UFCS 's demand. By solving this problem, this research aims to provide a practical, cost-effective solution for integrating BESS with UFCS, contributing to the wider transition towards sustainable transportation.

2.2. EV Charging

The transition to EVs stands at the forefront of a sustainable transportation future. Central to this revolution is the development and understanding of EV charging infrastructure. With many charging options, standardizing and understanding these methods becomes paramount for widespread adoption.

Within this section, there will be delved into the intricacies of EV charging, exploring topics such as the four predominant charging modes, the specifics of Direct Current (DC) charging, system configurations and components, and the power demands and implications of UFCS.

As EVs continue to gain traction globally, understanding these elements will be pivotal for researchers, policymakers, and industry stakeholders aiming to optimize the charging experience for end-users and ensure seamless integration with existing energy systems.

2.2.1. Charging Modes

EV charging encompasses a broad spectrum of technologies and approaches, differentiated primarily through their charging modes. These modes, classified from Mode 1 to Mode 4, are distinct in their charging speeds, current:Alternating Current (AC) orDC classification, and the requirement for on-board or off-board power conversion.

Several universal components are central to all charging types, including a charging cord, stand, plug attachment, power outlet, vehicle connector, and an integral protective system. When it comes to the actual charging, EVs can leverage either on-board or off-board chargers. On-board chargers, embedded within the vehicle, offer the flexibility of utilizing any standard AC connection. However, they're hampered by their power ratings due to the inherent constraints of weight, space, and cost in EVs. In contrast, off-board chargers bypass these limitations by situating the power electronics externally, enhancing charging capabilities.

Given the diverse array of charging options, standardization plays a crucial role. The IEC 61851-1 standard offers clarity on these modes, distinguishing them based on connection types and the speed of charging. The most common charging modes are described in the next section[37], and a pictorial representation is given in Fig. 2.1.

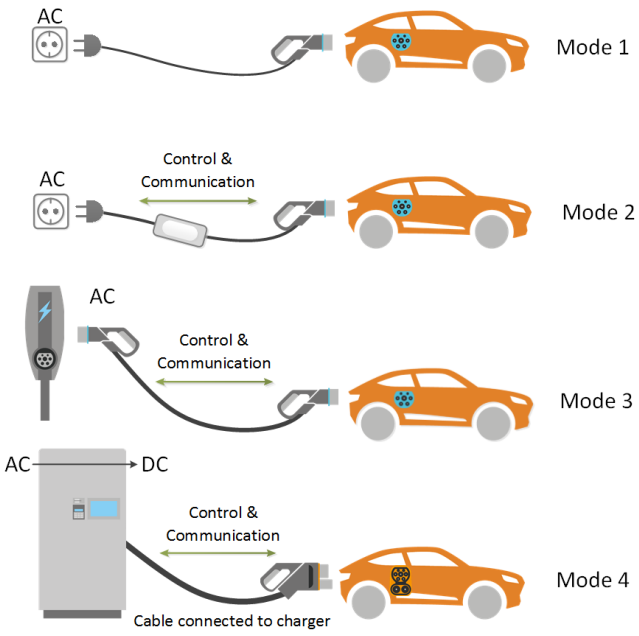

Figure 2.1: Charging modes [2].

Mode 1: Mode 1 charging is a fundamental yet effective method, commonly relying on standard household sockets without specialized EV equipment. It operates at slower speeds using alternating current (AC), with the vehicle's onboard system managing the conversion. Mode 1, also known as slow charging, delivers power rates of 2-3 Kilowatt (kW)as shown in Figure 2.2., utilizing common outlets like 110-120V in the United States or 220-240V in Europe. Despite its basic approach, it's particularly suited for homes or situations where the car remains parked for a longer duration, such as nightly at homes or during a full workday at offices. Yet, its prolonged charging intervals, often stretching across several hours, might not be optimal for those on the go or in need of a swift energy boost.

Mode 2 & 3: Mode 2 charging, commonly known as Level 2 or fast charging, employs dedicated EV charging cables with embedded safety mechanisms. Delivering power outputs ranging from 7 kW to 22 kW, this mode significantly shortens charging times compared to basic chargers. Using AC and with the conversion done onboard the vehicle, these chargers require specific infrastructure, such as a 240V connection in the US or a 400V connection in Europe. They are widely seen in public places, commercial establishments, and certain residences with the appropriate electrical setup.

In contrast, Mode 3 charging is chiefly tailored for public charging stations, offering even faster AC charging speeds than Mode 2. Although it also operates with onboard conversion, what sets Mode 3 apart is its emphasis on security. Often referred to as "Level 2" or "Type 2" as well, these chargers come with features that ensure secure and locked connections, preventing unauthorized access or tampering, making them particularly suitable for public environments where such considerations are vital.

Mode 4: Mode 4, or "DCFast Charging," uses DC for rapid off-board charging at UFCS, delivering up to 350 kW. This enables most EV batteries to charge in under 20 minutes. The technology demands advanced electrical systems, cooling solutions, and specially designed batteries to handle the power without compromising lifespan. More details follow in the next section.

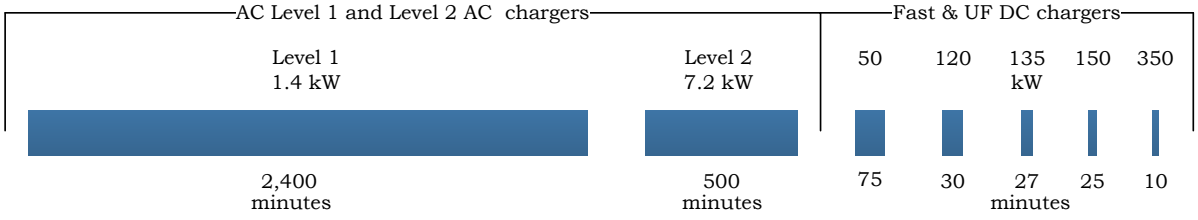

Figure 2.2: Charging levels and their corresponding charging power and charging times [23].

2.3. Mode 4: DC Fast Charging

This research is only interested in high-power DC charging. The other charging modes are not considered forUFCS. Therefore this paper will dive deeper into the mechanics of DC fast charging. The basics of DC fast charging will be covered first, secondly, the operational mechanics, and thirdly the different options within DC fast charging will be explained. Next the constraints and considerations of DC charging are discussed and finally UFCS configurations and components. Apart from charging power and time the biggest difference between Mode 4 and the other modes is that the conversion from AC to DC is done outside the EV which allows for much larger Power Conversion System (PCS) and therefore much higher charging power. A couple examples of the PCS have been given in Figure 2.3

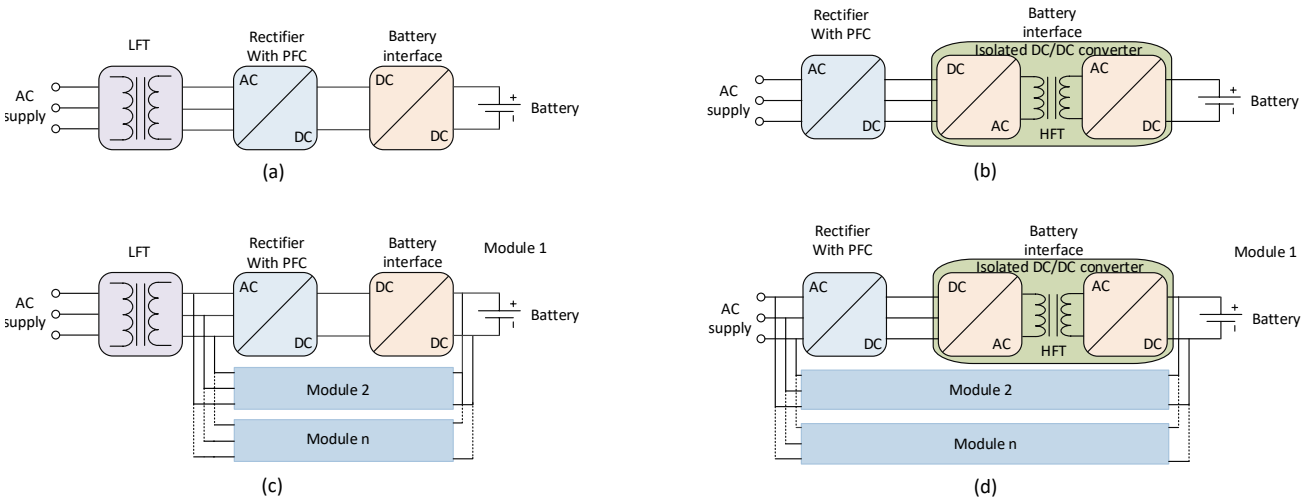

Figure 2.3: Illustration of AC to DC power conversion systems [23].

2.3.1. Basics of DC Charging

DC fast chargers are advanced tools devised to quickly recharge EV batteries. These charging solutions overshadow the conventional Level 1 and Level 2(&3) chargers by offering an extensive power output ranging from 50 kWto 350 kW.DC fast charging is mostly found in commercial charging stations, often connected to conventional gas stations.

2.3.2. Operational Mechanics

AC power, sourced from the grid, is converted into DC via a rectifier within the charging station. Post-conversion, a power control unit refines the voltage and current, overseeing the DC power channeled to the battery. A basic configuration of a DC fast charging station is presented in Figure 2.3. For safety, interlock and protection circuits are integrated, which can pause the charging process during faults or if improper connections are detected. Central to this operation is the Battery Management System (BMS) of the EV — It communicates with the charging station to regulate the battery's voltage and current levels, initiating safety protocols as necessary.

2.3.3. Types of DC Charging Connectors

Different regions and automakers use a variety of DC charging. connectors[3][37].The most common ones will be discussed in this section. The background of the connector and the characteristics will be evaluated to get a better understanding of the specific conditions the UFCS is subjected to. The 3 connector types that will be discussed are Combined Charging System (CCS), Charge de Move (chademo), the Tesla DC charger and Guobiao Standards (GBT) :

- **CCS/Combo 1 and CCS/Combo 2**:
  - *Voltage:* 200V to 1000V.
  - *Current:* Up to 350 Amps.
  - *Maximum Power Output:* 350 kW.

History and Details: A very common technology in the United States (combo 1) and Europe (Combo 2). These connectors emerged from the initiative of the CharIN association, spearheaded by several renowned automakers and companies. A distinctive feature of the Combined Charging System is its singular connector, which is compatible with both AC and DC charging through different pins.

- **CHAdeMO**:
  - *Voltage:* 50V to 500V (with expectations of up to 1000V in the future).
  - *Current:* Up to 400A.
  - *Maximum Power Output:* Currently 200 kW(400kWexpected in the future).

History and Details: Originating in Japan, chademo is a globally recognized DC charging standard with the most extensive installation base as of 2017. It facilitates V2X (Vehicle to Everything) communication and uses the Controller Area Network (CAN) for signaling.

- **Tesla DC Chargers**:
  - *Voltage:* Approximated between 350V to 400V (exact figures are proprietary to Tesla).
  - *Maximum Power Output:* 120 kW.

History and Details: In the US, Tesla employs a proprietary charging connector. However, in Europe, the Type 2 connector is the standard. A unique aspect of Tesla's approach is the shared connector for both AC and DC charging.

- **China GB/T Standard**:
  - *Voltage:* 750V or 1000V.
  - *Current:* Up to 250A.
  - *Maximum Power Output:* Up to 250 kW.

History and Details: China employs its own DC charging system rooted in the 20234.3-2015 standard. A distinct feature of this system is its capability to charge both the low-voltage auxiliary battery and the high-voltage traction battery.

2.3.4. Constraints and Considerations of Fast Charging

Fast charging, while advantageous, is bounded by technical limitations. Amplifying charging speed elevates losses in both charger and battery and may reduce battery lifespan due to heat[25]. Achieving more than 70-80% State of Charge (SOC) during fast charging becomes challenging. As charging power rises, cables become thicker, posing challenges in flexibility and user handling.

2.3.5. UFCS Configuration and Components

An UFCS is a complex assembly of components designed to deliver power levels up to 350 kW, enabling rapid charging of EV's. These components work in concert to ensure that the UFCs operate efficiently and safely.

At the heart of the UFCS is the PCS. This system, which consists of power converters, is responsible for transforming the AC power from the grid into the DC power that the EV batteries require. To minimize energy losses during this conversion process, these converters must operate at a high efficiency. Advanced converter topologies, such as dual-active bridge converters, are often employed in high-power chargers to achieve this level of efficiency.

Connecting the UFCs to the grid can be done via an AC or a DC bus. While an AC bus connection involves converting the grid's AC power to DC power at the station, a DC bus connection involves a centralized conversion from AC to dc, with the DC power then distributed to individual chargers. The

choice between AC and DC connections often comes down to a trade-off between flexibility and efficiency. AC connections are generally more adaptable and easier to integrate with the existing grid infrastructure, while DC connections can offer improved efficiencies and faster response times under certain circumstances. In addition to the power conversion systems and grid connections, inverters play a significant role in UFCS stations, particularly those equipped with renewable energy sources or energy storage systems. In these cases, inverters convert the DC power generated by these systems into AC power, suitable for supply to the grid or for use within the station itself.

Safety is paramount in the design of UFCs, with grid isolation serving as a crucial protective measure. Isolation transformers provide electrical separation between the grid and the charging station, protecting both from faults or electrical surges[4]. Finally, the ability to support different charging protocols is an essential feature of UFCS. EVs use various charging protocols, such as CHAdeMO, CCS (Combined Charging System), and Tesla's Supercharger system. To cater to a broad range of vehicles, multi-protocol charging controllers are used. These controllers can communicate with the EVs and control the charging process according to each vehicle's specific requirements.

In summary, the design of a UFCS involves making critical decisions to balance efficiency, cost, compatibility, and safety. With ongoing advancements in power electronics, communication technologies, and EV charging standards, there are continually evolving opportunities to optimize these designs for enhanced performance and cost-effectiveness.

2.3.6. Standards and Technological Advancements in DC Fast Charging

The development and adoption of EV necessitate a robust and standardized charging infrastructure. Two pivotal standards in this domain are the IEC 61851-1 and IEC-62196, which play a crucial role in ensuring interoperability and safety across various EV models and charging systems. The IEC 61851-1 standard provides comprehensive guidelines that cover various aspects of EV conductive charging systems. It lays out the general requirements for electric connections, addressing crucial factors such as safety, performance, and compatibility. This standard is instrumental in fostering a uniform and reliable charging infrastructure, facilitating ease of use and widespread adoption of EVs. The IEC-62196 standard complements the IEC 61851-1 by specifying particular plug and socket configurations tailored for fast charging applications. It categorizes these configurations into four distinct types, each designed to cater to different regions and voltage requirements. This standard ensures that EVs can access fast charging stations reliably and safely, regardless of the manufacturer or geographic location.

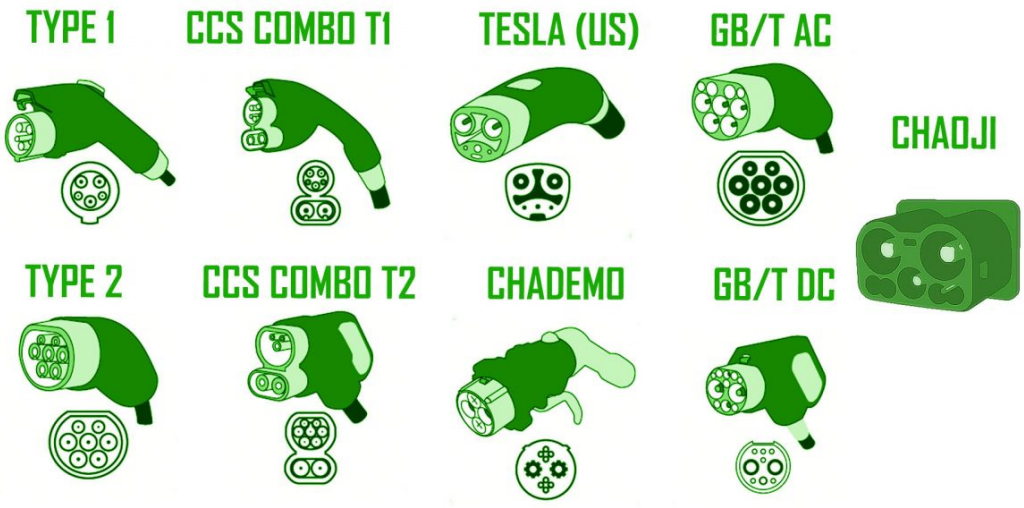

Figure 2.4: Current and Next-generation DC charging technology [83].

Tesla, a frontrunner in the EV industry, initially developed its proprietary charging standard. However, recognizing the importance of interoperability and the evolving landscape of EV charging, Tesla has integrated the CCS type 2 standard for its European models. This strategic move enables Tesla vehicles to access a broader network of charging stations, supporting charging speeds up to 175 kW.

Addressing the thermal and physical constraints of cables, especially at higher power levels, is paramount for the advancement of DC fast charging. Innovations such as liquid cooling for cables and wireless charging via Inductive Power Transfer (IPT) are at the cutting edge of research, showing promising potential for efficient and user-friendly charging solutions. IPT, in particular, is gaining traction for its capability to facilitate autonomous charging, enhancing the convenience and practicality of EV charging.

Looking ahead, next-generation charging technologies such as the Chaoji charging system (Figure 2.4) are set to redefine the standards of EV charging. Capable of delivering up to 900 kWwith operational voltages of 1500V and a maximum current of 600A[5], these technologies, although not yet available commercially, are expected to start permeating the market around 2025. They represent a significant leap forward, aligning with the industry's trajectory towards faster and more efficient charging solutions.

The emerging segment of electric trucks is propelling the need for even higher charging speeds. Collaborative initiatives like Charin are spearheading the development of the High Power Charging Consumer Charging (HPCCV) standard, targeting charging capabilities of up to 1MW. This concerted effort underscores the industry's commitment to evolving the EV charging infrastructure, ensuring it is poised to meet the demands of a diverse range of electric vehicles, including commercial fleets.

2.4. Understanding UFCS Demand Dynamics

With the understanding of the provider side of the charging station, it is important to combine this with the consumer side of the station. To optimally design, size, and deploy the BESS and necessary infrastructure it is important to what the behavior of the consumer of an UFCS is, to determine the total power demand over time. The chargers' characteristics determine the upper boundary of the UFCS but the characteristics of the consumers determine the actual demand. Previous studies have tried to predict charge load using algorithms and mathematical models[61][110] These algorithms are typically based on the assumption that charging power and time are determined by the SOC, the arrival time of an EV and the type of EV that is charged. Furthermore, day types such as holidays and weekends have a significant impact when determining charge demand [110][96][70][71][32][26][74][104]. Air conditioning and for example, the use of heating appliances greatly influences the total energy usage of a car, and battery drainage occurs more quickly at lower temperatures. Thus, seasonal and weather information has also been used in several studies [[61][108][69][111][110][96][70],[74][104],,29]. It is clear many factors are at play when using these prediction methods, luckily for this research it is not necessary to know what kind of car is charging at the charge location. This research only needs to know the cumulative demand of all charging spots at a certain period. Another method to determine the charge demand is using data available from existing fast charging stations. This data would model the demand based on the number of cars that are present at a specific period for a charging station. The number of cars combined with the charge demand of a car can be another method to model the demand for the fast charging station.

2.4.1. Influence of EV Characteristics on FCS Demand

Every EV model exhibits unique charging behavior, primarily dictated by its battery specifications and manufacturer's design choices. As portrayed in 2.5, when subjected to 175kWchargers, different EV models display distinct charging curves. Notably, the SOC markedly affects the charging speed. As the SOC ascends, charging velocity diminishes, with an evident deceleration as it nears the 80% threshold. This safety inflection exists to thwart overcharging, which could precipitate expedited battery degradation [103]. It is expected that EV's using DC fast charging are there to charge for a significant range in a short period of time rather than charging up to the upper limit of the battery. This is because the opportunity to charge at home or at work will allow the EV to charge up to the upper limit. It is therefore assumed that an arriving EV has a state of charge of <25% and will leave once the SOC reaches 80% therefore staying within the fast charging range. Other research also indicates that for DC fast charging the EV charges an average of 60% of its battery capacity per charging session[41]. For a 100 kWh

battery that would mean that on average about 60 kWh is charged every session.

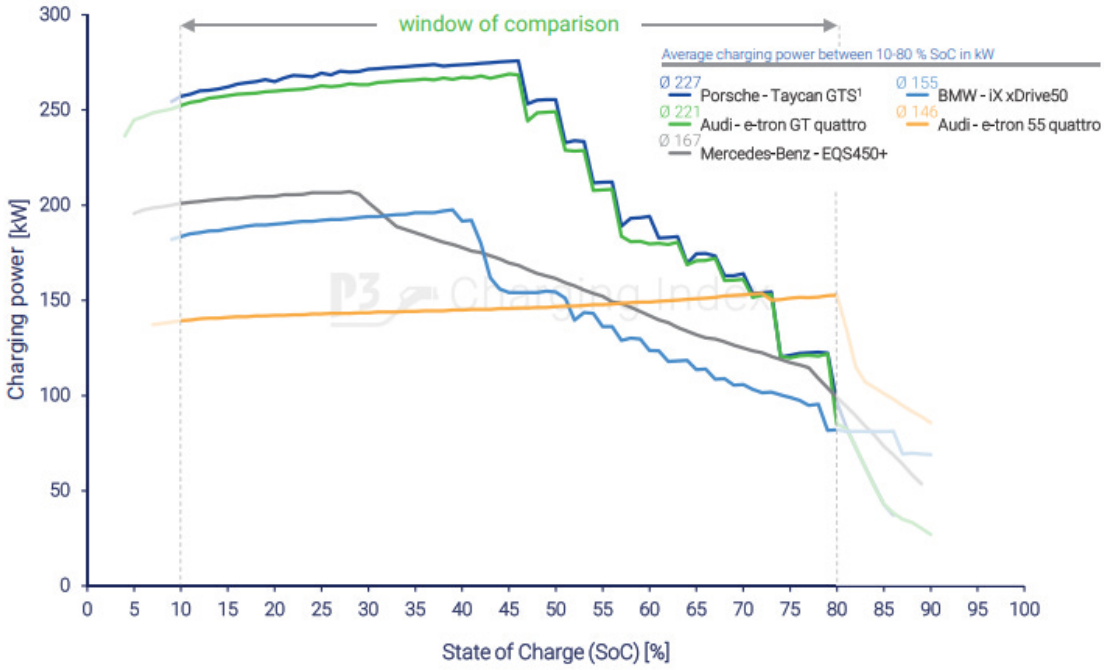

Figure 2.5: Charge power as a function of SOC for different types of cars.[33]

Another important variable is the capacity of the battery in kWh. Nowadays the average EV battery capacity is 50 kWh [36] and with newer models having increasingly larger capacities, as can be seen in 2.6 the average battery capacity of newly sold EV's has reached 100 kWh [54]. The capacity and SOC combined determine the charge speed, charge energy, and time of charging of the EV.

2.4.2. Synthetic Generation of FCS Demand Profile

Although studies have found that the charge demand is higher on weekends[47] on a national level it is also found that that statement does not hold for individual charging stations[61], where randomness and unpredictability were observed when comparing different UFCS. It is found that in urban areas, where EVs are mostly used for short commutes, the charge demand on the weekend is expected to be lower [55][48]. This is because during workdays EV owners typically commute to work using their car while weekend trips are not done every weekend, and are less likely to be in an urban area. The further away from cities the chargers are, the more variable the demand between weekdays and weekends will be in general [20] Also during weekdays, the peak is expected at different moments of the day. During weekdays the peak is expected around midday [39][62], and the peak during weekends is expected a couple of hours later in the day [98].

2.4.3. Annual UFCS Demand Fluctuations

On an annual scale, the oscillations in FCS demand stem from myriad sources, including seasonal changes in mobility behavior and climatic variances. Factors like increased freeway use during holidays or the heightened appeal of vehicular travel during winter months influence FCS demand. Furthermore, the vagaries of extreme temperatures can modulate both charging speeds and battery storage capacities [64], adding layers of complexity to FCS demand forecasting. An interesting observation is the surge in FCS activities during the December-January and summer holiday corridor, a byproduct of the confluence of extreme temperatures and elevated holiday travels [31][41].

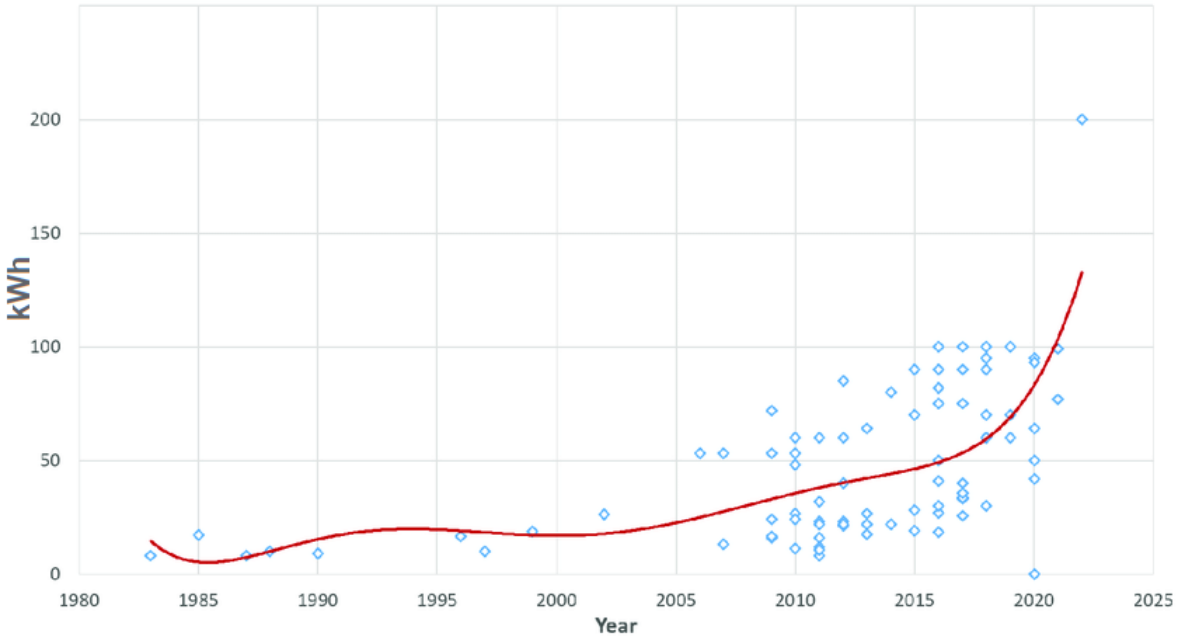

Figure 2.6: Average battery capacity for newly sold EV's [54].

2.4.4. Charging Pole Utilization Rates

Other studies have used data provided by UFCs about the utilization percentage of the available charge poles for a specific time period[62]. This data is in line with the expected peaks during week and weekend days as was found in the previous section. This data is based on all-time averages making it hard to predict the demand for a specific month, especially months with surges in demand due to holiday commutes. It is, however, very effective in analyzing yearly demand since the average does take into account the peak demand periods. The utilization dynamics of charging poles are instrumental in shaping the demand profile since they don't have to take into account the specifics of individual cars. It will base the power demand on the range of average power demand a group of cars needs. Data from Fastned, a leading UFCS provider in the Netherlands, reveals a maximum of 50% utilization rate during peak hours (spanning from 7 am to 11 pm) and an average of 20% beyond these hours [40]. This data can be used together with hourly utilization percentages for specific charging stations based on historical data. This allows the construction of a charging profile for a specific charging station based on the data of similar charging stations. This will allow to model the randomness of the charging demand on a single day but remain bound to the yearly expected behavior of such UFCs[61].

2.5. Battery Technology Selection

A battery-integrated UFCS's thriving design and operation hinges on selecting an appropriate battery technology. Many factors contribute to this decision, including the battery technology's energy density, power density, cost, safety, reliability, and longevity. As of 2023, three primary battery technologies are used: nickel-cadmium (NiCd), lead-acid batteries, and lithium-ion [78]. In Figure 2.7 the volumetric and gravimetric energy densities of these technologies can be seen.

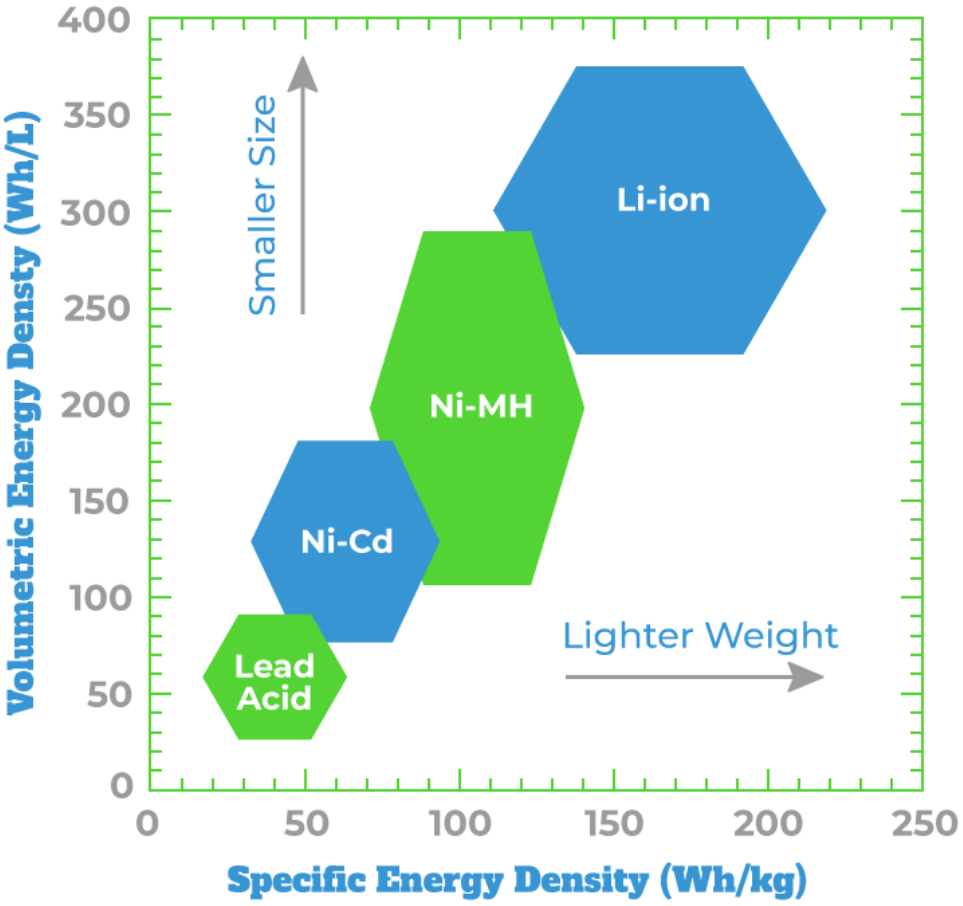

Figure 2.7: Gravimetric and volumetric energy densities of different battery technologies(2022) [35].

From the figure, it becomes clear that on both energy density metrics, the Li-ion battery comes out as superior. However, there are many more characteristics to consider to choose the best fit for an UFCS, for example, costs, voltage stability, and longevity. Below an in-depth analysis for each technology is done to get a better insight into the performance of different chemistries.

2.5.1. Nickel Cadmium

Working Principle NiCd batteries have a nickel oxyhydroxide (NiOOH) cathode, a cadmium (Cd) anode, and a potassium hydroxide (KOH) electrolyte. During discharge, the NiOOH gets reduced to nickel hydroxide (Ni(OH)2), and the cadmium oxidizes to cadmium hydroxide (Cd(OH)2). The reverse reactions occur during charging. NiCd cells have a nominal voltage of 1.2 volts.

Efficiency NiCd batteries have a relatively stable efficiency across a wide range of temperatures and discharge rates. They generally exhibit a round-trip efficiency of 70%[58]. However, they can suffer from the “memory effect,” where incomplete discharge/charge cycles can lead to a decrease in capacity and efficiency. Additionally, the efficiency can be affected by the rate of discharge; high discharge rates can lead to a drop in voltage and efficiency. The internal resistance is relatively low, which contributes to high efficiency during high discharge rates, but this can also lead to higher self-discharge rates compared to other battery types.

Energy and Power Density: Nickel Cadmium (NiCd) batteries possess an inherent balance between energy and power density. While the energy density of NiCd batteries is admittedly lower compared to newer technologies, such as lithium-ion, they do perform decently in power density[6]. It means NiCd batteries can deliver high bursts of power in short durations—a crucial requirement in several

applications. Their fast charge capability accentuates their standing in applications where rapid energy replenishment is more vital than long-term energy storage. NiCd batteries could offer a practical solution for UFCs or scenarios that demand quick power boosts, although with the trade-off of increased volume or weight due to their lower energy density.

Cost per kWh and Deployment: From an economic standpoint, NiCd batteries often present themselves as a cost-effective solution[100]. Their price per kWh, especially when factoring in their prolonged service life, can offer economic advantages over their lifespan. This affordability makes them attractive for large-scale deployments or regions where budget constraints supersede the demand for the absolute highest energy densities. Their versatility in design allows them to be tailored for specific scenarios, providing flexibility in deployment strategies.

Longevity: One of the standout merits of NiCd batteries is their longevity. With the capability to endure over 1,000 charge/discharge cycles [100], they can significantly outlast several competing battery technologies under similar conditions. However, without regular maintenance, this number can go up to 3 times lower[78],[100]. This lifespan is particularly impactful when considering total ownership costs, as longer service lives can reduce replacement frequencies and associated labor costs. Furthermore, their robust nature ensures consistent performance, even under rigorous and challenging operational conditions, further amplifying their effective lifespan.

Safety and Reliability: NiCd batteries have historically proven to be reliable and safe [6], especially when juxtaposed with some of the challenges seen in other rechargeable batteries. Their chemistry is resistant to issues such as thermal runaway, a problem sometimes encountered in lithium-based cells. Their tolerance to abuse, whether from deep discharges, overcharging, or operational rigors, makes them a dependable choice. Their established history has allowed for the refinement of charging and management systems, further enhancing their safety profile.

In conclusion, while NiCd batteries may seem overshadowed by newer technologies on certain fronts, they still hold significant merits that warrant their consideration. Their power density, cost-effectiveness, longevity, and safety balance solidify their position as a viable option for various applications. Decision-makers would be well-advised to consider these advantages, especially when NiCd batteries can effectively meet operational demands.

2.5.2. Lead Acid

Working Principle: Lead Acid batteries consist of a lead dioxide cathode, a sponge lead anode, and a sulfuric acid electrolyte. During discharge, lead sulfate forms at both electrodes, while during charging, the lead sulfate decomposes back to lead dioxide at the cathode and sponge lead at the anode. The electrolyte's sulfuric acid concentration decreases during discharge and increases during charging. These batteries maintain a voltage of about 2.1 volts per cell.

Efficiency: The efficiency of Lead Acid batteries is influenced by several factors including the rate of discharge, temperature, and the age of the battery. Typically, these batteries exhibit a coulombic efficiency of about 85-95%, but their energy efficiency (the ratio of output energy to input energy during charging) can be as low as 70%[86]. Peukert's Law in Lead Acid batteries implies that as the discharge rate increases, the available capacity decreases, which leads to lower efficiency. High temperatures can increase the efficiency but may also lead to faster degradation of the battery, while low temperatures can significantly reduce the efficiency. Over time, sulfation (the accumulation of lead sulfate crystals) can occur, especially if the battery is not fully charged regularly, which leads to a decrease in efficiency and capacity.

Energy and Power Density: Lead-acid batteries have been a cornerstone in energy storage due to their consistent energy and power density attributes[7]. Though they don't possess the highest energy density compared to technologies like lithium-ion, they offer a reliable power density profile[78]. It enables them to deliver sustained power over prolonged periods. Lead-acid batteries find their niche, particularly in applications where the energy demand is steady and predictable, such as backup power systems or grid energy storage.

Cost per kWh and Deployment: Regarding energy storage economics, lead-acid batteries frequently emerge as one of the most affordable options on a per kWh basis[100]. Their widespread use and mature manufacturing processes have increased economies of scale, reducing their overall Cost. This affordability makes them a prime choice for large-scale installations and regions where cost-effectiveness is paramount. Moreover, the simplicity of their design and Deployment has made them a staple in diverse applications, from automotive starters to renewable energy storage.

Longevity: The longevity of lead-acid batteries is context-dependent. They can offer a respectable service life when appropriately maintained and operated within their design parameters. Regular maintenance, like ensuring electrolyte levels and preventing over-discharge, can extend their operational life[8]. Additionally, innovations like the Valve Regulated Lead Acid (VRLA) design have further enhanced their lifespan and reduced maintenance requirements.

Safety and Reliability: Lead-acid batteries have a legacy of reliability, having been used for over a century in various applications. Their chemistry is inherently safe, posing a minimal risk of catastrophic failure such as explosions or fires. Furthermore, their robust design means they can tolerate various environmental conditions, from temperature fluctuations to vibrations. It has made them a go-to choice in applications where reliability is non-negotiable, such as emergency power systems and Uninterruptible Power Supply (UPS)[106]. In summation, lead-acid batteries, with their blend of energy and power density, affordability, dependability, and safety, continue to hold substantial relevance in the modern energy landscape. While newer technologies garner attention for their advanced features, the lead-acid battery remains a steadfast and proven solution, especially when its strengths align with specific application demands.

2.5.3. Lithium-ion

Working Principle: Li-Ion batteries consist of a lithium compound cathode, a graphite anode, and an organic electrolyte. During discharge, lithium ions move from the anode to the cathode through the electrolyte and the separator. During charging, the lithium ions move back to the anode. Li-Ion batteries typically have a cell voltage of 3.6-3.7 volts.

Efficiency: Li-Ion batteries are known for their high efficiency, typically ranging from 85-95%[58] for round-trip efficiency. They have a low internal resistance, which contributes to high efficiency even at high discharge rates. However, the efficiency can degrade over time due to factors such as high temperatures, overcharging, deep discharging, and aging. The degradation leads to an increase in internal resistance, loss of active material, and formation of the Solid Electrolyte Interphase (SEI), all of which contribute to a decrease in efficiency. Proper battery management is crucial to maintaining high efficiency over the life of the battery.

Energy and Power Density: Li-ion batteries possess considerably higher energy and power densities compared to NiCd and Lead-Acid batteries [78][100]. This remarkable density allows Li-ion batteries to store more energy and deliver more power per unit volume, which is a critical advantage in applications where space efficiency is vital, such as UFCSs. The inherent compactness of these batteries makes them suitable for deployments where minimizing the station's footprint is a priority. This high energy and power density directly translate into a higher charging capacity, enabling more EVs to be served at a UFCS with the same space.

Cost: Although Li-ion batteries might require a higher initial investment than NiCd and Lead-Acid batteries, they deliver superior value in the long run [52]. Their extended lifespan and enhanced energy efficiency lead to a lower total cost of ownership, which is a critical factor for commercial UFCS deployments. While the upfront fees may appear daunting, considering the total lifecycle costs paints a different picture. Over their operational life, Li-ion batteries often prove more economical due to their longer-lasting performance and lower maintenance needs.

Safety and Reliability: In terms of safety and reliability, Li-ion technology generally outperforms its counterparts. NiCd batteries suffer from a ”memory effect,” leading to a reduced capacity over time if they do not undergo complete charge-discharge cycles[73]. This effect could be detrimental to the operation of a UFCS, which demands consistent power availability. On the other hand, Lead-Acid batteries can emit harmful gases if improperly charged or discharged and necessitate regular maintenance—issues not present with Li-ion batteries [99]. Increased safety and reliability are crucial in a UFCS context, where battery failures could lead to significant downtime and economic losses.

Longevity: Li-ion batteries typically enjoy a longer lifespan than their NiCd and Lead-Acid counterparts when operated under comparable conditions [78]. This extended lifespan means they can continue delivering high-quality performance over many charge-discharge cycles, minimizing replacement and maintenance costs for UFCS operators. The long lifespan also translates into reduced waste generation, contributing to the overall environmental sustainability of the UFCSs.

Table 2.1: Comparative Analysis of NiCd, Lead Acid, and Li-ion Batteries

Characteristic	NiCd	Lead Acid	Li-ion
Cost per kWh	+	++	-
Efficiency	++	+	+++
Energy Density	-	–	+++
Power Density	++	+	+++
Safety	+	++	+++
Longevity	++	+	+++

2.5.4. Li-ion Batteries: The Preferred Choice for UFCS’s

Ultra-fast charging (UFCS) stations, tailored for the burgeoning electric vehicle (EV) market, necessitate robust and efficient energy storage solutions. Li-ion batteries, with their superior energy and power densities, long lifespan, and operational reliability, emerge as the optimal choice for powering UFCS stations.

Energy and Power Density: Li-ion batteries excel in providing high energy and power densities, a critical requirement for the space-constrained environments of UFCSs. With a cell voltage typically ranging from 3.6-3.7 volts and efficient lithium-ion movement between the anode and cathode during charge and discharge cycles , Li-ion batteries ensure a compact yet powerful energy storage solution. This capability is crucial for UFCSs, particularly in urban settings where space is at a premium, enabling them to cater to a large number of EVs without necessitating extensive land use. Moreover, this high energy and power density directly translates to a higher charging capacity, allowing UFCSs to serve more EVs within the same footprint, as illustrated in fig. 2.7.

Efficiency: Li-ion batteries are known for their high roundtrip efficiency, typically ranging from 85-95%[58]. This high efficiency ensures that a significant portion of the electrical energy stored during charging is available for use during discharge, making them highly suitable for the demanding operational cycles of UFCSs. Furthermore, their low internal resistance contributes to maintaining this high efficiency, even under high discharge rates, ensuring a consistent and reliable power supply for fast-charging EVs.

Cost Considerations: While the initial investment for Li-ion batteries may be higher compared to other battery technologies, their prolonged operational life and higher energy efficiency result in a lower total cost of ownership over time[52]. This aspect is vital for UFCS operators, as it enables them to provide competitive charging rates while ensuring the profitability and economic viability of the charging station.

Safety, Reliability, and Longevity: Li-ion batteries offer unparalleled safety and reliability, steering clear of issues such as the ”memory effect” seen in NiCd batteries and the maintenance challenges associated with Lead-Acid batteries[73][99]. Their stability and resilience ensure a consistent power supply, crucial for UFCSs, where downtime can result in significant operational disruptions and financial losses. Furthermore, Li-ion batteries boast a longer lifespan than their NiCd and Lead-Acid counterparts, translating to fewer battery replacements, reduced maintenance costs, and enhanced operational efficiency[78].

Environmental Sustainability: The extended lifespan of Li-ion batteries not only contributes to the economic and operational efficiency of UFCSs but also aligns with global sustainability goals. By reducing the frequency of battery replacements, Li-ion batteries contribute to lower waste generation, underscoring their role in fostering environmentally sustainable energy storage solutions.

In summary, the high energy and power density, efficiency, economic benefits, safety, reliability, and environmental sustainability of Li-ion batteries make them the preeminent choice for UFCSs. As the world navigates towards a cleaner and more sustainable future, integrating Li-ion batteries in UFCSs stands out as a strategic and forward-thinking decision, ensuring reliability, efficiency, and sustainability in the fast-evolving EV charging landscape.

2.6. Battery Aging

The overall performance of BESS in reducing the operational costs of an UFCS is inherently connected to the lifetime of the battery. The battery must outlive the payback period to become profitable It is important to understand the mechanics behind the aging of batteries. In the method, section will be discussed how these different aging mechanics will be evaluated. Lithium-ion batteries, pivotal in various applications from mobile devices to electric vehicles, are prone to both calendar and cycling degradation mechanisms, which can significantly impact their operational longevity.

Calendar Degradation: in lithium-ion batteries is predominantly a function of time and is less influenced by the actual usage of the battery. A number of variables are responsible for the rate of aging due to calendar degradation.

- **Temperature:** Temperature plays a crucial role in calendar degradation. At elevated temperatures, the rate of parasitic reactions between the electrodes and the electrolyte increases. These reactions can cause a thicker SEI layer to form on the anode[65], leading to lithium loss and increased internal resistance. Furthermore, high temperatures can also accelerate the decomposition of the electrolyte and lead to gas formation inside the cell.
- **State of Charge:** Maintaining a battery at a high SOC for extended periods can exacerbate the potential for harmful side reactions, particularly at elevated temperatures. For instance, holding a battery at a high SOC can promote cathode dissolution and migration of transition metal ions to the anode, disrupting the SEI layer and increasing cell impedance[24].
- **Time:** Naturally, as the battery ages, even without undergoing charge-discharge cycles, there’s an inherent degradation in the electrode materials and electrolyte, causing a decrease in capacity and a rise in internal resistance.

Cycling Degradation: is associated with the battery’s regular charge and discharge operations. This will likely have the most impact on the total aging of the battery but also allows for more control in regulating the aging rate than compared to calendar aging.

- **Voltage:** The operating voltage range significantly impacts the battery’s cycle life. Charging a lithium-ion battery to its maximum voltage can lead to cathode material oxidation, resulting in a capacity drop[76]. Conversely, over-discharging can lead to excessive lithium-ion of the anode, causing an unstable SEI layer and potential copper dissolution.

- **High Currents:** Charging or discharging at high currents generates more heat within the battery. This can induce local hotspots, leading to uneven electrode utilization and faster degradation[75]. High currents can also magnify side reactions, further exacerbating the wear and tear of the battery.
- **Depth of Discharge:** The extent to which a battery is discharged during each cycle also influences its lifespan. Frequent deep discharges can strain the electrodes, promoting mechanical degradation due to the continuous expansion and contraction of the active materials[59].
- **Mechanically**, with each cycle, there's an expansion and contraction of the electrodes. Over time, this can cause particle cracking in the cathode and anode materials, reducing their structural integrity and ability to host lithium-ions effectively[29].
- **Electrolyte Oxidation**, more prominent at high voltages, is another cycling degradation mechanism. This oxidation can result in the consumption of the electrolyte and the formation of gas, causing swelling and potentially increasing the risk of rupture or leakage.
- **Side Reactions**, especially in the presence of impurities, can also occur during cycling, forming undesirable compounds that increase internal resistance and decrease overall cell capacity.

In summation, while lithium-ion batteries are a cornerstone of modern technology, their degradation mechanisms necessitate careful management and understanding. Proper temperature control, a reasonable choice of charging voltages, and understanding the implications of Depth of Discharge (DOD) can significantly mitigate these degradation pathways. Integrating advanced battery management systems can further optimize the operational parameters, ensuring both the safety and longevity of these cells.

2.7. AC vs. DC Bus Systems:

In the quest for designing efficient EV charging infrastructures, the choice arises between working with an AC or DC bus system. Both forms of electricity are present in the system; the source of electricity is the grid, of course, which is AC, while the delivered power is DC since fast charging is preferred. The integrated battery energy system also works with DC power for charging and discharging. Both these systems present unique benefits and challenges.

AC bus systems seamlessly align with most of our existing infrastructure, as most grid power is delivered in AC form. This compatibility makes the integration of such systems smoother. Moreover, the universal implementation of AC power means that components for AC systems are often widely available and can be more cost-effective[85]. Furthermore, an AC bus is inherently suited to serve a charging station with significant AC loads, like lighting or auxiliary systems. However, the benefits come with a downside to be cautious of.

In AC-bus stations, the secondary side of an MV/LV distribution transformer serves as the shared AC bus [87], [94]to which the EV chargers are linked. Take, for example, commercially available DC fast chargers like those offered by ABB, which operate with an AC input voltage ranging from 400 to 440 V and a DC output voltage ranging from 150-920, reaching up to 360 kWof charging power[9]. In a multiport station utilizing these chargers, each charger is connected to the typical AC bus.

To facilitate this connection, power electronic converters play a crucial role by offering rectification, Power Factor Correction (PFC), isolation, and voltage control. These converters bridge the main AC bus with the DC EV ports, as well as with BESS and Renewable Energy Sources (RES) when applicable. The AC-bus architecture necessitates multiple power conversions to establish connections with DC loads and sources, resulting in a more intricate control system [28], especially when serving DC-centric loads like EVs or BESS. Each conversion introduces potential inefficiencies and energy losses. Especially in the DC/AC stage from the battery to the AC bus. As seen in Figure 2.9, this DC/AC conversion step has both the lowest minimum efficiency and the lowest maximum efficiency of 90%. This multi-conversion system also complicates the direct integration of renewables, such as solar panels, which produce DC, as it necessitates multiple inversion stages.

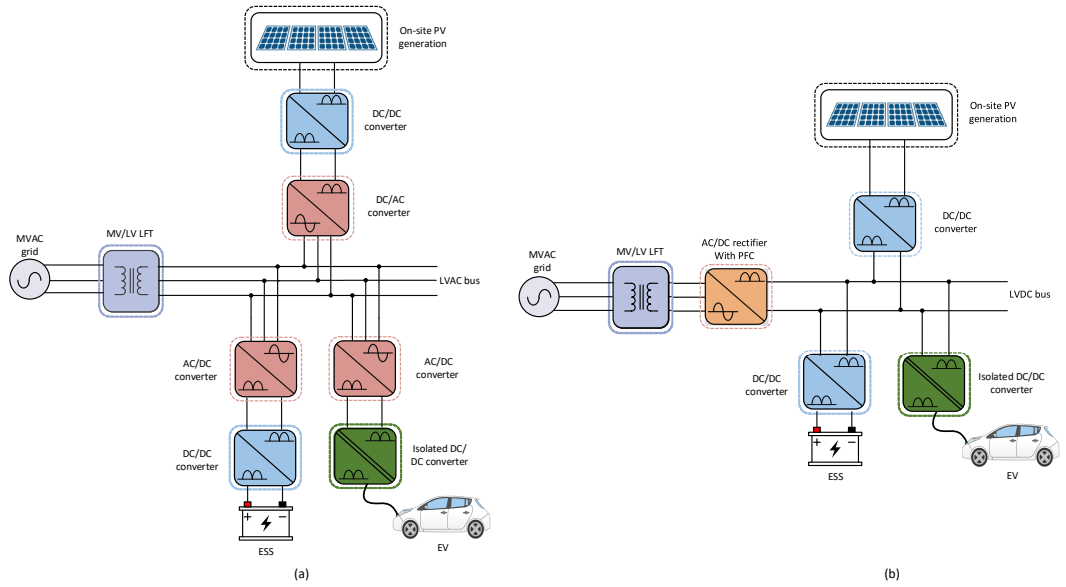

Figure 2.8: A basic configuration of an AC and DC common bus UFCS [23].

In contrast, the DC bus system offers a potent set of advantages, particularly in the context of UFCSs. Foremost among these is efficiency. Reducing the number of conversion stages minimizes energy losses, leading to an overall increase in efficiency[88],[53]. DC systems also provide a straightforward platform for integrating DC-producing renewable. This advantage cannot be understated as renewable energy sources and storage become more integral to our power infrastructure. Expansion and scalability are other aspects where DC systems shine. Whether adding more DC chargers or integrating storage solutions, the process is notably less complex than with AC systems. However, DC bus systems have their own set of challenges. The components for DC systems can sometimes be more expensive than their AC counterparts[68], although this price gap has been narrowing. Managing a DC system, particularly if varying voltages are involved, can also introduce its own set of control and safety complexities.

After an in-depth assessment of AC and DC bus systems, the scales tip in favor of the DC system for UFCS with integrated BESS. Its advantages of efficiency, direct integration of renewables, and scalability make it a more promising choice for future-ready infrastructure. In dc-bus stations, the EV chargers are all connected to a common DC bus, meaning that only isolated DC/DC converters are required between the dc bus and the EV port. Thus, the DC-bus architecture generally has a lower cost, smaller size, and better dynamic performance compared with the ac-bus architecture[10]. This way, the DC/AC converter is avoided, and a 95% efficiency can be assured for all power electronic components2.9. Although the other three power electronic devices can exhibit efficiencies lower than 95% at low loading percentages, this can easily be fixed using multiple lower-rated converters that combined make up the necessary power. This can be done for AC and DC bus systems and systems with and without a Bess. The size and number of converters can be determined based on the average, maximum, and minimum power flowing through that given conversion stage.

In a charging station utilizing a DC fast charger structured with a shared DC bus and an integrated BESS, several functionalities are crucial[85]. These include converting alternating current to direct current (AC/DC rectification), PFC, and regulating voltage levels. Additionally, it is vital to establish a barrier between the grid and the battery to prevent the potential transfer of ground faults, particularly in scenarios where the battery casing might be deteriorated or damaged. This isolation requirement,

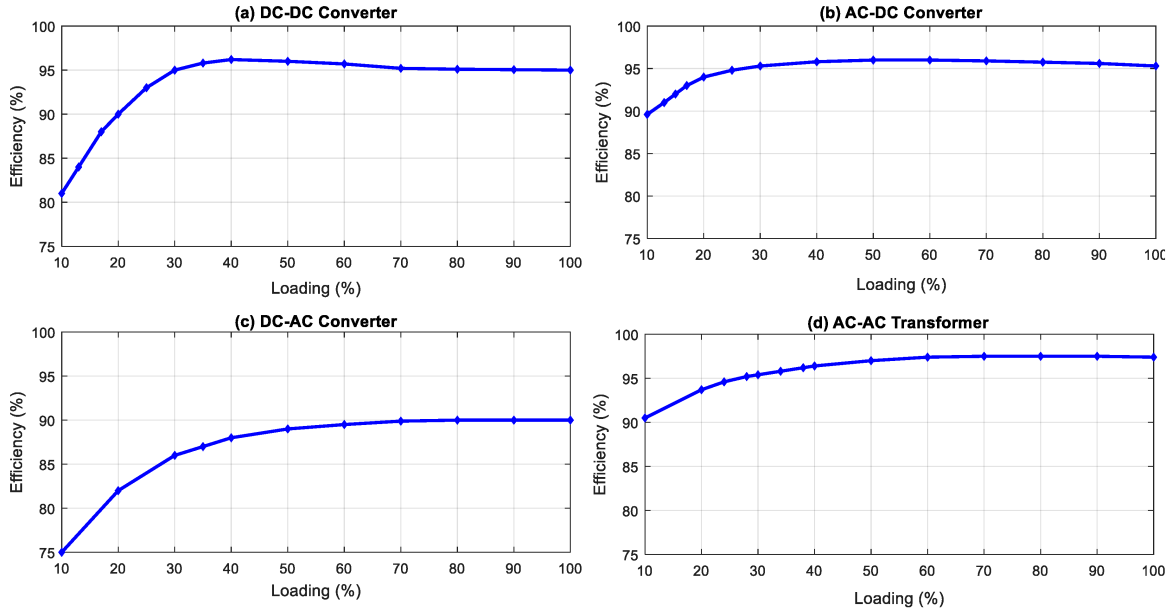

Figure 2.9: load-based efficiencies of power electronic devices [42].

documented in references [60], [11], and [4], presents an extra layer of complexity that doesn't apply to DC UFCS's that don't incorporate energy storage systems. In those setups, only isolation is necessary between the electrical grid and the EV

In high-power DC fast charging stations, particularly those integrated with BESS, the configuration of the DC bus voltage plays a pivotal role in determining the system's performance, flexibility, and reliability. The two primary configurations under consideration are a fixed voltage DC bus and a varying voltage DC bus.

A fixed voltage DC bus offers simplicity and reliability. Standardizing the voltage streamlines component sourcing and replacement, engendering a robust system with fewer active components. Such design simplicity not only mitigates the risk of failures but also ensures the system's resilience, which is preferable. Because despite the inherently lower risk of failure in a DC system compared to an AC system, the implications of a failure in the former can be more severe due to the singular point of failure in the centralized conversion step, as opposed to the multiple failure points in an AC bus system. However, the adaptability of a fixed voltage system might be limited as EV technology evolves. Given that modern electric vehicles operate within a voltage range of 200 to 1000 volts, a high fixed bus voltage, such as 1000 volts, at the upper end of this spectrum, appears sufficient for the foreseeable future. Such a design choice anticipates the demands of EVs in the coming years, ensuring the charging station's continued relevance. The schematic UFCS with integrated BESS with a fixed voltage is shown in Figure 2.10. In the green area the PCS can be seen and in this case is a Solid State Transformer (SST) which has proven to provide superior efficiencies compared to more conventional Low Frequency Transformer (LFT) in the AC to DC conversion step.[51]

Conversely, a varying voltage DC bus exhibits versatility. Its ability to dynamically adjust to the demands of diverse loads makes it adept at serving a wide range of EVs. By delivering power precisely at the requisite voltage level, energy usage is optimized, curtailing unnecessary conversions. Yet, this versatility comes at the cost of increased complexity. Accommodating a wide voltage range necessitates intricate control mechanisms and rigorous safety protocols. Moreover, a direct battery connection to a fluctuating DC bus complicates the design of the EV DC/DC converter. Achieving soft switching across a broad range of input and output voltages poses significant challenges[45], [92].

Soft switching in power electronics, notably Zero Voltage Switching (ZVS) or Zero Current Switching (ZCS), is praised for its potential to minimize switching losses and enhance system efficiency[27],[72]. In DC Fast Charging stations operating at elevated power levels, these efficiency gains are pronounced,

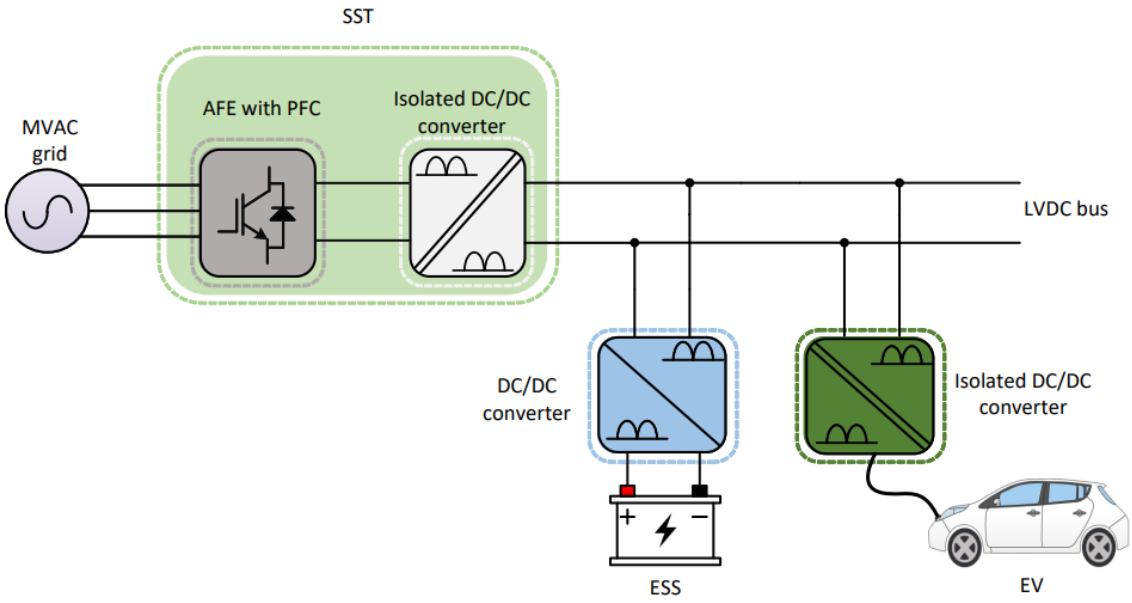

Figure 2.10: Schematic of BESS integrated DC bus of an UFCS [85].

making soft switching a compelling choice. Furthermore, by reducing the rate of change in voltage or current during switching, soft switching substantially diminishes the Electromagnetic Interference (EMI) produced, ensuring smoother operation. The efficiency, combined with reduced EMI

Considering the advantages of soft switching, reliability and the foreseeable voltage demands of modern EVs, a fixed high voltage system emerges as the optimal choice for a battery-integrated DC fast charging station. Such a system can harness the benefits of soft switching while obviating the need for adaptability inherent to a varying voltage system. In conclusion, a fixed voltage system strikes a well-judged balance between performance, reliability, and future readiness, making it well-suited for contemporary DC fast charging applications.

2.8. Electricity Cost

Electricity costs, a critical aspect of the operational expenditures for a UFCS, are fundamentally driven by two distinct entities: the Energy Provider and the Network Operator. The energy provider calculates costs based on total consumed energy and operates within different markets and contracts, for example, the day-ahead market, adjusting prices based on supply and demand dynamics, thereby influencing the cost of the actual energy consumed (kWh). Periods of low demand and high supply can potentially lead to negative prices, which present unique opportunities for entities like BESS-equipped UFCSs to store cheap or effectively 'free' energy.

Conversely, the network operator focuses on the infrastructure side, levying charges for the use of the grid based on the size of the grid connection and the peak power demand. The load profile of the UFCS fundamentally impacts these costs. As the power drawn from the grid increases, so too do the costs from the Network Operator, making it essential to manage the power draw efficiently. Thus, understanding and managing these dual aspects of electricity costs form a central theme of this study, where a BESS at a UFCS can offer a balanced solution for optimal cost management.

2.8.1. Energy Market and Prices

Within the broader methodology of this research paper, an essential component lies in comprehending the structure of the European and therefore the Dutch energy markets. This understanding aids in establishing the operating conditions and parameters for the BESS integrated UFCS.

In the Netherlands, 44% of all contracts are enorm contracts [12]. It means that energy consumed is charged at a set tariff. For the duration of the contract, this price will not change. According to Centraal Plan Bureau statistiek (CBS), the average price per MWh before taxes in 2022 was €156/MWh or €0,156/kWh for companies consuming between 2000-20000 MWh per year [13]. These contracts with set tariffs might offer predictability and reasonable prices, however, they might not necessarily be the most profitable contracts. The Dutch energy market offers a number of options. Using a variable contract gives the opportunity to exploit these markets.

The Dutch energy market comprises three segments: the day-ahead, intraday, and balancing markets[14]. In the day-ahead market customers can sell or buy energy for the next 24 hours in a closed auction. Orders are matched to maximize social welfare while taking network constraints provided by transmission system operators into consideration. The prices are announced a day ahead of the time that the power is traded. On the Intraday market, market participants trade continuously, 24 hours a day, with delivery on the same day. As soon as a buy- and sell-order match, the trade is executed. Electricity can be traded up to 5 minutes before delivery and through hourly, half-hourly, or quarter-hourly contracts. As this allows for a high level of flexibility, members use the Intraday market to make last-minute adjustments and to balance their positions closer to real-time. The balancing market works in actual real-time. The balancing market's core purpose is ensuring grid stability and responding immediately to unexpected deviations in supply or demand. Prices in the day-ahead and intraday markets are typically settled in advance based on bids and offers. In contrast, prices in the balancing market can change frequently and reflect real-time conditions. These prices can be more volatile as they respond to the immediate needs of the grid. In the balancing market, participants are typically providers of reserve power, energy storage operators, and demand response aggregators. They offer resources and services to balance the grid in real-time.

The day-ahead market, wherein energy for the following day is traded based on projected supply and demand, has a particular interest in this study. The combination of prices fluctuating every hour while being known the day before makes the day ahead market very lucrative for lowering electricity costs by (dis)charging the BESS on specific periods and their corresponding price points. The intraday market allows for adjustments closer to real-time, while the balancing market, operated by the Transmission System Operator, ensures that supply and demand are balanced in real-time.The UFCS is not an energy trader but it can exploit the price fluctuations of the intra-day market, without jeopardizing the quality of service for charging customers. The (near) real-time characteristics of the intra-day and balancing market make it impossible for the BESS to constantly and reliably provide for the UFCS

The model will be designed to utilize the day-ahead market's characteristics optimally. This is due to the unique capability of BESS to charge the energy storage during periods of lower demand (and thus lower prices) and to release energy during times of high demand (and, correspondingly, higher prices). This feature of BESS makes UFCSs more economically viable and contributes to the grid's overall stability.

An intriguing feature of the day-ahead market, which the chosen model considers, is the occurrence of negative prices. These emerge when a high supply of inflexible power, which cannot be efficiently shut down and restarted, coincides with low demand. During negative pricing periods, generators pay to maintain their output, as the costs associated with halting and restarting their plants might outweigh the price for which they can sell their energy. In such situations, the BESS offers a unique solution: it can absorb this excess energy, storing it during high demand and higher prices. With an increasing renewable energy penetration in electricity markets, price volatility is expected to increase due to the intermittent nature of renewables, in the absence of sufficient energy storage[49]. The bigger the price volatility the bigger the opportunity to reduce operational cost by BESS deployment optimization.

Therefore, understanding the Dutch energy market, particularly the day-ahead market, plays a significant role in the literature study. This comprehension feeds into the simulation and optimization models, helping generate valuable insights that mirror practical scenarios. As a result, this research stays grounded in the realities of the market, thereby enhancing its relevance and applicability. This research will use an optimization method to exploit the day ahead market to reduce the average energy price of a set tariff contract of €0,156/kWh while prioritizing the power demand of a charging EV

2.8.2. Network Operator Cost

The other component of operational cost is due to the Network Operator (NO). The network operator charges fees for the use of the electrical infrastructure rather than the energy itself. In the Netherlands, the job of the network operator is privatized. In Figure 2.11 it can be seen which companies are active in which area of the Netherlands. The implementation of a BESS has multiple effects on network operator costs.

Figure 2.11: Operating area per network operator [21].

Firstly, implementing a BESS influences the initial agreement with the network operator regarding the size of the grid connection required for the UFCS. This relationship is vital because the network operator charges for grid connectivity based on the capacity of the connection; the larger the connection, the higher the cost. By integrating a BESS into the UFCS, energy can be stored during off-peak hours and used during peak hours. This strategy reduces the station's direct dependency on the grid to provide peak power, allowing for a smaller grid connection. Consequently, this leads to savings in grid connection costs, which are usually significant upfront expenses for the UFCS. These impacts play out over a yearly or even more extended time frame, impacting the foundational infrastructure costs of the station.

Secondly, the BESS contributes significantly towards managing the UFCS's monthly operational costs. The network operator primarily determines these costs based on the maximum power drawn from the grid within a billing cycle, commonly referred to as demand charges. By strategically charging the BESS during off-peak periods and discharging it during peak periods, the UFCS can flatten its demand curve, reducing the peak power drawn from the grid. This approach, in turn, results in lower demand charges, hence reduced monthly operational costs.

In summary, both roles involve the strategic deployment and use of a BESS, yet they distinctly impact the UFCS's cost structure differently. One role pertains to reducing upfront infrastructure costs related to grid connection size, and the other to minimizing recurring operational costs imposed by the network operator based on demand charges.

3

Optimization

In this thesis, a large-scale optimization problem with several variables and constraints needs to be solved. To ensure this is done properly the optimization method is chosen carefully. In the previous chapter the optimization objective, the scheduling of the battery charge and discharge power to minimize energy cost based on hourly electricity tariffs, was described. This chapter will cover what optimization method will be most suited for both the deployment and the sizing of the BESS. The first section of this chapter will discuss what kind of approach is used for the deployment of the battery. Since there are multiple options possible for this optimization method the best contenders will be discussed. Once the best-suited approach is selected. The general working principle of this approach will be explained next, and how the problem described in this research can be expressed in a useful form suitable for the optimization method. In the second section, the specific algorithm that will drive the optimization is selected and explained. In the third section, the optimization method for the sizing of the battery is described, and how it complements the optimization of the deployment. The final section will discuss which software is used and how it contributes to this research.

3.1. Optimization Approach

In the quest for optimal glsBESS deployment and sizing for maximal cost reduction, selecting the appropriate optimization method is paramount. This decision depends on the problem structure, computational efficiency, and solution quality, among other factors. The three prominent contenders for this task include Genetic Algorithm (GA), Particle Swarm Optimization (PSO), and Linear Programming (LP).

Inspired by biological evolution, GA offers a robust search process across complex spaces. Thanks to their population-based approach and the application of genetic operators (selection, crossover, and mutation), they provide the advantage of potentially discovering global optima even in multi-modal landscapes. However, GA can be computationally intensive [46], particularly in large and complex problems. Additionally, GA 's required careful tuning of parameters [57] (e.g., population size, mutation rate, etc.) and do not guarantee the optimal solution in every case [93].

Particle Swarm Optimization is another heuristic method inspired by social behavior patterns of bird flocking or fish schooling. PSO has the advantage of being conceptually simple and requiring fewer adjustable parameters than GA. It can effectively explore large-scale spaces and tends to converge quickly [63]. However, PSO may suffer from premature convergence [77], leading to local optima instead of global optima, especially in complex and non-linear optimization problems. Moreover, its performance can significantly fluctuate depending on the problem type and parameter settings.

On the other hand, linear optimization provides a robust [43] mathematically rigorous approach to finding the optimal solution in problems where the objective function and constraints are linear. The main advantage of this method lies in its computational efficiency [97], transparency, and ability to provide unique, globally optimal solutions. It can efficiently manage large problem sizes [30] while pro-

viding interpretable results. However, its applicability is limited to problems that can be linearized or are inherently linear.

Given the nature of the current problem—optimal glsBESS deployment and sizing—which involves balancing grid power, battery power, and total demand power, linear optimization is the most suitable approach. The problem can be formulated as a linear problem, as the objective function (minimizing the cost) and constraints (power and energy balance, battery operation limits, grid maximum power) are linear relationships. The linear optimization approach, notably the Dual Simplex algorithm, offers a combination of computational efficiency, optimal solutions, and direct alignment with the problem structure, making it the preferred choice for this problem.

3.1.1. Objective and Constraints

At its core, linear optimization seeks to find the best possible outcome (maximum or minimum) for a particular situation while adhering to a set of constraints. Consider the design of a production process, resource allocation, or supply chain optimization. Constraints can be divided into equality and inequality constraints. The objective is to maximize profits, minimize costs, or achieve some other goal, subject to limitations on resources, time, or capacities. In this case, the available energy, the maximum and minimum storable energy, and the fulfillment of demand are some constraints, while the minimization of energy cost is an objective.

3.1.2. Linear Relationships

Linear optimization revolves around linear relationships. This implies that both the objective function (the quantity to be maximized or minimized) and the constraints (the limitations to be upheld) can be expressed as linear equations(equalities) or inequalities. This linearity simplifies the problem and permits the use of mathematical techniques to efficiently find solutions.

3.1.3. Mathematical Representation

To mathematically represent a linear optimization problem, several components are defined:

1. **Decision Variables:** These are the quantities under our control or allocation, often denoted as symbols (e.g., x, y, z).

2. **Objective Function:** It represents the goal to be achieved, such as profit maximization or cost minimization. The objective function is a linear combination of decision variables.

3. **Constraints:** These consist of linear equations or inequalities that express limitations or requirements. Constraints ensure compliance with acceptable bounds for resources, capacities, and other factors.

Linear constraints are mathematically formulated as follows:

$$A_{\text{eq}}\mathbf{x} = \mathbf{b}_{\text{eq}} \tag{3.1}$$

Inequality constraints are generally formulated in the following way:

$$\begin{aligned} A_{\text{ineq}_1}\mathbf{x} &\leq \mathbf{b}_{\text{ineq}_1} \\ A_{\text{ineq}_2}\mathbf{x} &\leq \mathbf{b}_{\text{ineq}_2} \\ &\vdots \\ A_{\text{ineq}_m}\mathbf{x} &\leq \mathbf{b}_{\text{ineq}_m} \end{aligned} \tag{3.2}$$

Finally the objective function, the solution multiplied by a decision variable that must either be minimized or maximized looks as follows.

$$\text{Maximize: /Minimize: } f(\mathbf{x}) \tag{3.3}$$

3.1.4. Optimization Techniques

Solving a linear optimization problem involves determining values for the decision variables that maximize (or minimize) the objective function while adhering to all constraints. Various mathematical methods exist for this purpose, with the Simplex Method being the most commonly employed. It iteratively explores the feasible region (the area where constraints are satisfied) until the optimal solution is reached.

3.1.5. Feasible Region and Optimal Solution

The feasible region encompasses all feasible combinations of decision variable values that satisfy the constraints. The Simplex Method efficiently traverses this region to identify the optimal solution. The optimal solution represents the best course of action within the constraints, where the objective function attains its maximum (or minimum) value. Below an example is given of a linear problem. The corresponding feasibility region and optimal have been given as well.

$$\begin{aligned} \text{Maximize } & J(\mathbf{x}) = 10x_1 + 2x_2 \\ \text{Subject to } & x_1 + x_2 \leq 20 \\ & x_1 - 3x_2 \leq 3 \\ & -20x_1 + 2x_2 \leq -10 \\ & x_1, x_2 \geq 0 \end{aligned} \tag{3.4}$$

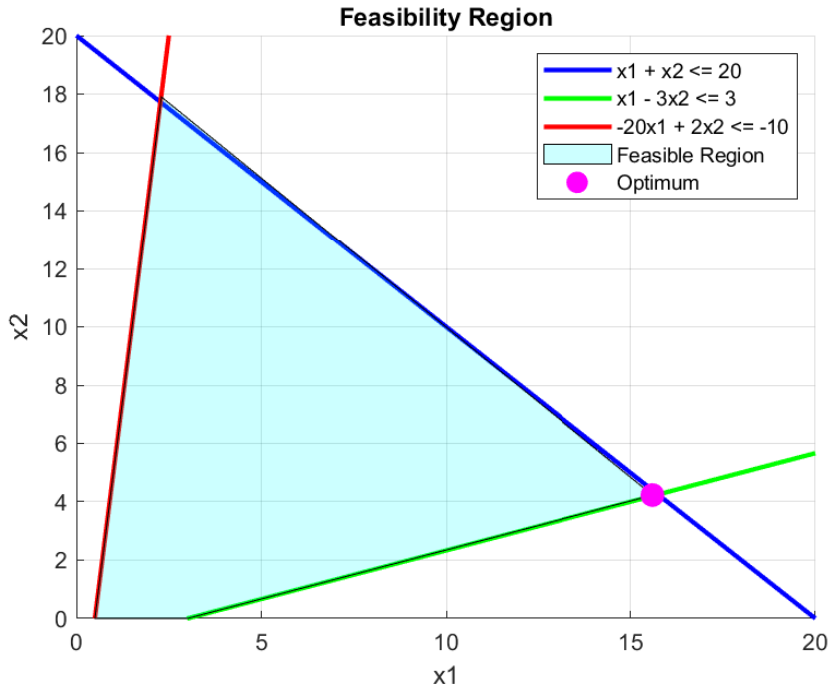

Figure 3.1: Feasibility region and optimal solution.

3.1.6. BESS scheduling Application

The next step is to write the equation that would turn the best-integrated ufc with MV grid connection into a solvable linear problem. Below the equation will be given step by step and their role in the linear optimization problem and their role in the real-life situation will be given.

The most important equation is the equation for Power Demand. The equation is written down also followed. ($P_{\text{demand}}(t)$):

$$P_{\text{demand}}(t) = \sum_{t} Pe_v(t) \tag{3.5}$$

Physical Representation: This equation represents the total power demand at time t, which is the sum of power demands of all-electric vehicles at time t. Linear Programming Role: In a linear programming problem, this equation represents the equality constraint that ensures the electricity demand matches the electricity supply and storage at each time step.
The equation for Power Balance between all suppliers and demand:

$$P_{\text{grid}}(t) + \eta\hat{}(k) \cdot (k) \cdot P_{\text{battery}}(t) = P_{\text{demand}}(t)) : \tag{3.6}$$

The physical power balance this equation represents is the balance between power supplied from the grid, power supplied from or to the battery, and the power demand at time t. The efficiency factor η accounts for losses in battery charging and discharging. And the factor$k$ determines if the battery is charging or discharging. In Linear Programming the role of this equation is also an equality constraint that ensures power balance between grid supply, battery operations, and demand at each time step.

Formulating the variables and constraints related to the grid connection:

$$0 \leq P_{\text{grid}}(t) \leq P_{\text{gridmax}} \tag{3.7}$$

The physical representation of this constraint is that this formula ensures that the power taken from the grid at time t does not exceed the maximum grid power capacity and that no power can be delivered to the grid. In linear programming, this formula represents an upper and lower limit constraint on the decision variable $P_{\text{grid}}(t)$, restricting it to be less than or equal to P_{gridmax}.
Constraints on Battery Power:

$$-P_{\text{batmax}} \leq P_{\text{battery}}(t) \leq P_{\text{batmax}}$$

The physical representation of this constraint is that this formula ensures that the discharging and charging power flowing into or out of the battery at time t stays within the specified limits. In linear programming, this formula sets upper and lower limits on the decision variable $P_{\text{battery}}(t)$, restricting it within the range of $-P_{\text{batmax}}$ to P_{batmax}. Constraints on Battery Energy Level:

$$E_{\text{batmin}} \leq E_{\text{battery}}(t) \leq E_{\text{batmax}}$$

This formula ensures that the battery's state of charge (energy level) at time t remains within specified minimum and maximum limits. In the linear programming problem, this is considered an inequality constraint for $E_{\text{battery}}(t)$, constraining it to be between E_{batmin} and E_{batmax}.

3.2. Discussion on Linear Programming Algorithms

In linear programming, there are several algorithms made available by Mathworks, the chosen software tool. The reason for this choice will delved into in the next section. 3 possible algorithms will be discussed below and the most suited one will be chosen.

3.2.1. Overview of Algorithms

- **Interior-Point Algorithm:** A widely-used approach for large-scale linear programming problems. It navigates through points inside the feasible region, making it effective for problems with numerous constraints.
- **Interior-Point-Legacy Algorithm:** An older rendition of the interior-point technique Though still effective, it may be less optimized than its contemporary counterpart. Certain problem structures or compatibility requirements might necessitate its use.
- **Dual-Simplex Algorithm:** Contrasting the primal simplex method that starts from a feasible solution and moves towards optimization, the dual-simplex method initiates from an infeasible solution, iterating towards feasibility while optimizing. It is particularly beneficial when changes in constraints render a previously feasible solution infeasible, necessitating an efficient return to feasibility.

3.2.2. Algorithm Suitability for Optimal BESS Deployment

The provided optimization method aims to optimize power and energy flows over multiple days in an electric grid scenario while adhering to constraints on energy storage and grid demand. Considering the problem's dynamism, where minor constraint modifications can lead to infeasibility, the dual-simplex algorithm appears optimal. Its strength lies in addressing situations wherein small constraint alterations render the current solution infeasible.

The state-dependent constraints, emphasized by the cumulative inequality matrices, suggest frequent in-feasibilities might arise due to dynamic constraint changes. In such scenarios, the dual-simplex method remains robust, ensuring optimization even as parameters evolve.

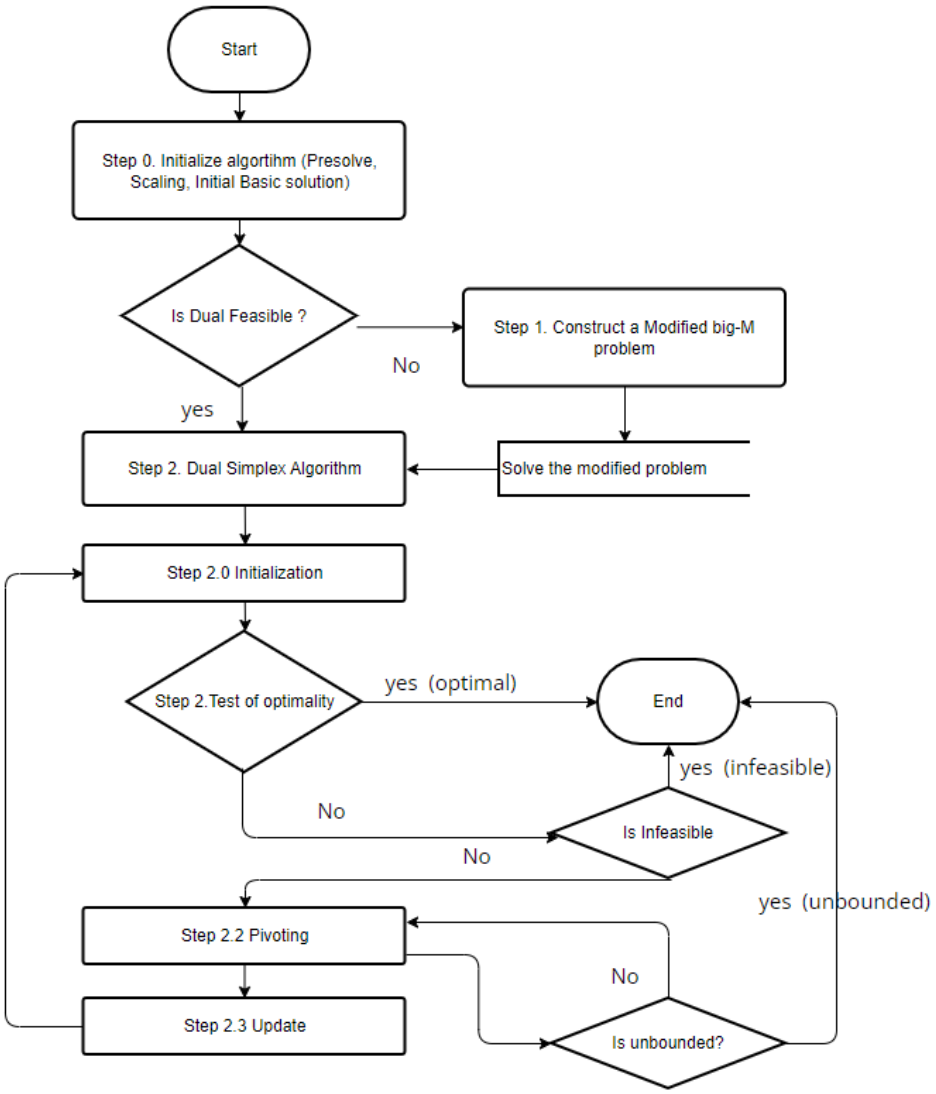

Figure 3.2: Process flow chart of dual simplex algorithm [84].

While the interior-point methods can efficiently tackle large-scale problems, they aren't tailored for frequent infeasibilities arising from dynamic constraint changes. Moreover, the legacy version of the interior point might not provide specific advantages for this problem's structure. Given the dynamic nature of the described electric grid problem and the potential for frequent infeasibilities from evolving constraints, the dual-simplex method stands out as the preferred choice among the discussed algorithms. In Figure 3.2 the process flow chart of a dual simplex algorithm, as described by the book Linear Programming using Matlab[84]

3.3. Grid Search in Power System Optimization: A Comprehensive Approach to Identify Global Optimum

Grid searching is a cornerstone technique in the realm of optimization, defined by its systematic and exhaustive exploration of a specified parameter space. Essentially, grid search meticulously evaluates a problem at varying parameter configurations, ensuring a thorough examination of all conceivable combinations. Despite its computational demands, this brute-force method delivers impressive precision and depth, rendering it useful for challenges with ambiguous or multifaceted parameter landscapes.

In the specific context of this research's power system optimization task, grid search is ingeniously employed to examine two pivotal parameters: grid power capacity and battery power. Each parameter is varied in defined intervals, spanning from 0 to 3500, thus crafting a multidimensional grid of feasible configurations. It will actually run the linear optimization problem over and over again for different combinations of grid power and battery power. The rationale behind adopting this approach can be encapsulated into the following tenets:

- **Granularity of Analysis**: Through systematic evaluations across diverse power spectrums, a granular landscape of system behavior emerges. Such intricacy is pivotal to pinpointing distinct power thresholds where vital performance indicators, such as cost efficiency or operational resilience, are maximized. It will also give insight into the general effect on operational costs of increasing or reducing both grid power and battery capacity. This will be insightful to be able to extrapolate the results of this research into similar problems.
- **Robustness in Solution**: By encompassing an expansive array of scenarios, grid search guarantees that the deduced solutions exude adaptability, aligning with fluctuating real-world contingencies and thus fortifying system resilience. The borders of the grid will show the outer edges of feasibility, and the grid will be able to compare different local optima to put results into perspective.
- **Detection of Global Optimum**: While each discrete configuration might yield a local optimum, the overarching objective of the grid search remains the revelation of the global optimum—a singular configuration that transcends all others in the designated parameter domain. Using this grid searching technique the absolute best solution can be found for this single objective multivariable problem
- **Revelation of Inter dependencies**: Iterative evaluations across the parameter spectrum demystify the intricate interplay between grid and battery power. This could materialize as synergistic efficiencies in specific configurations or spotlight thresholds where returns diminish.

Integrating grid search into the optimization equation enhances the analytical depth, offering a comprehensive perspective of the system's dynamics. By exploring diverse local optima, grid search facilitates a holistic analysis, culminating in the identification of an optimal solution that combines both the network operator costs and energy costs. This way the shortcomings of the deployment algorithm are nullified. It also easily allows to alter the search area and application of this optimization method.

3.4. Software and Tools

The selection of software tools for research is pivotal to the successful implementation of the study. In this case, MATLAB and Simulink were chosen to model the optimization problem and the physical system, respectively, owing to several advantages these software tools offer, particularly for this type of engineering problem.

MATLAB, a multi-paradigm numerical computing environment, is often favored for its interactive interface and robust library of mathematical functions that make it suitable for algorithm development, numerical computation, and data visualization. The MATLAB optimization toolbox was utilized in this research context for the deployment optimization problem. MATLAB's advanced computational capabilities enable efficient implementation of linear optimization algorithms, such as the Dual Simplex method, to determine the glsBESS's most cost-effective charging and discharging times.

In contrast to MATLAB, Python is a more general-purpose programming language, and while it can certainly handle numerical and scientific computations with packages like NumPy and SciPy, MATLAB's

dedicated focus on numerical computing may give it an edge in ease of use and speed for such tasks. MATLAB also excels in the availability of toolboxes designed for specific tasks, such as optimization, making it an excellent choice for this research.

Simulink, a block diagram environment for model-based design, complements MATLAB in this research. It is ideal for modeling, simulating, and analyzing dynamic systems, such as the glsBESS under study. In this research, Simulink is used to model the physical system and calculate the battery lifetime, a task that Simulink is particularly well-suited for due to its capacity for simulating real-world systems.

An alternative to MATLAB and Simulink could have been Wolfram Mathematica. It is a powerful tool for symbolic computation, numerical computation, data analysis, visualization, and algorithm development. However, it might be less practical for modeling dynamic systems like Simulink or have as extensive and specialized toolboxes as MATLAB.

In summary, the selection of MATLAB and Simulink was primarily influenced by their specialized optimization and system simulation capabilities, the robustness of their toolboxes, and the ease and efficiency of implementing engineering computations and visualizations, making them well-suited for this research.

4

Methodology

This chapter will delve into the method this research has used to answer the research question. The first section of this chapter will cover the problem definition and the assumptions that have been made. In the third section, the method to determine and model the power demand of the UFCS is covered. In the next section, the model-chosen variables and working conditions of the battery system will be explained. In the fourth section, the physical and economic properties of the electrical infrastructure are covered. The following section will provide the energy balances that shape the mathematical model of the UFCS. Afterwards, the characteristics and the calculation of the operational expenses will be explained. In the second to last section the evaluation metrics that will determine the optimal solution will be discussed. The final section of this chapter will discuss the sensitivity analysis done in this research.

4.1. System Model and Assumptions

The system being analyzed encompasses the BESS, UFCS, the electrical grid, and several power electronic units. The BESS has the capability to both absorb and supply power, whereas the grid solely supplies power, and the UFCS exclusively consumes it. Energy from the grid charges the BESS, which then discharges to satisfy the UFCS's energy needs. It's presumed that the BESS doesn't have to be entirely depleted before recharging, and any surplus grid power can be stored in the BESS. The UFCS's total energy requirement, pre-calculated and based on methodologies outlined in the literature review, will be elaborated upon in this chapter.

A UFCS station, intricate in its composition, is engineered to provide power ranging from 50 kW to 350 kW per charging slot, facilitating quick charging for electric vehicles (EVs). Each vehicle will receive an identical amount of energy. These elements collectively ensure the efficient and safe functioning of the UFCS. Located near Delft, an urban locale, the UFCS includes 10 charging slots, each offering equal power output capabilities.

Central to the UFCS is the power conversion system. This setup, comprising power converters, converts the grid's AC power to the DC power needed by the EV batteries and BESS. To reduce energy loss during this transformation, these converters must be highly efficient. Advanced converter designs, like dual-active bridge converters, are often utilized in high-power chargers to attain such efficiency.

The UFCS's connection to the grid is via a DC bus. While an AC bus involves converting the grid's AC power to DC at the charger, a DC bus involves a centralized AC to DC conversion, distributing DC power to individual chargers. All system components have a predefined efficiency level. Although real-life power electronic components have load-dependent efficiency, a fixed value is chosen for optimization purposes.

Besides the BESS's capacity reduction, it's assumed that other component performances remain unaffected over time. Maintenance costs are considered only for the BESS, disregarding other components. The battery will have a 1C rating,meaning it's power in/output is less than or equal to the capacity

Pricing assumptions imply that selected prices reflect costs throughout the entire evaluation period. Additional expenses like taxes and insurance are not included. The aging rate, determined for a specific

battery chemistry, may not directly apply to different battery systems.

Considering temperature impacts on battery efficiency and capacity, a climate control system is suggested. It will maintain optimal battery temperature (25C) within a standard 40 ft insulated container, up to a 25-degree external temperature variance. The power requirement for this system can be calculated through a heat transfer formula, ensuring the battery operates at around 25 degrees Celsius. Although this system may consume extra power, it significantly boosts battery performance under extreme temperatures. The power required to maintain a battery at a specific temperature in an insulated container can be calculated using the formula for heat transfer through a surface, given by:

$$Q = U \cdot A \cdot \Delta T$$

where:

- Q is the heat loss in watts
- U is the heat transfer coefficient in W/(m²·K)=1.5
- A is the surface area of the container in m²=136
- ΔT is the temperature difference between the inside and outside of the container in °C=25

Next, considering the COP of the heat pump, the electrical power required to compensate for this heat loss can be calculated as:

$$P_{\text{electrical}} = \frac{Q}{\text{COP}}$$

where:

- $P_{\text{electrical}}$ is the required electrical power in kW
- COP is the coefficient of performance of the heat pump

In this case, with an estimated heat loss of 5.07 kW and a COP of 4, the required electrical power is:

$$P_{\text{electrical}} = \frac{5.07\,\text{kW}}{4} \approx 1.25\,\text{kW}$$

Since the power requirement is so small in comparison to the rest of the demand it is chosen to neglect the power requirement of this system. The purchase and installment of such a system is unlikely to exceed 2000 euros and is also deemed insignificant.[22]. Therefore it is decided that the battery temperature can be assumed to be constant at 25 degrees with the corresponding efficiencies capacity and cycle life.

4.2. Demand Modeling

In the rapidly growing EV market, the role of UFCS is pivotal. These stations bear the significant responsibility of meeting the charging demands of EVs swiftly and efficiently. Understanding and predicting the demand at these stations is a cornerstone of this study, aiming to craft a nuanced model that adeptly mirrors real-world scenarios. A MATLAB model has been made to create a 30-day demand profile with time steps of 10 minutes.

To forge a precise and representative demand profile, the study leans heavily on meticulous data analysis and simulation over 30 days, built upon a set of well-defined parameters. The primary focus is on high-speed charging sessions encompassing 50 kW, 175 kW, and 350 kW speeds, with each car assumed to necessitate a charge slightly exceeding 58 kWh. This translates to charging times of 70 minutes, 20 minutes, and 10 minutes for the corresponding charging speed respectively. In Figure 4.1 the charging speed over time can be seen for each of the 3 chosen possibilities.

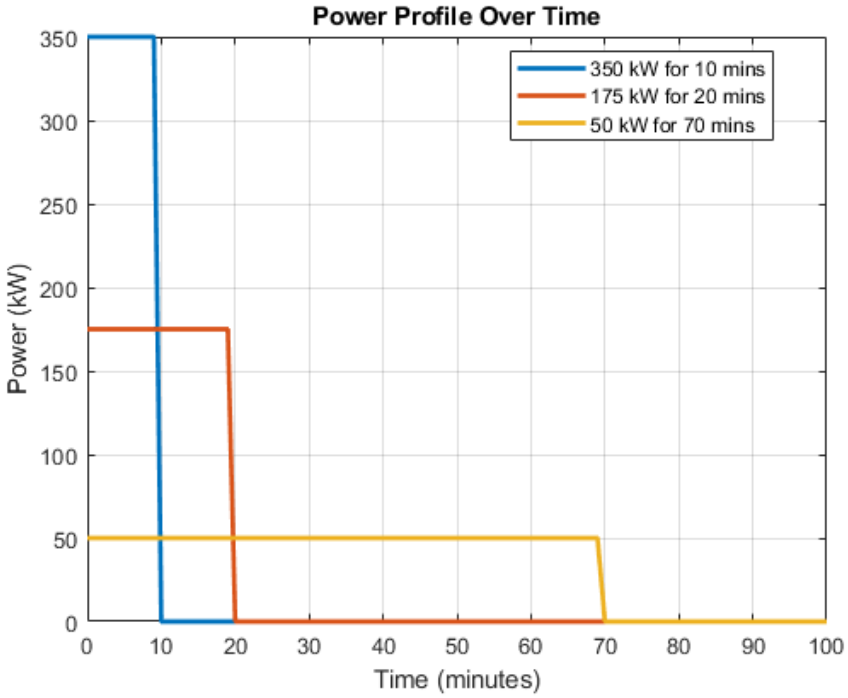

Figure 4.1: 3 possible charging profiles for an arriving car.

Although in actual scenarios, charging requirements might vary based on various factors such as the vehicle's SOC, model specifications, and user preferences, this study adheres to these predetermined charging speeds to maintain a streamlined approach. The intricate variables and fluctuating charging speeds warrant a separate, detailed investigation and are considered to have a marginal impact on the outcome of this study.

The modeled UFCS, positioned in an urban locale in the Netherlands near the city of Delft, is equipped with 10 charging poles, each having 144 10-time slots per day, with each slot spanning 10 minutes. Each pole is capable of providing each of the three defined charging speeds. This forms a critical facet of the simulation, facilitating a deep dive into the utilization dynamics of the charging stations over a day.

Real-world data serves as the bedrock of this study, guiding the simulation to portray an accurate representation of the demand dynamics at the UFCS. The hourly utilization percentages for every day of the week of Five Fastned charging stations, a leading provider in the Netherlands, were carefully analyzed. Using this data the average utilization rates for two distinct periods of the day - 00:00 to 12:00 and 12:00 to 24:00, for both weekdays and weekends were derived. This will The results can be seen in the table below. This data steers the MATLAB model to dynamically adjust the utilization rates, ensuring a faithful replication of the actual demand patterns. This data aligns with and is supported by the literature as discussed in the previous chapter.

Table 4.1: Utilization percentages for different time slots during weekdays and weekends

Time Slot	Weekdays (%)	Weekends (%)
00:00 - 12:00	27.3	17.9
12:00 - 24:00	35.8	25.1

The MATLAB script employed in this study showcases a robust simulation model, iterating through each day with a keen differentiation between weekdays and weekends. It initializes a three-dimensional matrix to record the charging status across the 10 charging spots at 10-minute intervals. Each matrix representing a day will have 10X144 indices representing the charging spots and their charging time slots. A pivotal component of the script is the assign values function, a custom-built tool that adeptly

populates the matrix with charging sessions. The function will randomly assign a spot in the empty matrix with a charging speed and the corresponding charging time until the average utilization percentage presented in the Table 4.1 is reached. This step will repeated 30 times, while counting whether a weekend or weekday is modeled starting from a Monday until a 30-day period demand profile is constructed and finished. Each day will output a different demand profile but will mirror the realistic, varied distribution witnessed in real-world scenarios, maintaining the data's integrity while offering the randomness of the potential demand patterns.

As the simulation completes its 30-day cycle, the three-dimensional 30X10X144 matrix morphs into a two-dimensional format(30X144), allowing for an analytical study of the total demand and the individual charging power demands over the month. This transition is not just a transformation of data but symbolizes the culmination of a complex, dynamic model into a comprehensible, analytical format.

This analytical format will represent the power that is provided by the bus system sent to the charging EV's and corresponding power electronics. The optimization algorithm will deploy a mix of power from the BESS and the grid to fulfill this power demand while minimizing operational expenses.

4.3. Empirical Model of UFCS

The ufc and its sub-components consist of several mathematical equations. In this section, the overall model of the energy balance is discussed. The equations given below describe the power balance or energy balance in this system. These equations therefore represent the equality and inequality constraints and the upper and lower bounds of the linear optimization problem.

4.3.1. Energy Balance

Within these equations the total demand is the sum of all charging spots i with charging speeds p for time step t. The efficiency eta is extracted from Table 4.4 and the variable k represent wether the battery is charging(-1) or discharging (k=1)

$$P\,\mathrm{demand}(t) = \Sigma Pev(p,i,t) \tag{4.1}$$

$$\mathrm{Pgrid}(t) * \mathrm{eta} + \mathrm{eta}^{\wedge}(k) * (k)P\,\mathrm{Pattery}(t) = \mathrm{Pdemand}(t) \tag{4.2}$$

$$\mathrm{Pgrid}(t) \leq Pgridmax \tag{4.3}$$

$$-Pbatmax \leq Pbattery(t) \leq Pbatmax \tag{4.4}$$

$$Ebatmin \leq Ebattery(t) \leq Ebatmax \tag{4.5}$$

$$\begin{aligned} p &= 50, 175, 350 \\ i &= 1, 2, \ldots, 10 \\ t &= 1, 2, \ldots, 144 \end{aligned} \tag{4.6}$$

$$\begin{aligned} k &= -1, 1 \\ Eta &= \mathrm{Efficiency\,of\,Battery\,or\,PCS} \\ \mathrm{Ebattery}(t) &= \mathrm{Ebattery}(0) + \Sigma(-k)\,\mathrm{Pbattery}(t) * T \\ \mathrm{Ebattery}(t) &= \mathrm{Ebattery}(t-1) + (-k)\,\mathrm{Pbattery}(t) * T \end{aligned} \tag{4.7}$$

4.4. Battery selection

After opting for the Li-ion battery technology, the next choice concerned the specific battery chemistry to adopt. Among the many Li-ion chemistries available, Lithium Iron Phosphate (LFP) was chosen due to its several advantageous properties:

- **Efficiency:** LFP batteries are renowned for their high efficiency, characterized by a consistent discharge voltage[102] that contributes to effective energy utilization. They exhibit low internal resistance, which enhances their charge and discharge efficiency, especially beneficial in applications requiring high current outputs. LFP based BESSs offer efficiencies in the range of

94%–98% [66], depending on series and parallel cell connections and cell type. LFP batteries maintain a stable efficiency over a wide range of temperatures, making them reliable in diverse operational environments.

- **Thermal and Chemical Stability:** LFP batteries demonstrate excellent thermal stability and robustness, thanks to the inherently safe iron phosphate cathode material [102]. This stability is of paramount importance for UFC stations, which frequently operate at high charging rates. Excessive heat generation could lead to premature degradation or even catastrophic failure of the batteries, a risk mitigated by the LFP chemistry.

- **Long Cycle Life:** LFP batteries are renowned for their extended cycle life, outperforming other Li-ion chemistries. They can endure a larger number of charge-discharge cycles before experiencing significant capacity loss [38]. This increased cycle life is essential for UFC stations, which often undergo numerous charge and discharge cycles each day. This aspect directly contributes to lower lifetime costs and reduces the need for frequent battery replacements, ensuring continuous operation of the UFCS.

- **Cost:** Over recent years, the cost of LFP batteries has been trending downwards, making them an increasingly economical choice for large-scale deployment [52]. The utilization of iron, a cheaper and more abundant element than the cobalt used in other Li-ion chemistries, contributes to cost-effectiveness. The reduced manufacturing costs associated with LFP batteries make them a more attractive option for UFC station developers who aim to balance performance and affordability. The Cost of Capacity (COC) a lithium-ion battery has been declining steadily with costs ranging from$151-$203/kWh [90][82]. These however only represent the COC. To install a battery at the site the cost of Cost of Commissioning (C&C) has to be taken into account as well, these cost range from $87-$105/kWh[44][15]. In this research paper, the mean estimate is taken in euros. It can be seen in Table 4.5 that the cost of a li iron phosphate battery is €285/kWh. Next to the investment to purchase the battery, there are Operation and Maintenance (OM) costs involved as well. These occur every year. The OM costs are (€6.9/kW-yr)[105].

- **Environmentally Friendly:** From an environmental standpoint, LFP batteries are a more attractive option within the Li-ion family. Their manufacturing process involves no heavy metals, and their operation poses no risk of thermal runaway [80]. This eco-friendliness is particularly relevant in today's world, where there is a growing emphasis on the environmental impact of technology.

Table 4.2: BESS project costs for LFP chemistry and associated maintenance and commissioning.

	COC(€/kWh)	C&C(€/kWh)	OM(€/kWh/year)
Cost range	151-203	87-105	6.9
Cost mean estimate	189	96	6.9
Total cost	285(€/kWh)		6.9(€/kWh/year))

In conclusion, the choice of Li-ion batteries, and specifically the LFP variant, creates a balance between the requirements of energy and power density, cost, safety, reliability, and longevity. This equilibrium results in an optimal design and operation of UFC stations for the research at hand.

4.5. Battery and Aging Model

The lifetime of a li-ion phosphate battery can range from 10 to 15 years [79], but high cycling rates and calendar lifetime will affect the actual lifetime of the battery. Since the battery is used in a very specific and unique way a unique model is used to calculate the lifetime of the battery. To do that the results of the empirical model have to be implemented in a mathematical model that incorporates the characteristics of an LFP battery. The results of this mathematical model are used to calculate the battery degradation. First, the calendar degradation will modeled, and second the cycling degradation model.

4.5.1. Mathematical Model

This battery model, specifically for lithium-ion batteries, intricately maps how a battery's performance varies with temperature and current flow. It uses a set of mathematical equations to represent both charging and discharging processes, factoring in the impact of ambient and internal temperatures, battery capacity, and voltage changes.

In this model, the current at any given time ($i(t)$) is determined by dividing the power output or input ($P(t)$),obtained from the empirical model, by the battery's voltage at that time ($Ebatt(t)$).Where the initial battery voltage is 1000 volts. For discharging (when current i is positive), a complex function $f1$ calculates the battery voltage considering factors like the constant voltage ($E0(T)$), polarization effects ($K(T)$), and the maximum capacity ($Q(Ta)$), among others. The same approach, with slight variations, is applied for charging (when current i is negative). These calculations help in understanding the nonlinear behavior of the battery's voltage during different operating conditions.

The model also considers the temperature dynamics within the battery cell. The internal temperature ($T(t)$) is calculated using a formula that includes the thermal resistance (Rth), thermal time constant (tc), and the heat generated during charge/discharge ($Ploss$). This aspect is crucial because temperature significantly affects battery performance and longevity.

Moreover, the model incorporates several temperature-dependent parameters, like the reversible voltage temperature coefficient ($\frac{\partial E}{\partial T}$), polarization constant (K), and internal resistance (R), which change according to an Arrhenius-type behavior. These components are essential for accurately predicting battery behavior under different thermal conditions. The equations for these calculations are detailed in equations 4.1 to 4.11.

$$i(t) = \frac{P(t)}{Ebatt(t)} \tag{4.8}$$

Discharge Model (i > 0)

$$f_1(it, i^*, i, T, T_a) = E_0(T) - K(T) \cdot \frac{Q(T_a)}{Q(T_a) - it} \cdot (i^* + it) + A\exp(-B \cdot it) - C \cdot it \tag{4.9}$$

$$E_{\text{batt}}(T) = f_1(it, i^*, i, T, T_a) - R(T) \cdot i \tag{4.10}$$

Charge Model (i < 0)

$$f_1(it, i^*, i, T, T_a) = E_0(T) - K(T) \cdot \frac{Q(T_a)}{it + 0.1 \cdot Q(T_a)} \cdot i^* - K(T) \cdot \frac{Q(T_a)}{Q(T_a) - it} \cdot it + A\exp(-B \cdot it) - C \cdot it \tag{4.11}$$

$$E_{\text{batt}}(T) = f_1(it, i^*, i, T, T_a) - R(T) \cdot i \tag{4.12}$$

With

$$E_0(T) = E_{0|T_{\text{ref}}} + \frac{\partial E}{\partial T}(T - T_{\text{ref}}) \tag{4.13}$$

$$K(T) = K_{|T_{\text{ref}}} \cdot \exp(\alpha\left(\frac{1}{T} - \frac{1}{T_{\text{ref}}}\right)) \tag{4.14}$$

$$Q(T_a) = Q_{|T_a} + \frac{\Delta Q}{\Delta T} \cdot (T_a - T_{\text{ref}}) \tag{4.15}$$

$$R(T) = R_{|T_{\text{ref}}} \cdot \exp(\beta \left(\frac{1}{T} - \frac{1}{T_{\text{ref}}}\right)) \tag{4.16}$$

The cell or internal temperature, T, at any given time, t, is expressed as:

$$T(t) = L^{-1}\left(\frac{P_{\text{loss}}}{R_{\text{th}}} + T_a \frac{1}{1 + s \cdot t_c}\right) \tag{4.17}$$

$$P_{\text{loss}} = (E_0(T) - E_{\text{batt}}(T)) \cdot i + \frac{\partial E}{\partial T} \cdot i \cdot T \tag{4.18}$$

Where:

- R_{th} is thermal resistance, cell to ambient (°C/W).
- t_c is thermal time constant, cell to ambient (s).
- P_{loss} is the overall heat generated (W) during the charge or discharge process and is given by
- T_{ref} is the nominal ambient temperature, in K.
- T is the cell or internal temperature, in K.
- T_a is ambient temperature, in K.
- $\frac{\partial E}{\partial T}$ is the reversible voltage temperature coefficient, in V/K.
- α is the Arrhenius rate constant for the polarization resistance.
- β is the Arrhenius rate constant for the internal resistance.
- $\frac{\Delta Q}{\Delta T}$ is the maximum capacity temperature coefficient, in Ah/K.
- C is the nominal discharge curve slope, in V/Ah.
- E_{Batt} is the nonlinear voltage, in V.
- E_0 is the constant voltage, in V.
- Exp(s) is the exponential zone dynamics, in V.
- Sel(s) represents the battery mode. Sel$(s) = 0$ during battery discharge, Sel$(s) = 1$ during battery charging.
- K is the polarization constant, in V/Ah, or polarization resistance, in Ohms.
- i^* is the low-frequency current dynamics, in A.
- i is the battery current, in A.
- it is the extracted capacity, in Ah.
- Q is the maximum battery capacity, in Ah.
- A is the exponential voltage, in V.
- B is the exponential capacity, in Ah^{-1}.

The model is utilized to verify if real-life battery models can replicate the results from the empirical model. It accounts for voltage variations due to charging and discharging rates and the SOC. This approach not only tests the empirical model's reliability but also facilitates more precise battery degradation calculations for specific configurations and uses. As discussed later in this section, battery aging is influenced by various factors, which are determined using the battery model, as described by equations 4.12 to 4.15.

For the lithium-ion battery type, these equations where provided by matlab[75] whom based there model on previous research[34]. The input of the model are the (dis)charge power profile provided by the empirical model, the cyclic aging characteristics, the initial battery voltage, the battery capacity and the ambient temperature. All other variables for the LFP battery were provided by Matlab simulink. According to the literature the experimental validation of the model shows a maximum error of 5%, when SOC is between 10% and 100%, for the charge (when the current is 0 through 2 C) and discharge (when the current is 0 through 5 C) dynamics. Which well within the operating conditions proposed in this research.

4.5.2. Calendar Degradation

The calendar degradation of a battery is highly dependent on the storage time, the state of charge at which the battery is kept and the temperature the battery is kept. Since the battery is cycling it will be assumed that the average soc is 50% while temperatures will ambient temperature will be kept constant at 25 degrees. Studies using measurements from experimental setups have determined that a lithium iron phosphate battery, under conditions very similar to the assumed conditions in this research, will change its capacity ranging from 98%-101% over an 8-month period[59][56]. While a study using a linear regression model has calculated that an LFP battery under these conditions will lose 20% capacity over a lifespan of 23.8 years. Using the average loss per year of the literature, respectfully -2.4%, +1.5%, and -0.84%, an average is taken of a loss due to calendar life of 1% per year. Other literature confirms this estimate. As can be seen in Figure 4.2 the Battery will lose 20% capacity in about 240 months(20 years) when kept at 50% state of charge.

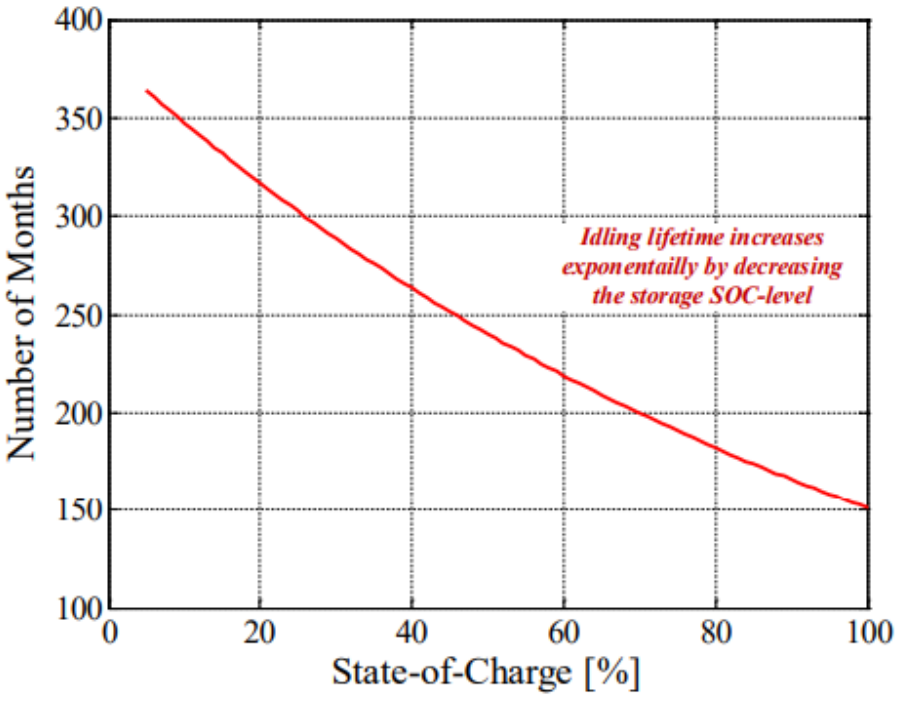

Figure 4.2: . Calendar lifertime characteristic of the LFP/C battery cell idling at 25°C and various SOC-levels (valid for a 20% capacity fade end-of-life criterion) [95].

when the battery is kept at 90-100% SOC year round the capacity losses can increase significantly

with the most optimistic expectations being a lifetime of 150 months, just a bit more then 12 years. This is without considering aging due to cycling.

4.5.3. Cycle Life Degradation

Conventional cyclic aging methods incorporate something called the cycle life vs depth of discharge curve like in Figure 4.3. This curve will show how many cycles a battery will last when a constant DOD is used assuming that charging and discharging are constant and repeated. This method however is way too simple to predict the lifetime of the battery used in a way as proposed in this research. This method only provides an endpoint and will not consider the capacity loss between beginning and end of life. Also does it not specify what the capacity is at the end of life? Because the optimization algorithm will deploy the battery to reduce the operational cost the discharge and charge power are not predictable and repeatable. A constant current constant voltage (dis)charging protocol will not allow to full use potential economic benefits of this model. The factors of voltages and temperatures have also been left out of the equation. To accurately determine the cyclic aging of the battery a model has been used that incorporates the dynamic currents, voltages, depth of discharge, and temperature of a specific battery. In this case a LFP battery.

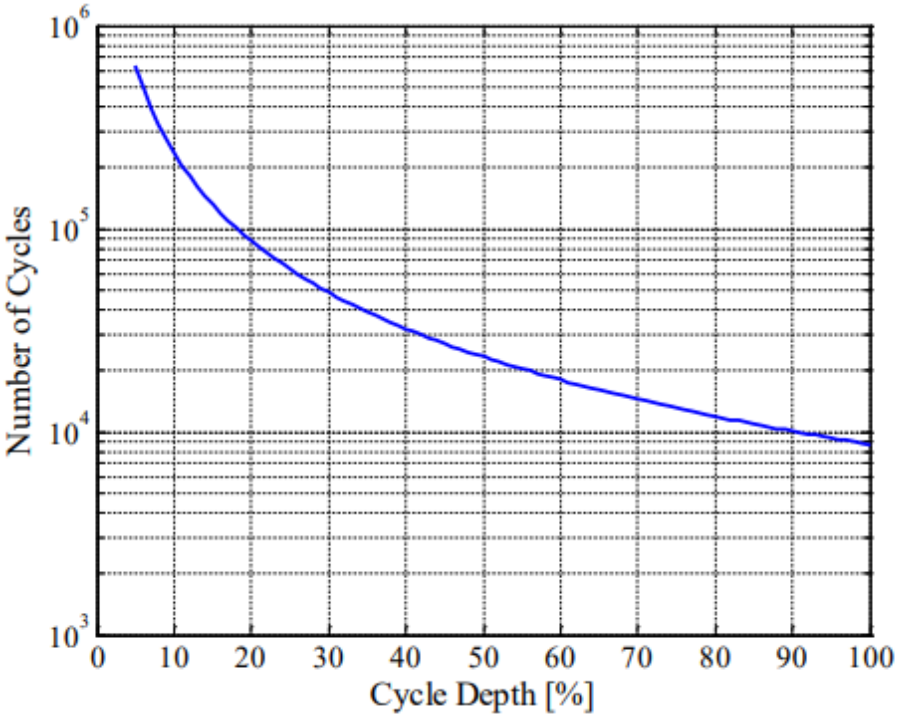

Figure 4.3: Lifetime characteristic of the LFP/C battery for cycling at 25°C (valid for a 20% capacity fade end-of-life citerion) [95].

From this chart the number of cycles the LFP battery can run for a specific cycle depth before it reaches the end of lifetime criterion of 80% of original capacity. From the graph the following values have been extracted.

Table 4.3: Lifetime characteristic of the LFP/C battery for cycling at 25°C (valid for a 20% capacity fade end-of-life citerion).

Cycle Depth	number of cycles
25%	60.000
50%	22.000
75%	15.000
100%	9.000

The problem however is that the optimized model only works with power and energy and will not provide any useful data regarding temperature current and voltage, it does however provide DOD. The (dis)charge profile in k over time needs to be implemented into a model representing an actual battery, having the properties of a battery.

4.5.4. Aging Model

This section of the research presents a model for estimating the usable lifespan of a lithium-ion battery, considering various operational factors and their impact on battery aging. The model calculates the battery's maximum capacity ($Q(n)$) and internal resistance ($R(n)$) over time, taking into account the battery's condition at the beginning of life (BOL) and end of life (EOL). This model will use the results from section 4.5.1-3 to calculate the degradation over time.

The model operates on a cycle-by-cycle basis, with each cycle represented by a half-cycle duration (T_h). The capacity and resistance at each cycle (n) are calculated using the BOL values (Q_{BOL}, R_{BOL}) and the EOL values (Q_{EOL}, R_{EOL}), modified by an aging factor ($\epsilon(n)$). This aging factor is determined based on the battery's depth of discharge (DOD) and other operational parameters.

The aging factor ($\epsilon(n)$) itself is a dynamic value that evolves with each cycle, influenced by the change in DOD and the number of cycles ($N(n)$). The number of cycles is affected by the average discharge and charge currents ($I_{dis\_ave}(n), I_{ch\_ave}(n)$), whom are obtained from the results of the mathematical model from section 4.5.1, and the ambient temperature ($T_a(n)$) in relation to a reference temperature (T_{ref}). For the LFP battery type, the impact of aging (due to cycling) on the battery capacity and internal resistance is represented by these equations [81][89][109][75]:

$$Q(n) = \begin{cases} Q_{BOL} - \varepsilon(n) \cdot (Q_{BOL} - Q_{EOL}) & \text{if } k/2 \neq 0 \\ Q(n-1) & \text{otherwise} \end{cases} \tag{4.19}$$

$$R(n) = \begin{cases} R_{BOL} + \varepsilon(n) \cdot (R_{EOL} - R_{BOL}) & \text{if } k/2 \neq 0 \\ R(n-1) & \text{otherwise} \end{cases} \tag{4.20}$$

with

$$n = kT_h \quad (k = 1, 2, 3, \ldots \infty)$$

where: - T_h is the half-cycle duration, in s. A complete cycle is obtained when the battery is discharged and charged or conversely.
- Q_{BOL} is the battery's maximum capacity, in Ah, at the beginning of life (BOL) and nominal ambient temperature.
- Q_{EOL} is the battery's maximum capacity, in Ah, at the end of life (EOL) and nominal ambient temperature.
- R_{BOL} is the battery's internal resistance, in ohms, at the BOL, and nominal ambient temperature.
- R_{EOL} is the battery's internal resistance, in ohms, at the EOL, and nominal ambient temperature.
- ε is the battery aging factor. The aging factor is equal to zero and unity at the BOL and EOL.
The battery aging factor, ξ, is expressed as

$$\varepsilon(n) = \begin{cases} \varepsilon(n-1) + \frac{0.5}{N(n-1)} \left(2 - \frac{DOD(n-2) + DOD(n)}{DOD(n-1)}\right) & \text{if } k/2 \neq 0 \\ \varepsilon(n-1) & \text{otherwise} \end{cases} \tag{4.21}$$

where: - DOD is the battery DOD (%) after a half-cycle duration.
- N is the maximum number of cycles and is given by

$$N(n) = H \left(\frac{DOD(n)}{100}\right)^{-\xi} \cdot \exp\left(-\psi\left(\frac{1}{T_{ref}} - \frac{1}{T_a(n)}\right)\right) \cdot \left(I_{dis_ave}(n)\right)^{-\gamma_1} \cdot \left(I_{ch\_ave}(n)\right)^{-\gamma_2}, \tag{4.22}$$

where:
- H is the cycle number constant (cycles).
- ξ is the exponent factor for the DOD.

- ψ is the Arrhenius rate constant for the cycle number.
-T_{ref} is the nominal ambient temperature, in K
-T_a is the l ambient temperature, in K
- I_{dis_av} is the average discharge current in A during a half-cycle duration.
- I_{ch_ave} is the average charge current in A during a half-cycle duration.
- γ_1 is the exponent factor for the discharge current.
- γ_2 is the exponent factor for the charge current.

As (dis)charge currents of the battery increase the maximum number of cycles N decreases. As N decreases the age factor ϵ becomes larger. As ϵ becomes larger the battery will creep closer to End of Lifetime (EOL) capacity. This way the aging for different (dis)charge currents and different DOD's can be calculated.

Using this model it can be calculated for how many years the battery can be used when (dis)charge profiles based on optimization for reduction of operational cost are applied ,before it reaches the end of life (EOL). For lithium-based battery chemistries the most common definition of (EOL) is the time that the capacity reaches its 70–80% of the nominal capacity, which means the corresponding state of health SOH decreases to 70-80%[101],[67],[107].In this research the EOL criterion is chosen at 80%. This means that the BESS will be retired when the capacity reaches 80% of the original capacity. To make sure that the battery performance is the same in the first month as in the last month it is also chosen that the minimum battery state of charge is 15% and the maximum battery state of charge is 85% meaning that only 70% capacity is used to perform in the first month and therefore in the last month. Since modern-day LFP can reach 100% DOD the bess will still be functional[16]. Although 100% DOD is not beneficial for the lifetime of the battery this will only occur in the last month.

4.6. Bus System

The chosen DC microgrid will need several components. As described in Chapter 2 there were multiple possible microgrids but for the UFCS DC bus system with a fixed voltage seems the most reliable and most cost-effective. This is because the only consumer of power, the UFCS, is DC and the added battery is also DC by nature. The chosen bus system is shown in Figure 2.10. This means that the isolation is on the grid side of the system, this is also where active frond-end rectification with PFC is ensured. The battery could be connected directly to the DC bus voltage, but by installing a bidirectional non-isolated DC/DC converter in between the battery and the DC bus a fixed voltage can be guaranteed. This way the range of voltages the the DC/DC converters on all three sides of the DC bus can be much smaller. leading to higher efficiencies and lower costs as well as minimising system failure . The isolated DC/DC converter shown as the dark green square is an important part of the system but will not change regardless of the chosen microgrid or size of the battery. Therefore it will be left out of the scope of sizing of the components. So in this research there are two main conversion steps. The efficiency of the SST[51][91] that converts the AC power to DC power and the BESS combined with the biderectional DC/DC converter[50],which has an efficiency of 99% under sof switching conditions, can be seen in Table 4.4 . It is chosen that the combined efficiency for thee SST is 95% and for the BESS combined with the DC/DC converter is also 95%.

Table 4.4: Efficiencies of power electronic components

	PCS(SST)	DC/DC	LFP
Efficiency range	91-98%	99%	94-98%
Efficiency mean estimate	95%	99%	96%
Total efficiency	95%		95%

All the components in this system have to be bought and the grid searching optimization method will reveal the combination of grid power and battery where the cost of components is favorable. The cost can come from either the isolated active front end rectifier with pfc, this is the power conversion system (PCS) illustrated by the light green square in 2.10, and from the bidirectional isolated dc/dc converter illustrated by the light blue converter in 2.10. With the PCS there will also be some miscellaneous costs

(Misc) involved, these costs are linked to the size of the PCS system. The range of costs the PCS, Misc and the DC/DC converter are €184-€329/kW, €75-€115/kW[44][15] and €69-€130/kW[17][18]. This means a system with large grid power and a small battery will have higher PCS and Misc costs but lower DC/DC costs. Vice versa a system with a smaller grid power and a larger battery will have lower PCS and Misc costs but higher costs for the DC/DC converter.

Table 4.5: Marginal costs of power electronic components and related costs

	PCS(€/kW)	MISC(€/kW)	DC/DC(€/kW)
Cost range	184-239	75-115	69-130
Cost mean estimate	211	95	100
Total cost	€306/kW		€100/kW

4.7. Electricity Cost

As discussed earlier the electricity cost is determined by consumed energy and the network operator cost. To calculate the energy cost the power drawn from the grid at a specific time step is divided 6 by to obtain the amount of consumed energy in kWh. This energy is then multiplied by the price in EUR/MWh from that specific timestep. This is done for both a winter month and a summer month. Both monthly total cost is multiplied by 6 to obtain the yearly (12-month) cost of energy. To calculate the baseline cost the same method is used however and the consumed energy from the grid at a specific timepoint is equal to the demand at that specific time point. The hourly tariffs are obtained from Entsoe a transparency platform that provides data for Electricity generation, transportation, and consumption for the European market. From there the historic day ahead hourly tariffs for January and July 2023 have been extracted.

The network operator cost calculation is a bit more complicated. A lot of different components determine both monthly and yearly costs. For the comparison, the total yearly costs are calculated. Since different network operators have different tariffs and structures it is chosen that in this research the tariffs of the network operator stedin from 2023 are used. This is mainly because this is the network operator in the same area as the Fastned stations that have been used for the demand modeling. It is also the network operator in Delft the city where this research has been conducted. The following section will discuss the structure and tariffs of the billing when stedin is used as a network operator. It must be noted that although the network operator costs for different companies in the Netherlands are different than the do share a lot of similarity

4.7.1. Stedin Network Operator Cost

The first part of the operator cost is one time costs. These are the costs that have to be paid when someone wants to get their grid connection for the first time. Based on the power that is requested the price changes. When no battery is present a 3500 kVA connection is necessary to ensure demand. This requires an initial investment of nearly a quarter million euros. When the grid power can be reduced to 1000-1750 kVA the price drops to around 75.000 euros and from 650-1000 kVA the price drops again to 25.000 euros. The full range of costs can be seen in the figure below. A lower initial investment for the grid connection frees up funds for the initial investment for the battery system.

The next part of the costs are cost to maintain the infrastructure on a yearly basis. A set yearly fee is paid to maintain the infrastructure. These costs also increase as the amount of the power infrastructure increases. But these costs are minimal compared to the costs covered in the first part and the next. Nevertheless, they have to be included

The third en last part of the cost are the costs of actual power consumption. The transport fee for large consumers consists of a fixed and a variable part (table 3). The fixed part is the transport-independent rate (fixed charge). The variable part consists of the transport-dependent rate - dependent on the contracted transport capacity and the actual maximum power consumed - and a part that is dependent on the consumption. The contracted transport capacity is the maximum power that you expect to need at any point in the year. You also pay for any additional reactive consumption This last part of the reactive consumption is not considered in this research.

Table 4.6: one-time connection fee [19].

Connection capacity	Costs (€ excl. BTW)	
	Connection fee/connection	Length rate/meter
> 3 x 80A - 3 x 125A	5.296	81
> 3 x 125A - 175 kVA	6.528	85
> 175 kVA - 630 kVA MV with LV-measurement	25.059	152
> 630 kVA - 1.000 kVA MV with LV-measurement	26.929	156
> 1.000 kVA - 1.750 kVA MV with MV-measurement	75.470	302
> 1.750 kVA - 5.000 kVA	245.224	381
> 5.000 kVA - 10.000 kVA	328.114	429
> 10.000 kVA	Connection fee based on precalculated project costs	

Table 4.7: Connection fee [19].

Connection capacity	Description	Costs (€ excl. BTW)	
		per year	per month
	LS5	56	5
> 3 x 80A - 175 kVA	Trafo MV/LV	122	10
> 175 kVA - 1.750 kVA	MV-distribution	1,092	91
> 1.750 kVA - 5.000 kVA	Trafo HV+TV/MV	2,650	221
> 5.000 kVA - 10.000 kVA	Trafo HV+TV/MV	13,099	1,092
> 10.000 kVA	TV	custom	custom

Table 4.8: Variable tariffs (Stedin 2023) [19].

Transport Category	Range Contract	Standing Charge	Tariffs	
			contract	Max
		(€/month)	(€/month/kW)	(€/month/kW)
LV	t/m 50 kW	1.50	1.18	-
Trafo MV/LV	51 t/m 150 kW	36.75	3.17	2.43
MV	151 t/m 1.500 kW	36.75	1.61	2.43
Trafo HV+IV/MV reserve	> 1.500 kW	230.00	1.52	1.41
Trafo HS+IV/MV	> 1.500 kW	230.00	3.05	4.06
IV reserve	> 1.500 kW	230.00	1.47	1.39
IV	> 1.500 kW	230.00	2.94	4.02

Since this research is interested in an active MV grid connection it must be noted that the tariffs used for either a reserve connection or an intermediate voltage (IV) connection are not considered in the cost calculations regardless of the size of the grid connection.

4.7.2. Operational Cost Calculation

To obtain the final cost the energy expense and the network operator expenses are combined. This is done for every possible configuration of the battery and gird power combination which produces a viable solution. The price is calculated on a monthly bases for both a summer(July 2023) and a winter (January 2023) price profile. The consumed grid power at a specific time point is multiplied the corresponding price at that time point. This will calculate the energy cost of that configuration. The network operator cost for a specific combination of battery and grip power is based on the grid power. As discussed earlier the network operator cost consists of 3 parts. However only the costs described in Table 4.7 and Table 4.8 will account for costs on a monthly bases. In contrast the costs described

in Table 4.6 represent one-time cost and are harder to incorporate in comparing monthly/yearly costs of a system with or without a BESS. Therefore the cost described in Table 4.6 will be incorporated in the payback time of the battery. This will be discussed in the next subsection. The cost reduction for both months will be evaluated and the average cost reduction of both will be considered as an average month. The following formulas have been used to calculate the operational costs.

$$CostEnergy\,\text{month} = \Sigma(Pg(t) * Price(t)) \tag{4.23}$$

$$\begin{aligned} CostStedin\,\text{month} = C.n.o.2.2(Pgmax) + C.n.o.3.1(Pgmax) \\ +C.n.o.3.2(Pgmax) * Pgmax + C.n.o.3.3(Pgmax) * max(Pg(t)) \end{aligned} \tag{4.24}$$

$$\text{Total Cost month} = CostStedin\,\text{month} + CostEnergy\,\text{month} \tag{4.25}$$

$$\text{Total Cost year} = 6 * \text{Total Cost month summer} + 6 * \text{Total Cost month winter} + Qbat * OM \tag{4.26}$$

$$\begin{aligned} Pgmax &= 0, 100, \dots, 3500 \\ t &= 1, 2, \dots, 4320 \end{aligned} \tag{4.27}$$

The C.n.o.x.y describe the Cost of network operator, x describes the table number for NO cost, 1 means Table 4.6,2 means Table 4.7 and 3 means Table 4.8. While the y value described the column in that given table, assuming the columns contains a tariff. The cost per month will be multiplied by 6 for both the winter and summer pricing, together combined these will form the yearly operational cost of the UFCS

4.8. Payback Period

The payback time of the battery is calculated by dividing the reduction in yearly operational compared to the system with no battery system, by the difference in capital investment costs CIC from the system with no battery and the system with a battery. The formula is used to calculate the payback time in years. The total cost per year is calculated as described in the last section. To comprehend the way the CIC is calculated exactly will be discussed later this section.

$$\textit{Payback period} = \frac{\textit{CIC with BESS} - \textit{CIC no BESS}}{\textit{Total cost year no BESS} - \textit{Total cost year with BESS}} \tag{4.28}$$

4.8.1. Capital Investment Costs

The CIC comprises of two main contributors. Battery related capital investment costs and grid related initial investment costs. The battery related CIC comprise of the COC, the C&C and the cost of the bidirectional DC/DC converter. The larger the battery system the larger the battery the larger the CIC. The grid related CIC is comprised of the PCS, MISC and the network operator initial connection fee, C.n.o.1. It must be noted that when a battery is integrated into an existing DC UFCS to reduce the size of the grid connection it can be expected that the CIC from the grid side have already been done, meaning that only the battery is responsible for the CIC.

$$\text{C. I. C.} = Qbat(kWh) * (COC + C\&C + DC/DC) + Pgmax * (PCS + Misc + C.n.o.1.1) \tag{4.29}$$

4.9. Evaluation Metrics

Evaluation metrics serve as critical tools to assess the performance and effectiveness of an implemented solution, offering quantitative insight into whether the solution achieves the intended objective. In the realm of Battery Energy Storage System (BESS) sizing and deployment for an UFCS, evaluation

metrics are employed to discern the efficacy of the BESS in cost and demand tariff reduction, and in meeting the UFCS energy demand.

A primary evaluation metric in this context is **Energy costs Savings**. This metric quantifies the reduction in the electricity bill as a result of the BESS implementation with the optimized deployement. The average cost per kWh is a good metric to see the effectiveness of sizing and deployment of the battery to exploit the volatility in the day ahead market. The lower the average cost per kWh the better the system performs. Closely related to the Total Cost Savings is the **Demand Charge Reduction**. This metric specifically focuses on the reduction of NO costs, a fee based on the peak power demand from the grid. As demand charges often constitute a significant part of the electricity bill, a BESS deployment that significantly lowers the demand charge demonstrates efficient usage of stored energy and load shifting. When combining these two metric the total cost reduction of the system can be found. Since an optimal sizing for the energy cost might not be the optimal size for the demand charge reduction. This way a global optimum can be found

Inversely to the operational cost reduction there the capital investment costs. The capital investment costs combined with the operational cost reduction will determine the payback time of the integrated battery system. The payback time is a much more complete metric when assessing the economic possibilities of the integration of a BESS. The lower the payback time the better the marginal performance of the initial investment. Although this metric is more complete it will not provide the full results. Additionally, **BESS Lifetime** provides an estimate of the expected operating life of the BESS. This is a key consideration as a longer lifetime can offset the high initial costs of the BESS over a longer period, resulting in a longer post-payback period and higher total savings over the lifetime of the system.

The next metric measures how large the size of the grid is. Apart from an economical purpose, it serves a public purpose by reducing the size of the grid power, therefore helping relieve the Dutch energy infrastructure from its congestion problems. Apart from net cost reduction another evaluation metric is the Peak to Average Ratio (PAR). This number describes the average power consumed from the grid with the maximum power drawn from the grid. The smaller this number the more efficient the grid power infrastructure is utilized. This means the maximum grid power is a lot smaller leading to a higher likelihood of obtaining a sufficiently large grid power connection. A lower peak-to-average ratio in an electricity grid indicates that the electricity demand is more uniform over time, avoiding sudden spikes. This consistent demand facilitates smoother operations, as power plants can operate at optimal levels without frequently ramping up or down, which can be resource-intensive and wear down equipment. Moreover, it reduces the necessity for substantial investments in peak power generation capacities, which may only be used infrequently, thus optimizing infrastructure costs. Lastly, a steadier demand can aid in the integration of renewable energy sources, which can sometimes be variable, into the grid by reducing the complexity of managing supply and demand fluctuations.

In essence, these evaluation metrics provide a comprehensive and multi-faceted assessment of the BESS configuration, considering not only the immediate cost-effectiveness but also the operational efficiency and long-term viability. Such a holistic evaluation is critical in guiding optimization efforts and decision-making processes in the deployment and sizing of BESS for UFC stations.

4.10. Sensitivity Analysis

First of all the UFCS is tested to handle the randomness and characteristics of power demand for such an UFCS. Which is both based on real life data as well as literature. This way it can be confirmed that the system can operate under a wide variety of situations. It must also be able to fulfill maximal power demand if necessary meaning that the total power that can be provided is as large as the total power that can be demanded of 10X350 kW=3500kW.

The prices of the day ahead market have been taken of a 30 day period, both in winter and in summer, showing wether the optimization is effective under different pricing conditions. The prices have also been taken without taxes giving a more reliable outcome on the performance regarding cost reduction. Taxes are not consistent for every consumer and will cloud the effect of the optimization method. Network operator costs have also been derived from real life tariffs ensuring a high reliability of the results but will also make them less representative for assessing the performance of other markets. However the optimasztion method can be used anywhere as long as the prices are updated.

The empircal model of the UFCS which only expresses the battery as a stored amount of energy is tested against a tested mathematical model that much better incorporates the working principles and

characteristics of a battery. This way it can be tested wether the results from optimal battery deployment can actually be done by a battery.

Batteries, especially lithium-ion types, are greatly affected by temperature extremes. High temperatures can accelerate chemical reactions within the battery, initially enhancing performance but leading to faster degradation and safety issues like thermal runaway, where the battery can overheat and potentially fail or explode. Conversely, low temperatures reduce battery performance by slowing down charge transfer reactions, resulting in longer charging times, decreased discharge capacity, and reduced lifespan, particularly in electric vehicles where cold weather can shorten driving range.

Repeated exposure to extreme temperatures, whether hot or cold, hastens overall battery degradation, emphasizing the importance of temperature management in battery system design and placement. Strategies to mitigate temperature effects include thermal management systems (like active cooling or heating) or insulative enclosures, and designing systems that accommodate local climate patterns and seasonal variations to maximize battery performance and lifespan.

5

Results and Discussion

Given the complexity arising from numerous variables in the results, this chapter will delve into the general effect sizing and deployment have on operational cost reduction. Afterwards, a selection of promising scenarios will be evaluated. These scenarios are formulated based on the guidelines and assumptions defined in the preceding chapters. The results will commence by examining the outcomes of the demand profile model, ensuring its alignment with empirical data and existing literature. Subsequently, the calculated costs of the UFCSin the absence of an integrated BESS with and without a dynamic price contract will be examined. Thereafter, the optimization process will be assessed, pinpointing configurations of grid and battery power that yield the most significant cost savings. Finally, by evaluating the lifetime and payback duration of this optimal configuration, the net cost benefits of integrating a BESS can be discerned. Finally when the optimal configuration is found this configuration will be explored in a case study, examining why this configuration is as effective as it is.

5.1. UFC Demand Profile

This section presents the outcomes of the demand profile analysis. The model's utilization percentages are compared with findings from the FastNEd data and existing literature. The analysis is segmented into daily and weekly time-frames, as these periods most effectively capture the expected patterns. Subsequent to this comparison, the actual power demand over a 30-day period, expressed in kW, is detailed. This quantified demand serves as the basis for the optimization of the system.

5.1.1. Utilization Percentage

The figures provided in this section offer a detailed view of the average utilization percentage on an hourly basis, differentiated for weekdays and weekends. The average is derived from data aggregated from five distinct FastNEd stations located in rural areas, each equipped with 9 to 12 charging points and offering charging capacities of 350, 175, and 50 kW. The specific stations analyzed include Hoogendoorn, Knorrestein, Elstgeest, Maatveld, and de Vink. Examination of Figure 5.1 indicates a utilization percentage peak around midday for a weekday, with a maximum value of up to 50%, consistent with literature findings. In contrast, Figure 5.1 also reveals that the peak during weekends materializes later, specifically around 5 pm. This observation aligns with the previous literature findings as well, with the occupation peak standing at 35%. When evaluating weekdays against weekends, occupation levels tend to be lower during weekends. Which was expected for UFCS in rural areas. However, it's essential to note that high occupation levels do not directly translate to elevated demand levels. While high occupation can be indicative of demand, situations can arise where many vehicles are present but predominantly utilize slower charging speeds, potentially shifting the actual demand peak.

Model outcome: Upon comparison of the anticipated data with the generated demand profile using the model described in Chapter 4, several correspondences are evident. The presented figures, which present the outcome of the power demand model, depict the count of vehicles at specific time intervals in blue, while the red trend line represents the average utilization percentage over time. Notably, in Figure 5.2 a, the timing and amplitude of peaks align with those in Figure 5.1. This includes the pronounced midday peak as well as the subtler peaks observed early in the morning and late in the

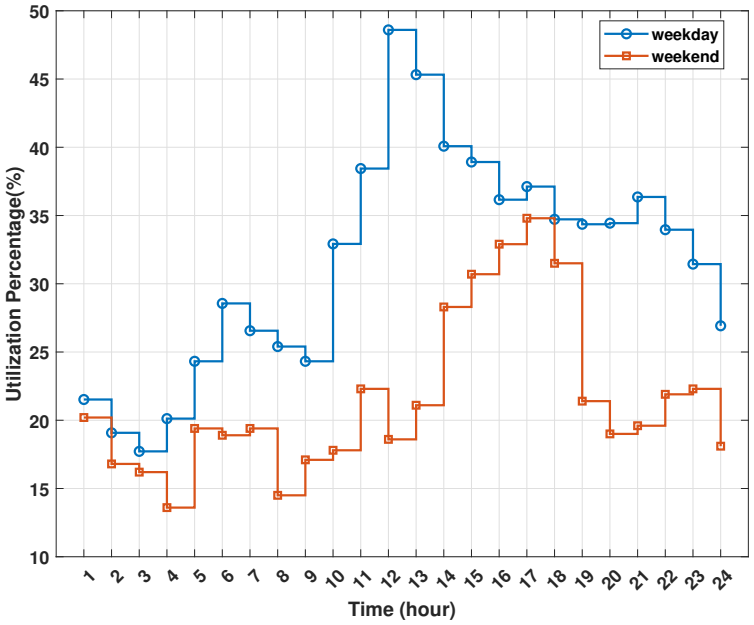

Figure 5.1: Data based: average utilization percentage of a UFCS on an hourly basis.

evening. However, it's pivotal to note that the peak in power demand might not necessarily coincide with the peak in occupation. Given the model's structure, each vehicle present has an equal likelihood of selecting any of the three charging speeds. Consequently, vehicles with slower charging speeds would necessitate a longer charging duration. Parallel observations can be drawn between Figure 5.2 a b and Figure 5.1. Here, the utilization peak manifests in the afternoon, reaching a maximum occupation of 35%. It's pertinent to mention that these outcomes can exhibit day-to-day variations. To incorporate a semblance of randomness and unpredictability, the average utilization percentage is computed over a span of 12 hours, rather than hourly, as was explained in the previous chapter.

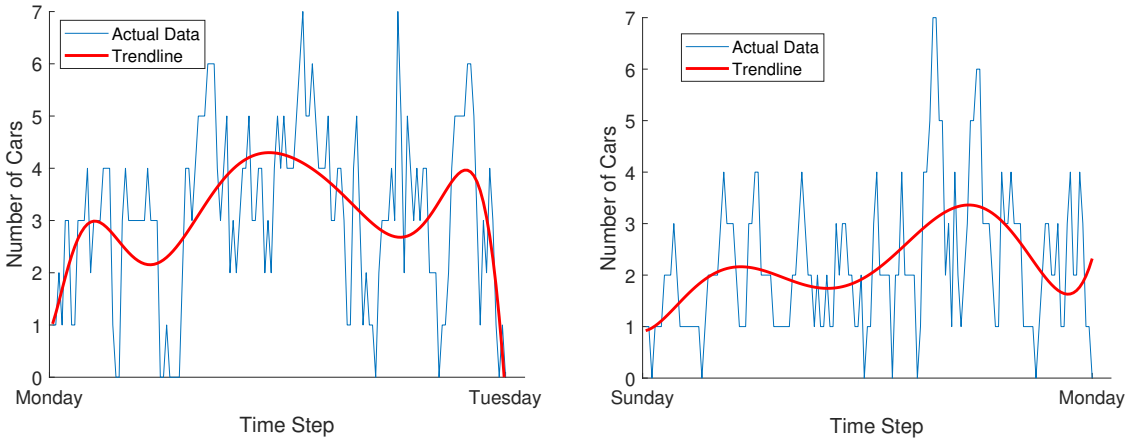

(a) During weekdays

(b) On weekend

Figure 5.2: Model-based: Number of cars present overtime at the UFCS

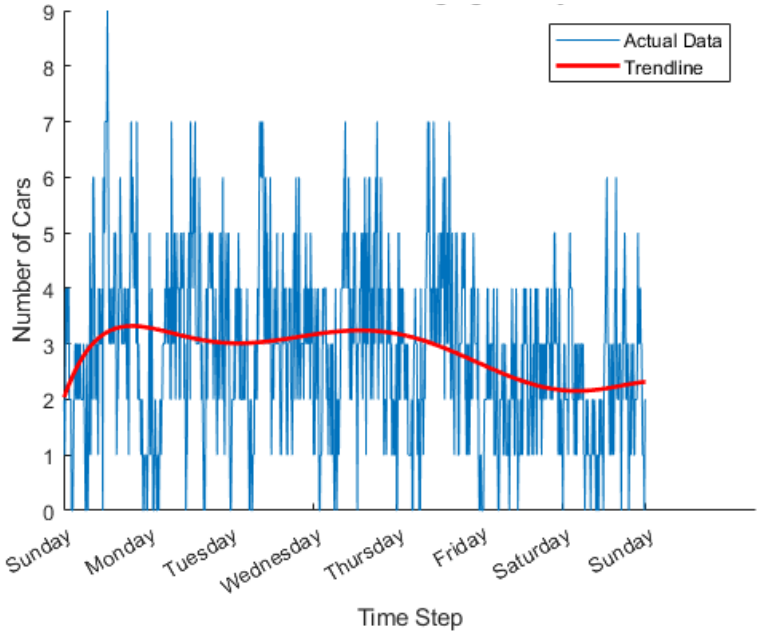

Figure 5.3: Model-based: the number of cars present overtime at the UFCS during the week from model

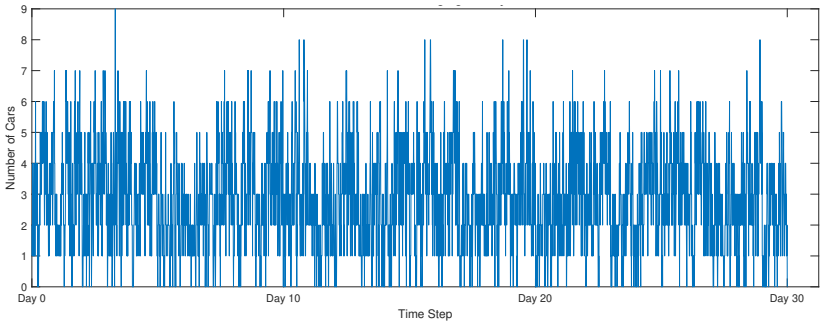

Figure 5.4: Model-based: amount of cars present overtime at the UFCS during a 30-day period

Extending the analysis to a weekly trend, an observable decline in average occupation during weekends versus weekdays can be seen in Figure 5.3. The data from the specific week under consideration reveals that at no point were more than 9 vehicles present simultaneously. A broader perspective is provided by Figure 5.4, which displays the total count of vehicles present at any given juncture over the 30-day period. Interestingly, there wasn't a single instance where more than 9 electric EV's were charging concurrently. The occurrence of 9 vehicles was an isolated event, 8 vehicles were seen approximately twice weekly, and the monthly average tallied to roughly 3 vehicles charging simultaneously.

5.1.2. Power Demand Evaluation

The power demand for the UFCS is derived from a two-pronged approach. Initially, it's contingent on the charging capacity of an individual EV, which can span across three levels: 350 kW, 175 kW, or 50 kW. Subsequently, the cumulative power demand is influenced by the number of EV's present at that instance. This figure factors in both the EV's arrival times and the charging duration, which is inherently dependent on the charging speed. This subsection will combine the utilization percentage approach with the characteristics of DC fast charging to determine the power demand profile of the UFCS.

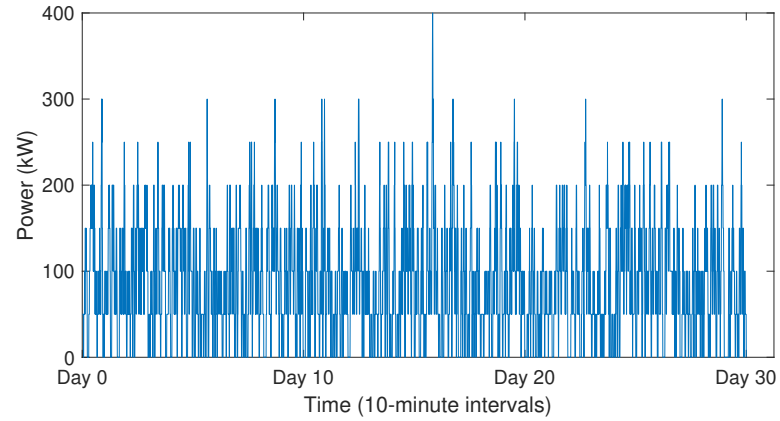

(a) Charging at 50 kW

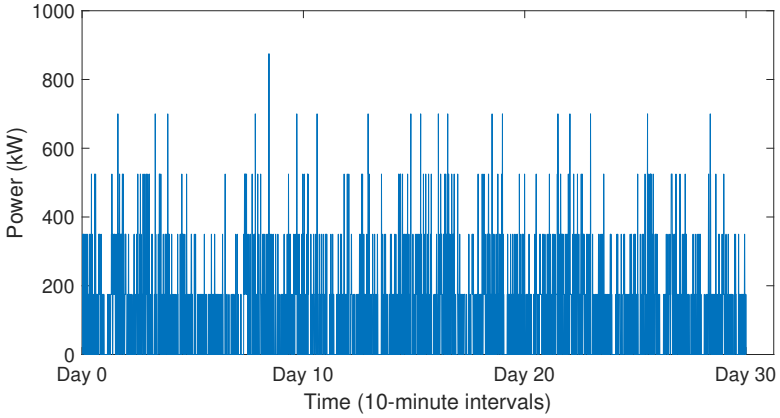

(b) Charging at 175 kW

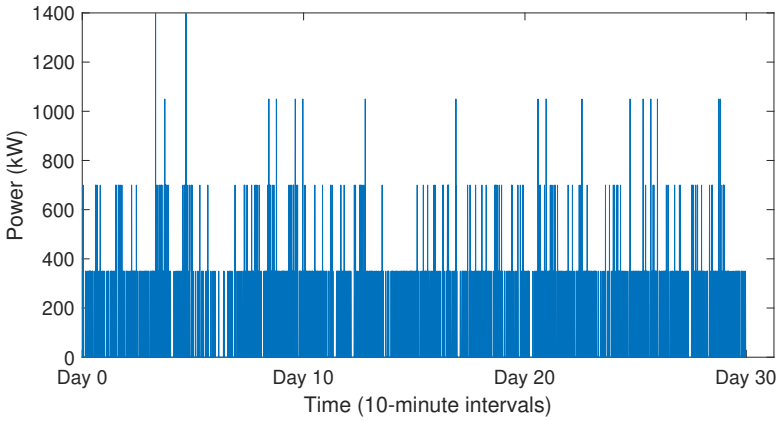

(c) Charging at 350 kW

Figure 5.5: Model based: Number of cars at specific charging speed at the UFCS over a 30-day period

It's imperative to consider that despite the outcomes of the demand model, there remains a remote possibility of an occasion where every available charging slot is occupied simultaneously by vehicles capable of charging at 350 kW. This scenario culminates in a peak power demand of 3500 kW. Ensuring that the UFCS is equipped to manage such worst-case scenarios is paramount; thus, this will be posited as the benchmark power rating.
The ensuing illustrations provide a graphical representation of power demand dynamics. Figure 5.5 describes the power demand specific to each charging speed. The power demand at each given time instance divided by the demand per car will give the number of cars at any given time instance charging at that specific speed.

In contrast, Figure 5.6 encapsulates the cumulative power demand of the UFCS over a span of 30 days. This is a combination of the power demand of all individual charging speeds and is the demand profile which the system will be optimized for.

Delving deeper into the 50 kW charging speed, it might intuitively seem to command the least power demand, given its lower charging capacity. However, the frequency of vehicles employing this speed is notably high. This isn't necessarily indicative of a preference for this speed but rather a byproduct of the longer charging duration it mandates. This extended duration translates to a higher occupancy of charging slots over time. As exemplified in Figure 5.5 (a), there's a particular instance around the 16th day where the power demand peaks at 400 kW. This surge, although seemingly modest, represents eight vehicles charging concurrently at 50 kW. For the remainder of the month, the demand for this charging speed never exceeds 300 kW. On average, the power consumed by vehicles operating at the 50 kW speed is 90 kW. This suggests that, on average, the UFCS accommodates nearly two vehicles charging at 50 kW concurrently.

The power demand dynamics of the 175 kW charging speeds are elucidated in Figure 5.5 (b). Given the intermediate magnitude of this charging speed, it stands between the 50 kW and 350 kW speeds in terms of power demand implications. As anticipated, fewer vehicles utilizing the 175 kW chargers generate a heightened power demand compared to their 50 kW counterparts. This expectation is manifested when a concurrent charging session involving five vehicles results in a peak power demand of 875 kW. Analyzing this further, on an average basis, vehicles employing the 175 kW charging speed are found to consume 125 kW. This observation reiterates the significant influence of the charging speed on the overall power dynamics at the charging station.

The power dynamics associated with the 350 kW charging speeds are illustrated in Figure 5.5 (c). Given the substantial charging capacity of this speed, it's anticipated that a fewer number of vehicles will be responsible for a notable power demand. This anticipation is validated when we observe that a peak power demand of 1400 kW arises from the concurrent charging of merely four vehicles. It's evident from this observation that vehicles employing the 350 kW chargers exert the most significant influence on the requisite power availability. On an average basis, EVs leveraging the 350 kW charging speed consume 118 kW.

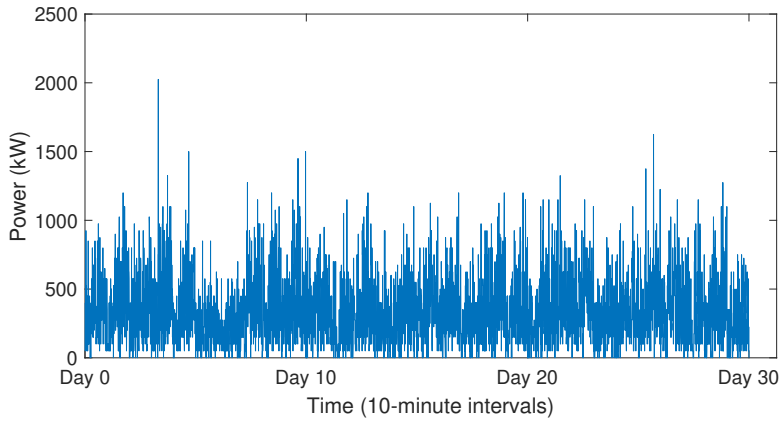

Figure 5.6: Total demand of the UFCS over a 30-day period

The comprehensive power demand over time is portrayed in Figure 5.6. This figure represents the aggregated demand across all charging speeds. It's crucial to underscore the significance of this collective demand: it dictates both the power and energy consumption, thereby influencing the strategic decisions regarding the scheduling and dimensioning of the Battery Energy Storage System (BESS) and grid power.

A notable observation from this figure is the peak power demand, which touches 2025 kW. Which is much lower than the maximum possible power demand of 3500 kW. Interestingly, this surge corresponds with the moment of maximum vehicular presence at the charging station, which is 9. This is the first indicator of the unlikelyness of maximum power demand. The chances of every charging spot being occupied at the same are quite small. Combined with the fact that there is a 1 in 3 chance that the car charging is at 350 kW the possibility of maximum possible power demand is small, but not impossible. Therefore to ensure that the station is prepared for a maximum possible power demand the combined power of the grid and battery is desired to be 3500 kW. The station's average power consumption stands at 333 kW. However due to the nature of day-ahead prices, where prices become available 24 hours upfront, the minimum grid size should be the maximum average power on a single day over a 30-day period. Which is 416 kW and occurs on the 4^{th} day.

Both these figures carry paramount importance for the UFCS's operational strategy. As the grid represents the exclusive source of energy consumption, its power capacity should not be inferior to the maximum average power demand for a 24-hour period. However, it should also be noted that the grid power in practice will be higher than the average consumed power due to losses in the conversion steps. When taking into account the efficiencies of the BESS and PCS as described in previous section the minimum size of the grid must 485 kW to ensure that the UFCS is able to provide for every single scenario. Due to the stepsize determined for the grid searching optimization the minimum gridd power isrouned of to 500 kW. Expanding this analysis over broader time frames, the UFCS's monthly and annual energy demands are computed to be 234 MWh and 2808 MWh, respectively.

5.1.3. Implications of Dynamic Pricing Strategy

The potential advantages and challenges of implementing dynamic pricing for a UFCS with a demand profile as depicted in Figure 5.6 are thoroughly examined. This assessment compares a consistent tariff of €0.156/kWh with a variable pricing strategy to determine which approach is more effective in reducing energy expenditure. Using the methodologies outlined in Section 4.7, the operational expenditure for the base scenario without a battery was calculated. To accommodate the simultaneous charging of 10 vehicles at 350 kW without the aid of a BESS, a grid capacity of 3.5 MW is required. This grid requirement remains constant across both contract types, ensuring consistent network operator costs. However, differences emerge when evaluating the energy consumption costs under these two pricing models. The variable pricing trends for winter and summer periods are presented in Figure 5.7.

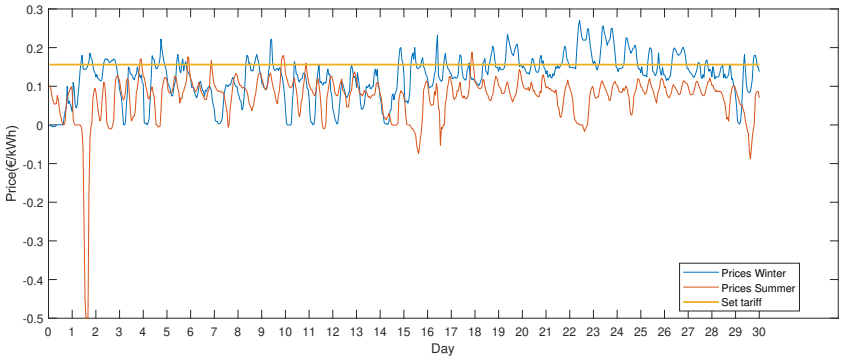

Figure 5.7: Winter and summer dynamic prices with a set tariff

The summer prices are based on the Day Ahead prices in the Netherlands of July 2023, and the winter prices are based on the Day Ahead prices in the Netherlands from January 2023. All prices were extracted from the EPEX spot market through the Entsoe transparency platform, which provides Central collection and publication of electricity generation, transportation, and consumption data and information for the pan-European market. A notable observation is a discrepancy in prices between summer with an average (€0.07/kWh) and winter with an average of (€0.13/kWh). The overall average cost is €0.10/kWh, which is considerably lower than the fixed tariff of (€0.156/kWh). However, sporadic peaks in price, which can reach up to €0.30/kWh, may increase costs if they align with peak

demand periods. The annual operational costs, divided into network operator fees and seasonal energy charges, are detailed in Figure 5.8. By introducing the dynamic prices the yearly operational costs have decreased by 24% from 706.000 to 535.000 euros. The reduction in costs for energy are solely responsible for these yearly operational cost reduction with a decrease of 36% going from 472.000 to 301.000 euros annually. This underscores the potential financial benefits of dynamic pricing for UFCS.

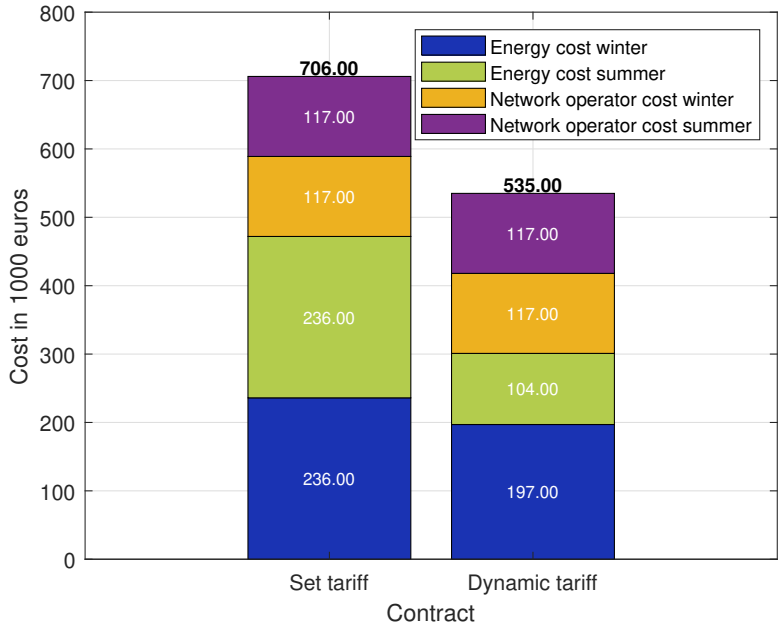

Figure 5.8: Price differences between set and variables tariffs

The alignment of the UFCS's demand profile with the periods of lower costs in the dynamic pricing model contributes to these savings. The UFCS experiences peak demand around midday, which often aligns with lower prices in the dynamic pricing model. With the increasing integration of renewable energy, particularly solar, there's an abundance of energy during midday, leading to reduced prices. Conversely, during the early mornings and evenings, when nation wide power demand increases, prices tend to rise. However, changes in either the time of peak demand or cost will expose the system's vulnerability to high and uncontrollable energy expenses. The incorporation of a battery system might offer further reductions in energy costs and will increase redundancy to shifts in demand and prices. The implementation of a battery will also lead to savings in network operator fees, due to lower possible grid power. The implications of such a battery integration will be discussed in the subsequent section.

5.1.4. Optimization Performance Assessment

To gain insights into the efficacy of the optimization technique, various graphical representations were developed to examine the impact of alterations in grid power and battery size on the overall costs, spanning both network operator expenses and energy consumption fees. The ultimate objective is to maximize cost savings over the battery's operational life. The figures in this section present all feasible solutions within the search space of this research. Configurations with larger combinations than presented in this section are deemed unnecessarily and ineffectively large, or too small and incapable of fulfilling the power demand. Each point in the figure represents a global optimum for that specific configuration. By combining all these points the grid is formed. By visual interpretation, the combined optimum of both the linear programming and grid searching optimization methods can be identified.

Figure 5.9 (a) depicts the minimized annual energy expenditure across numerous grid power and battery capacity configurations. Unsurprisingly, the total expenditure on energy consumption is predominantly influenced by battery capacity. As the battery's size increases, the energy costs tend to decrease. This decrease can be attributed to the battery's ability to purchase energy at a reduced price and use it at a premium price point. Additionally, a higher grid power availability marginally re-

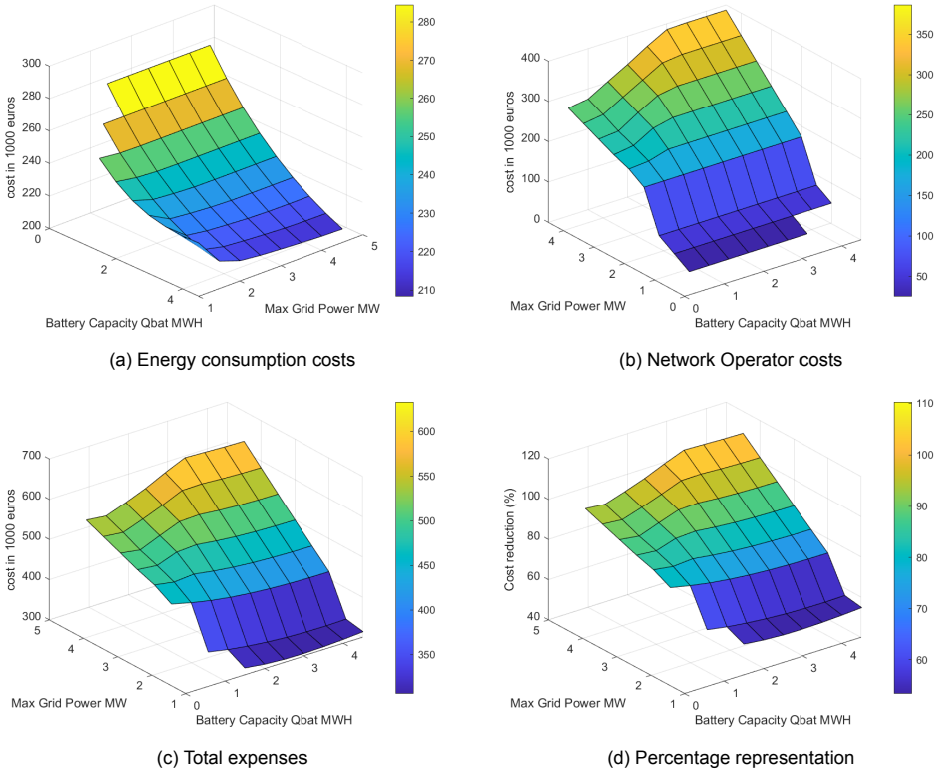

(a) Energy consumption costs

(b) Network Operator costs

(c) Total expenses

(d) Percentage representation

Figure 5.9: Per annum expenses of grid and BESS various configurations

duces energy costs. If the battery's capacity significantly surpasses the grid power, the limited power available for battery charging might restrict the acquisition of economical power.

In contrast, Figure 5.9 (b) displays the minimized costs associated with the network operator. Here, the costs are primarily driven by the grid power capacity; greater grid power directly correlates to increased network operator expenses. The role of the battery in influencing these costs is multifaceted. While the battery can curtail peak grid power usage during specific months by discharging during high-demand, high-price intervals, it might also augment grid power usage if low-demand and low-pricing coincide, prompting battery charging.

To optimize costs, a balance between battery sizing and grid power must be struck. This can be done by combining the results of Figure 5.9 (a) and Figure 5.9 (b). Since energy costs are not as much affected positively by lower grid power as no costs are affected negatively it can be expected that a combination of low grid power and high battery capacity will lead to the greatest recursion in costs. Figure 5.9 (c) confirms this expectation.As shown in Figure 5.9 (c), combining a 1 MW grid connection with a 2.5 MWh battery results in the most substantial cost reduction, with approximately 307.000 euros of yearly operational expenses. Much lower then the 535.000 found in the last section. The results from Figure 5.9 (c) can also been seen in Table 5.1. Here it can be seen that the optimal solution is either one of the options with a grid connection of 1000 kW and a battery of 2500,3000 or 3500 kWh. Decreasing the grid size further then 1000 kW will yielad infeasable solutions (Inf) and due to increased OM costs increasing the battery above 3500 kWh will increase yearly operational costs. The table also highlights the configurations that have the same power rating as the original system, a combined power rating of 3500 kW.

Figure 5.9 (d) further illuminates the cost benefits of specific configurations, expressing the costs as a percentage of scenarios without BESS integration. The lower the percentage in Figure 5.9 (d) the better the system performs in decreasing costs. Notably, maintaining grid power below 1.75 MVA is pivotal to network operator cost reduction. This is not only due to reducing the absolute of grid power but reducing the marginal cost per power unit as well.

However, larger batteries introduce additional complexities. Naturally larger systems, both on the grid and on the battery side, will introduce larger investment costs. The payback period of the battery therefore needs to be known before an optimal solution can be chosen. The payback period is determined by subtracting the capital cost of a system with a battery from the cost of a system without a battery and subsequently dividing the remainder by the cost reduction per year for that configuration. It's pertinent to highlight that configurations with either a small grid or battery allow for larger sizes in the counterpart, resulting in shorter payback periods.

Table 5.1: Yearly operational cost (€1k) per configuration

Battery Capacity (kWh) \Grid Power (kW)	500	1000	1500	2000	2500	3000	3500	4000
500	Inf	Inf	Inf	461	486	**501**	519	538
1000	Inf	Inf	349	449	**478**	496	512	532
1500	Inf	317	340	**439**	482	514	532	550
2000	Inf	311	**333**	431	474	517	551	569
2500	Inf	**307**	327	426	468	510	553	590
3000	Inf	307	323	422	463	506	548	591
3500	Inf	307	321	419	461	503	545	587
4000	Inf	310	321	417	459	501	543	585
4500	Inf	313	322	417	458	500	542	584

While these graphical analyses provide valuable insights into understanding why certain configurations excel in minimizing operational expenses, they don't definitively pinpoint which setup offers the most significant cost savings over the system's entire lifespan. It will also not filter out configurations that don't meet other conditions than the ability to fulfill power demand. Consequently, a selection of promising configurations, based on the above findings, was further evaluated to determine long-term performance by calculating the battery lifetime.

5.2. Potential optimal solution selection

Based on the results found in the previous section a selection of potential optimal solutions have been chosen. To fairly compare the situation with no BESS it is chosen that the total power of the system must be equal to the power in the system with no BESS. Therefore 4 different configurations with a battery have been chosen to compare to the starting situation. All 4 options have the same combined power rating of 3.5 MW. As can be seen in Figure 5.10 (a) the combinations range from a 0.5 MWh battery and a 3 MW grid connection to a 2.5 MWh battery with a 1 MW grid connection. A combination with a 500 kW grid connection and a 3 MW battery was found to be infeasible. Combinations with grid powers as low as 600 kW have been found feasible. Still, they will not provide significantly better results than the 1000 kW configurations and are considered outside the step-size chosen to evaluate possible configurations. Designing on the edge of what is possible will also limit the possible growth of the UFCS and make the system vulnerable to failure or unnecessary expenses when a larger average energy demand occurs than expected. These combinations will be compared using several metrics, cost reduction, payback time, and lifetime. Since summer and winter pricing lead to different decisions in the optimization, their effect will be analyzed separately.

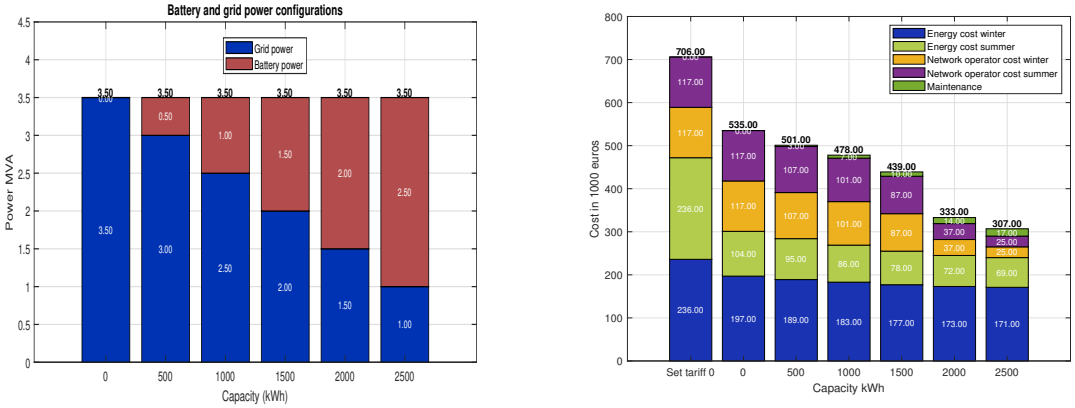

(a) Grid and BESS capacities

(b) Yearly Operational expenses

Figure 5.10: Various combinations of demand sharing among grid and BESS and corresponding operational expanses of a UFCS.

The first and most important metric is total yearly costs. In Figure 5.10 (b) the yearly cost for the situation when a conventional set tariff is used and no battery is used. This is also the most expensive option. The next 5 bars represent the 5 combinations from Figure 5.10 (a) with the dynamic tariff with no battery and 4 options with an increasingly larger battery. Immediately, the impressive cost reduction can be seen. As concluded earlier, the demand of UFCS is very suitable for dynamic pricing. Even more impressive are the results in terms of cost reduction when implementing a battery. Increasing the battery capacity and power while decreasing the grid power will consequently reduce the yearly operational costs. The combination found in the last section of 2.5 MWh BESS and 1 MW grid power reduces the cost by 42% compared to dynamic prices without a battery and an astounding 57% when compared to a conventional single tariff contract with no BESS. In the current energy market, this will lead to saving €280k and €399k a year on energy and network operator costs. The total reduction in energy cost for a battery-integrated UFCS compared to a UFCS with no battery and a dynamic contract can be seen in the table below. The cost reduction of the configuration with the smallest battery is only €34k while the cost reduction of the configuration with the biggest battery is €228k reducing the cost In Figure 5.10 (b) it can be observed that the yearly costs have been divided into 4 segments, energy

Table 5.2: Cost reduction per configuration compared to a UFCS with no BESS and dynamic prices

	Grid Power (kW)				
	3000	2500	2000	1500	1000
Cost Reduction (€1K)	34	57	96	205	228
Battery Capacity (kWh)	500	1000	1500	2000	2500

costs for winter and summer pricing, and network operator costs for winter and summer pricing. The network operator costs are not affected by the differences in prices during the year. They are however affected by the peak-to-average ratio.

A high peak-to-average ratio means that the size of the grid is dictated by an outlying peak. This will mean that a battery could substitute this unnecessary large grid power. In Figure 5.11 (a) it can be seen that an increased battery capacity, and therefore a smaller grid power will reduce the PAR. The network operator costs have been reduced from 302.00 euros a year to only 50.000 euros a year, shrinking by 83%. The peak-to-average ratio goes from 10 to 2.6, only 74% lower. This is because below a grid power rating of 1.75 MW the marginal cost per kW is also reduced. Leading to greater cost reduction than reduction in peak to average ratio.

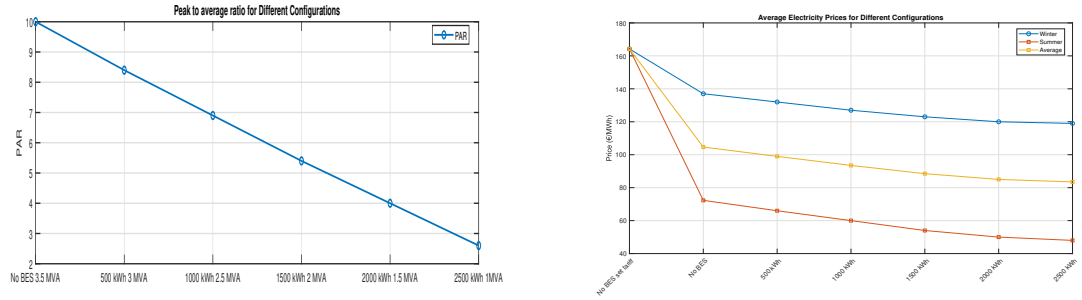

(a) PARs

(b) Electric price in €/MWh

Figure 5.11: PARs and average electric price in €/MWh for different BESS capacities

The performance of the energy cost optimization can be seen in Figure 5.11 (b). This figure shows the average net energy price that is paid per MWH to the UFCS. The average net price incorporates the losses in the system of the power electronic components. Since all system configurations provide the same amount of charged energy a fair comparison can be made. Since the energy costs are dependent on seasonal prices the price per MWh has been shown for both winter, summer, and together they form the yearly average. To the left of the figure, the net price for a regular set tariff contract is shown, €164/MWh. Since this is a set tariff the price does not differ based on the season. When dynamic pricing is implemented the average price drops to €137/MWh in winter and €72/MWh in summer, with a yearly average of €105/MWh. By introducing a battery this price will drop continuously with increasing battery capacity to €119/MWh in winter and €48/MWh, with a yearly average price of €83/MWh. This means that during winter using dynamic pricing the average energy cost is reduced by 16% and introducing a 2.5 MWh battery will reduce this price by another 20% points for a total of 36%. In summer this reduction is even more impressive, introducing dynamic pricing will reduce costs by 56%, and adding a battery will increase this number to a staggering 71%. The overall reduction in energy cost when a battery with dynamic pricing exploitation is introduced is just shy of half with costs reduced by 49% per delivered MWH. It is clear that the optimization method, for both sizing and deployment, is very effective in reducing costs, especially in configurations with large battery capacities and relatively small grid powers. However, from previous chapters, it was also found that larger battery capacities and grid power ratings will increase capital investment costs as well. To see if the increased cost reduction is worth the increased investment costs by choosing larger battery capacities will be examined in the next section. Using the lifetime of the battery and the payback period the overall performance of the system can be determined.

5.3. Lifetime

The lifetime of the battery is dependent on the aging due to calendar life and cycling life. For the calendar life, a standard loss of 1% per year was chosen based on previous literature. Next, the results for aging due to cycling will be presented. Finally, a yearly combined loss in % will be determined. This will be used to determine the lifetime in years until the EOL State of Health (SOH) is reached.

5.3.1. Aging due to cycling

The lifetime of a battery is calculated by the mathematical model in Simulink. The (dis)charge cycle corresponding to the five battery and grid configurations have been run for both the results from summer and winter pricing. In Figure 5.13 (a) the lost capacity per year, due to cycling, for each battery is presented. The red line represents the capacity loss based on the (dis)charge profile of the battery based on 6 months of cycling to exploit summer pricing. The capacity loss increases linearly with increasing battery size up until 2000 kWh and then starts to decrease. The blue line represents the capacity loss based on the (dis)charge profile of the battery based on 6 months of cycling to exploit winter pricing. Again the capacity loss increases linearly but only up to 1500 kWh. A small drop in capacity loss is seen compared to the 2000 kWh battery and a relatively sharp drop is observed for the 2500 kWh battery. The yellow line represents the total yearly capacity loss. This is the capacity loss that will be used to calculate the lifetime of the battery. With a yearly capacity loss of around 6 Ah due to cycling for the 500 kWh battery. Steadily increasing to 20 Ah for the 2500 kWh battery.

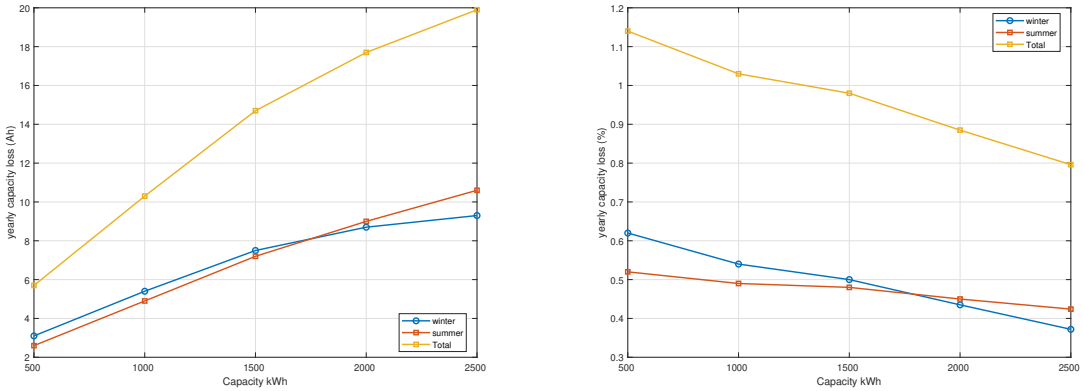

(a) Capacity loss (Ah)

(b) Capacity loss (%)

Figure 5.12: Yearly capacity's loss in terms of Ah and % due to cycling for 6 months summer and 6 months winter based electricity prices.

The loss in capacity in Ah, however, will not give a good estimation of the lifetime of the battery. This is because as the battery becomes larger it can lose more Ah before it reaches EOL SOH. To make an accurate comparison between the configurations the loss of capacity in % of original capacity is determined. The results can be observed in Figure 5.13 (b). The losses are presented again for summer, winter, and yearly total. Immediately it becomes clear that the increase in capacity loss is not as great as the increase in original battery capacity. This leads to a decrease in loss of percentage of total capacity as the battery size increases. From a maximum loss due to cycling of around 1.15% for the configuration with the smallest battery. And a much smaller relative loss of 0.8% percent for the configurations with the largest battery. When combining the results of both calendar and cycling aging the total capacity loss in % per configuration per year can be observed in Figure 5.13 (a). It must be noted that in this figure the losses for winter and summer represent half a year instead of a year, together they add up to the average yearly loss in percentage due to cycling. A steady decline in yearly losses can be observed. From just over 2.13% per year to 1.8% per year.

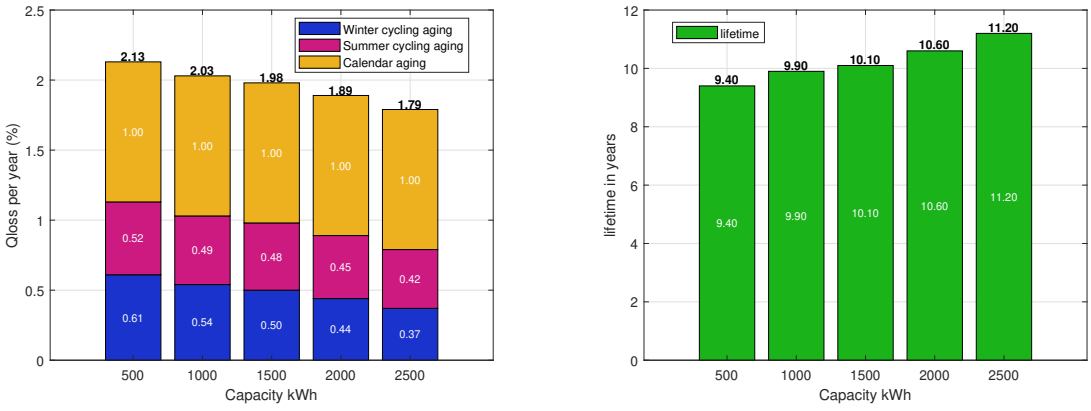

(a) Total capacity loss (%)

(b) Total lifetime (Years)

Figure 5.13: Total capacity loss in percentage per year and corresponding lifetimes of numerous BESS configurations

Using the results of Figure 5.13 (a) with the EOL SOH found earlier, which is 80%, meaning 20% can be lost before EOL is reached, the lifetime in years can be determined. by dividing this 20% by the yearly loss in % per configuration. As expected it can be seen in Figure 5.13 (b) that a steady increase in lifetime as the battery capacity increases, although the difference is limited. With the battery life ranging from 9.4 to 11.2 years the lifetime of the battery system is on the lower end of the expected

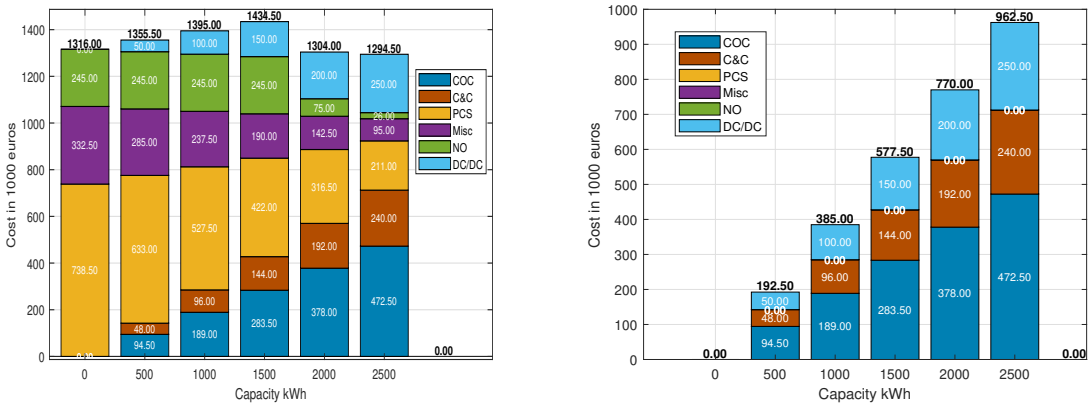

(a) New DC-bus UFCS

(b) Existing DC-bus UFCS

Figure 5.14: Capital investment in 1000 euros for BESS integration into UFCS

10-15 years lifetime found in the literature study. An EOL of 70% of the original capacity would move this to the higher end of the expectations.

5.4. Capital investment costs

The capital investment for battery-integrated UFCS is highly dependent on the situation of the DC bus UFCS. Particularly whether the UFCS is already existing and therefore PCS is already in place and the investor is looking into reducing the grid capacity using a battery, but this will mean that the costs of the original PCS have already been invested. Or if the UFCS has yet to be built which means that the PCS can be designed smaller due to the introduction of a BESS which would reduce investment costs on the grid side of the system. Both new and existing DC UFCS will be examined to see whether introducing a BESS is effective in reducing costs. The system with no BESS is considered the benchmark investment cost.

5.4.1. Capital cost of the integration of a BESS into new DC UFCS

First, the case of newly built DC UFCS will discussed by looking into the capital investment cost to obtain the electrical infrastructure of such a system. In Figure 5.14 (a) the Capital Investment Costs (CIC) for each configuration can be seen. Since capital has to be invested on both the grid and battery side of this UFCS, six parts contribute to the CIC. The initial network operator fee NO, the size of the PCS and the corresponding Miscellaneous (MISC), the rated power of the battery and equally large DC/DC converter and and OM, all decide on the total investment cost of the system. Immediately it can be noticed that the cost for each configuration is quite similar. The cost of systems with small grid power and a large battery even have smaller investment costs than a system with no battery, against all expectations. This is mainly because the size and therefore the cost of the PCS is linked to the grid power and will decrease the total capital investment of the system massively when the grid size is reduced, erasing the extra cost associated with the battery system. The same goes for the initial network operator fee. Since a battery has almost little to no effect on total capital investment it will likely favor a system that can reduce operational cost as much as possible.

5.4.2. Capital Cost of the Integration of a BESS into an existing DC UFCS

It is also interesting to see how the economical case would be for an existing DC UFCS that is looking into investing in a battery system, therefore being able to reduce their grid power capacity. Or they have a small grid power capacity and cannot or are not willing to expand but are looking into expanding the capacity of the UFCS. It is also important to know when the battery from the newly built DC UFCS reaches its EOL if the UFCS will run into high and mandatory investment costs when a new battery system needs to be purchased to ensure the same capacity as the UFCS had before. Since the PCS is expected to last several decades, much longer than the BESS.

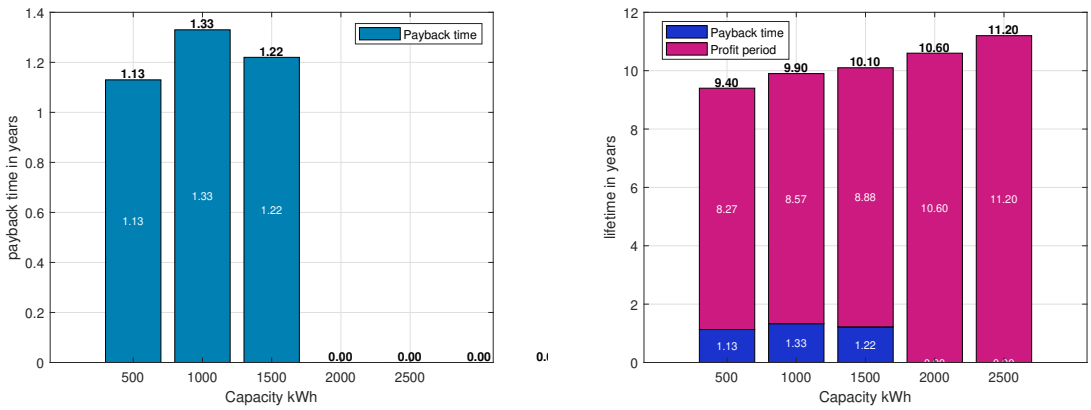

(a) Payback period

(b) Profit period and lifespan

Figure 5.15: Payback period, profit period and lifespan in years for BESS integrated into newly constructed DC-UFCS

In Figure 5.14 b the capital investment per configuration of an already existing DC UFCS is displayed. The results in this figure are drastically different. Since the UFCS already exists, only the battery side of the system will require additional investments. This is because the network operator fee has already been paid for and the same goes for the PCS and MISC costs. Therefore only the battery COC, the C&C and the DC/DC costs are responsible for the capital investment. As a results the configuration with no integrated BESS requires no additional investment while introducing an increasingly large battery will lead to increasingly large CIC. The configuration with the largest battery needs almost a million euros in additional funds. This possibly makes the introduction of a BESS not a wise investment as was found for a new DC UFCS.

5.5. Payback and Profit Period

Using the results from the lifetime, cost reduction and capital investment sections the payback and profit period can be determined. These then will be used to calculate the net yearly operational costs of an UFCS with integrated BESS and whether this is economically interesting. For both new and existing DC UFCS.

5.5.1. Integration of a BESS into new DC UFCS

Because the difference in capital investment cost is minimal and in some cases even negative for battery-integrated systems compared to systems without a battery the payback period is expected to be low. In Figure 5.15 (a) the payback period of all battery integrated systems is shown. The configurations with a battery system between 500-1500 kWh have a payback time of just more than 1 year with the longest payback time for the system with a 1000 kWh battery, having a payback time of 1 year and 4 months. The two largest configurations with a 2000 or 2500 kWh battery have a payback period of 0 years since the capital investment of these systems is lower mainly due to the reduced grid-related investments.

Profit Period: When combining the payback time of each configuration with the lifetime of each configuration, a calculation can be made on how many years the BESS-integrated system can run after the payback period is reached. This is called the profit period and can be seen in Figure 5.15 (b). Because of the low payback period, the profit period is quite long for each configuration. With the smallest configuration being profitable for 88% of its lifetime for a total of 8.27 years. The profit period keeps increasing as the battery size increases, reaching a profit period of 100% of their lifetime for the largest two configurations. The largest configuration has the longest lifetime as well, for a total of 11.2 years

5.5.2. Integration of a BESS into existing DC UFCS

With the PCS costs out of the equation the relative capital investment cost has changed dramatically compared to a new DC UFCS. Even though the total cost has decreased. This is because integrating

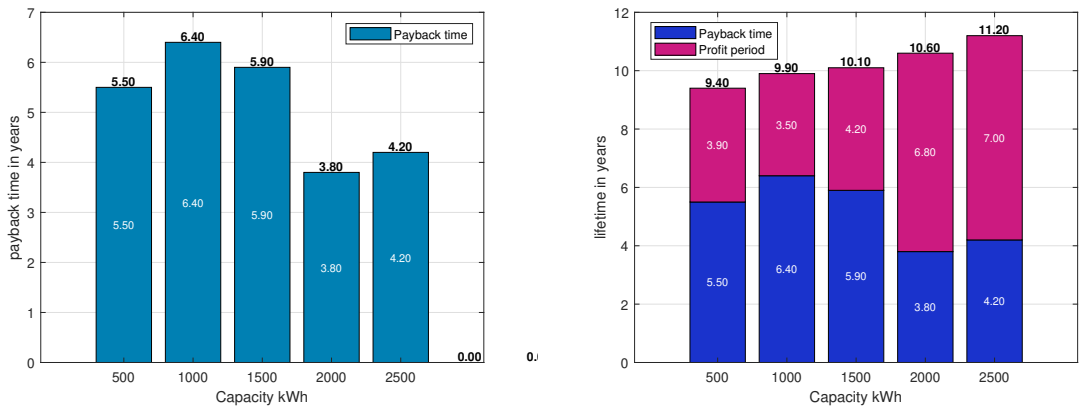

(a) Payback period

(b) Profit period and lifespan

Figure 5.16: Payback period, profit period and lifespan in years for BESS integrated into existing DC-UFCS

a battery will only cost investment money and will not save money on other components. This difference is also noticed in the payback period of the BESS integrated systemsFigure 5.16 (a). With an average payback period in Figure 5.15 (a) of only 0.75 years contrasted by 5.2 years Figure 5.16 (a). The payback time does not follow the linear increase in battery capacity that can be seen in the capital investment. This is because the operational cost reduction also increases with increasing battery capacity.

Profit Period The real interesting potential is shown by Figure 5.16 (b). Here it can be seen that the lifetime of the batteries for the first 3 configurations is barely larger than the payback period. This would surprise investors who assumed that integrating a battery would be a good idea from an economical standpoint. Just over half a decade later when the battery EOL is reached the financial benefits of integrating a BES will have dropped to nearly zero. In contrary to the range of 500-1500 kWh batteries is the profit period for the 2000 and 2500 kWh still substantial, respectively 4.4 and 6.4 years. When combined with the fact that the cost reduction of these two configurations is also substantially larger, makes these two configurations a great solution from an economical standpoint.

5.6. Net yearly operational costs

To make a fair comparison between all configurations it is important to express the cost per year over the lifetime of the battery. This metric takes into account yearly operational costs, the additional investment costs spread over the lifetime of the battery, and the maintenance costs of the battery. The configuration with the lowest yearly net cost is the best possible configuration for a 3.5 MW-rated UFCS.

5.6.1. Net yearly operational costs of new DC UFCS

When combining all these parameters the net total operational costs of the system over the lifetime of the battery can be calculated. And is depicted in Figure 5.17 (b).The graph contains two half circles. On the left side, in yellow the net yearly costs in absolute numbers can be seen. On the right side, the percentage of these net costs is shown for the network operator, energy, maintenance, and capital costs. As the battery size increases, and therefore the grid size decreases, a steady decline in net yearly cost can be seen. By introducing a battery to reduce grid size in combination with exploiting the volatile prices of a dynamic energy contract the cost can be reduced from 706.000 to 307.000 euros a year, by integrating a BESS with a dynamic price contract, constituting a net cost reduction of 56%.

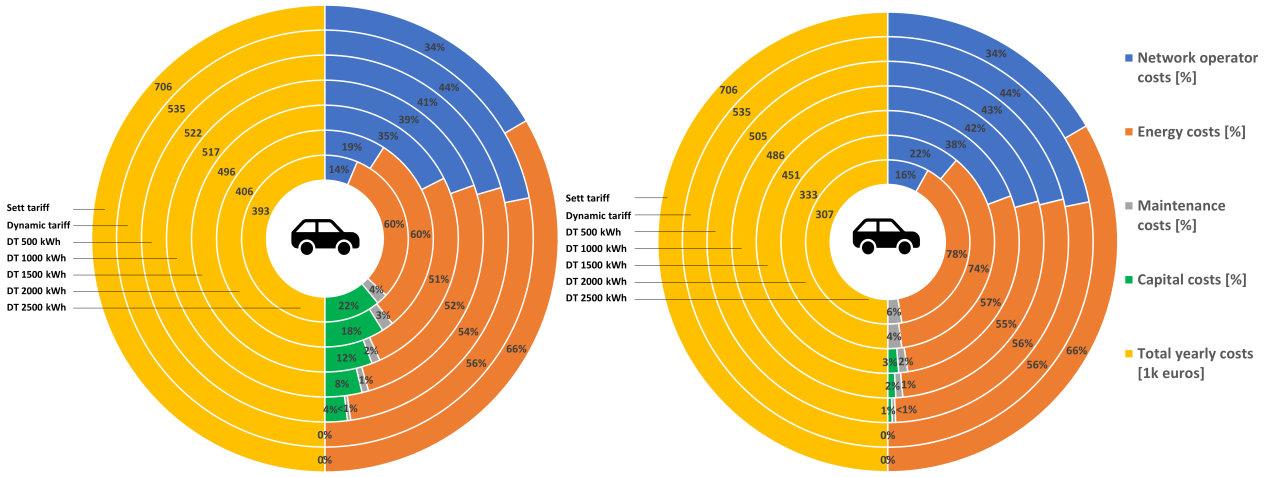

(a) Existing DC UFCS. (b) New DC UFCS.

Figure 5.17: Total net cost reduction over the lifetime of the BESS.

5.6.2. Net yearly operational costs of existing DC UFCS

When observing Figure 5.17 (a) the net costs can be seen on the left half of the circle, and on the right half of the circle the share of each cost component in the percentage of the total costs. The first thing that is observed is that after the implementation of dynamic tariffs, the smaller-sized batteries have little effect on the cumulative net costs and are not much lower than the cumulative net costs of the system without a battery. When the battery is 2000 kWh or larger the cost reduction rises significantly. The configuration with a 1MW grid power rating and a 2.5 MWh battery performs the best and has a net cumulative cost reduction of 44%, reducing costs from 706.000 to 393.000 euros.

Even though increasing battery size will increase the share of capital investment and maintenance, the decrease in operational costs is even larger. Even though it was found that the energy cost keeps decreasing the share in the total costs increases as the battery size increases. This is because the network operator costs decrease much faster than the energy costs. For both new and existing DC UFCS the largest battery configuration will allow for significant cost reduction making it an extremely interesting investment both economically as well as helping solve the net congestion problem.

5.7. Case Study of Optimal Configuration

In this section, the detailed individual performance of the best scoring configuration will be explored. This was the case where the battery capacity was rated at 2.5 MWh and the grid power was limited to 1 MW. In Table 5.3 all the results of the optimal and initial configuration are summed up again. It can be observed that the optimal configuration scores better on all but two fronts. Efficiency, due to the losses attributed to the battery and the DC/DC converter, and the capital investment costs for existing UFCS. Despite these costs and losses the optimal configuration shows impressive cost reduction.

To understand why this configuration performs as well as it does, the operation of the system is shown for a couple days. Only the summer pricing period will be discussed, as the battery will be used in the same way as the winter pricing. In Figure 5.18 (a) the power flow of the battery and the grid, the price, and the power demand can be seen for the first 3 days based on summer pricing. On the left y-axis, the price over time in cents/kWh is shown. The right axis represents the power in kW for the grid, the battery, and the demand of the UFCS. Since the battery is empty on the first day, it has to be charged within the first few hours, even though prices are high, since the minimum state of charge needs to be met. After that, it can be observed that at times of low prices, the black line, the grid power, shown in yellow, is used to its full extent, first providing the demand of the UFCS and using the rest of the available power to charge the battery, observed in red. But at times of high prices, the grid power is not utilized, and the battery will provide the demand, as shown in green. At some points, the demand is greater than the grid power, and the battery is forced to provide power regardless of price. This can

Table 5.3: Comparison of Initial and Optimal Configurations for UFCS

	Initial Configuration	Optimal Configuration
Configuration:		
Contract	Set tariff	Dynamic tariff
Grid power (kW)	3500	1000
Battery Capacity 1C (kWh)	0	2500
System efficiency:		
Energy delivered (MWh)	2876	2876
Energy consumed (MWh)	3028	3218
Efficiency	95%	89%
Energy:		
Total costs (€1000)	470	240
Price per MWh delivered (€)	164	83
Network operator:		
Total Costs (€1000)	334	50
Contract max (kW)	3500	1000
Consumed max (kW)	2012	1000
PAR	10	3
OM costs (€1000)	0	17
Capital investment costs:		
New UFCS (€1000)	1316	1294
Existing UFCS (€1000)	0	963
Lifetime (years)	-	11.2
Net yearly operational costs:		
New UFCS (€1000)	706	393
Existing UFCS (€1000)	706	307

be observed around the 42^{nd} hour.

In Figure 5.18 (b) the power flow of the battery and the grid, the price, and the power demand can be seen for the 4^{th} to the 6^{th} day, based on summer pricing. Here, the true potential of the battery is illustrated. Around the 3rd hour of these 3 days, the electricity price drops, demand is low, and the battery is charged. Only a couple hours later, just after the 6^{th} hour, a spike in demand occurs, over 2000 kW. Not only is this more than the grid can provide, but it also coincides with a peak in electricity prices. However, because of the decision to store cheap energy before the battery can fulfill this demand without needing to buy any expensive energy from the grid, these figures also show that network operator costs have been spent appropriately. There is no waste in extra capacity in the contract that is not used. And if the monthly maximum grid power is reached, it will not cost extra to max out your contract power many more times.

In Figure 5.19 the operation of the initial configuration is shown. There is no reduction in grid capacity and no smart charging battery system that exploits the dynamic price contract to reduce costs. The demand is just fulfilled by the grid and the price of electricity remains constant. The power capability of the 3.5 MW are not even remotely used to full extend, despite the corresponding costs.

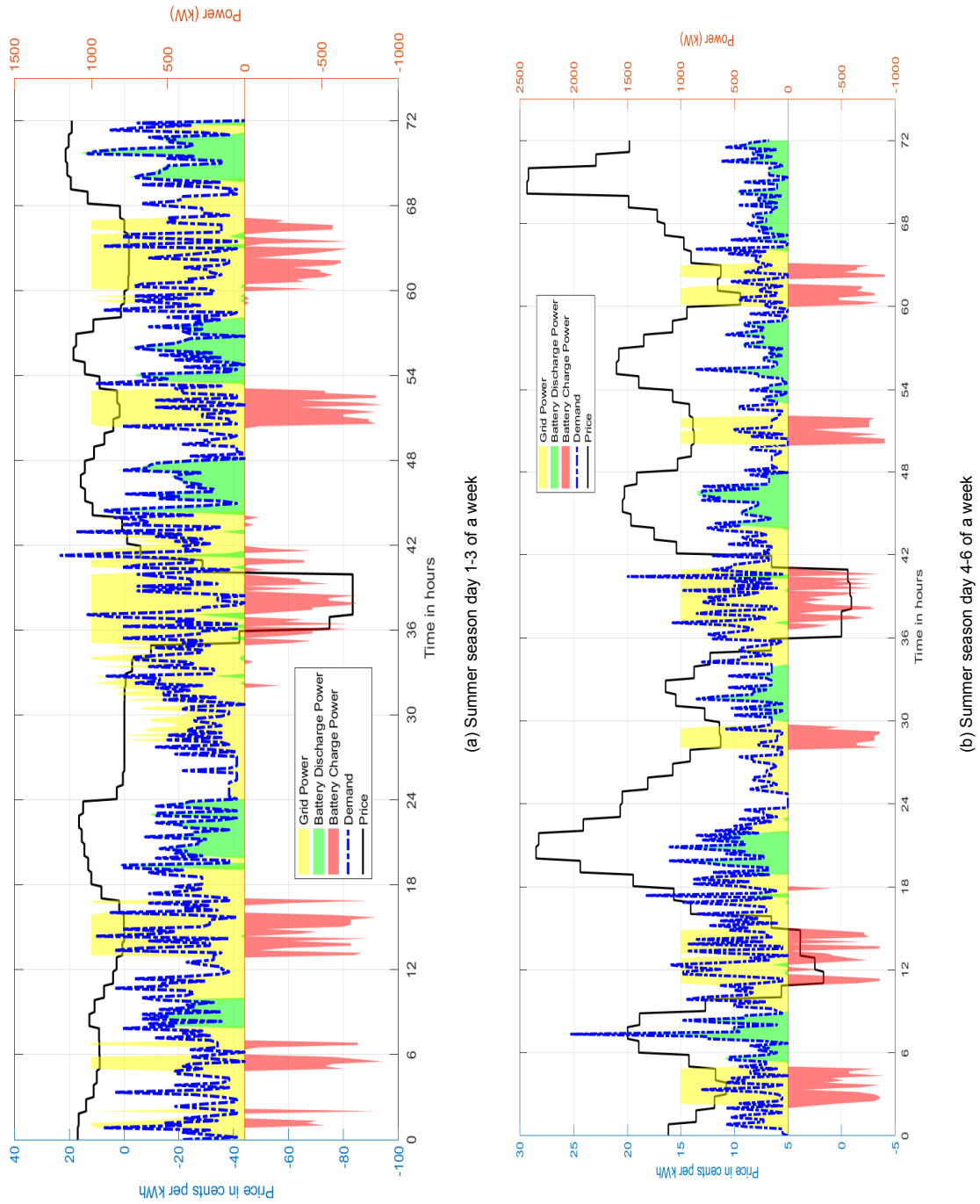

(a) Summer season day 1-3 of a week

(b) Summer season day 4-6 of a week

Figure 5.18: An overview of dynamic pricing, power demand and power flows for a week of summer season with optimal configuration

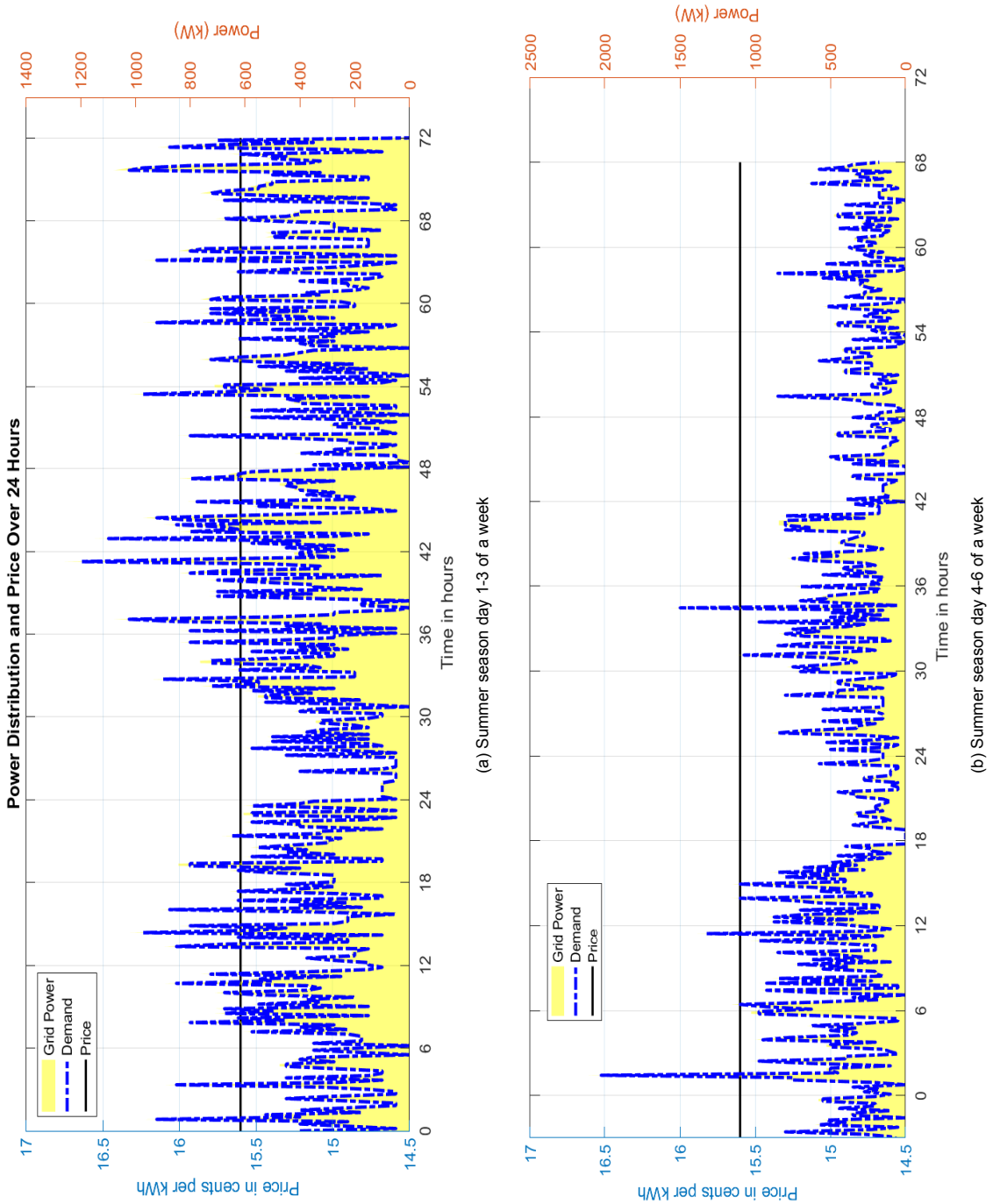

Figure 5.19: An overview of set tariff pricing, power demand and power flows for a week of summer season with initial configuration

5.8. Assessment of Battery Model

This section will show the results of the conversion of the empirical model to the battery model. First, the power output will be discussed, and the effect on the loss of capacity will be examined. Next, the voltage over time will be examined, which is the main driver in comparing the results of the empirical model to the battery model. Finally, the SOC of the battery model is shown, which will confirm whether the battery would function in real life similarly to the boundaries set by the empirical model.

In Figure 5.20 the (dis)charge power of the battery can be seen over a month. Apart from the spike in the first week, the battery does not need to provide more than half of its maximum power. This might explain the relatively low aging due to cycling compared to other configurations. The battery is also 2.5 times more powerful than the grid, therefore the power at which the battery can be charged is much lower than it is capable. These lower average (dis)charge currents are likely responsible for the longer lifetime compared to the smaller BESS configurations. This research did assume that there is no loss of power due to aging only loss of capacity. However, since the battery is much more powerful than is needed this configuration will be able to withstand these possible losses. Figure 5.21 shows exactly how the battery loses capacity as it cycles.

Another important variable to inspect is the voltage swing of the battery. Since the model optimizes the deployment of the battery and not the actual physical properties of the battery the proposed battery model will validate if the capabilities of the battery in the energy model are actually possible in a battery model. In Figure 5.22 the voltage swing is seen. The average voltage of this battery was around 1018 volts. It can be observed that with the voltage going no higher than 1024 and no lower than 1012. This means that the voltage swing is a maximum of 0.6%. Since the energy model assumes a constant voltage it does not take into account losses due to voltage swings. These small voltage swings confirm that under this research working conditions, an empirical model can confidently be represented by an empirical model which is much easier to use for optimization. This is also due to the carefully chosen battery chemistry LFP which has a very stable discharge voltage, especially within the SOC range chosen for this research.

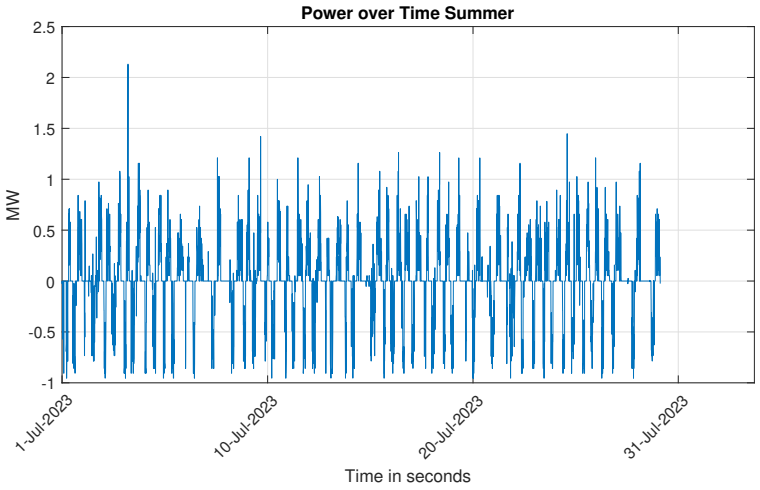

Figure 5.20: (dis)charge profile of the battery during summer

These voltage swings would account for losses that are not taken into account in the energy model. Due to these voltage swings, the battery loses up to 0.6% of its energy every cycle. In the battery model, a maximum of 0.6% of the total energy was lost compared to the empirical model. To account for these losses, the SOC of the battery was observed to be within the set limits. As can be seen in Figure 5.23. It also shows that the battery capacity is used to the fullest extent. Making more than one full cycle per day on average.

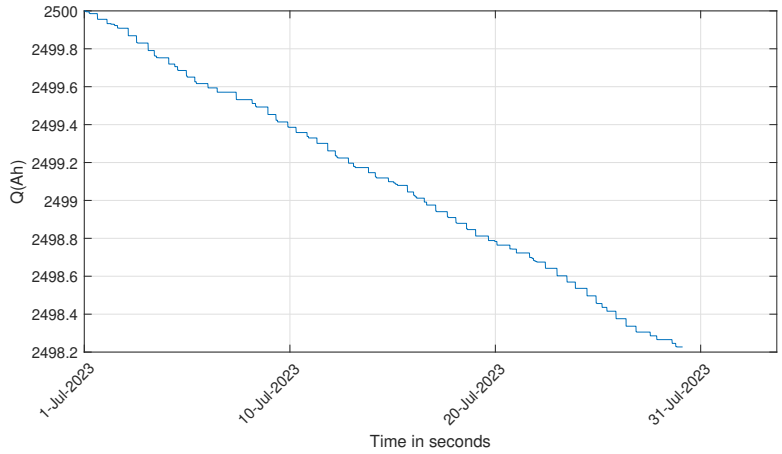

Figure 5.21: Capacity loss due to cycling of the battery during summer

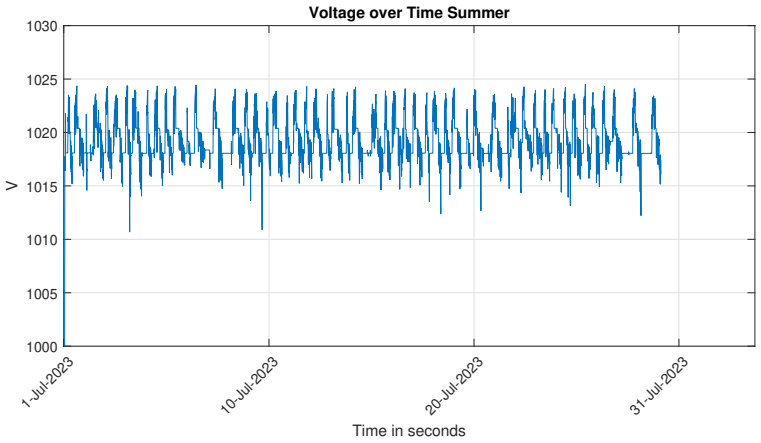

Figure 5.22: Voltage swing of the battery over summer.

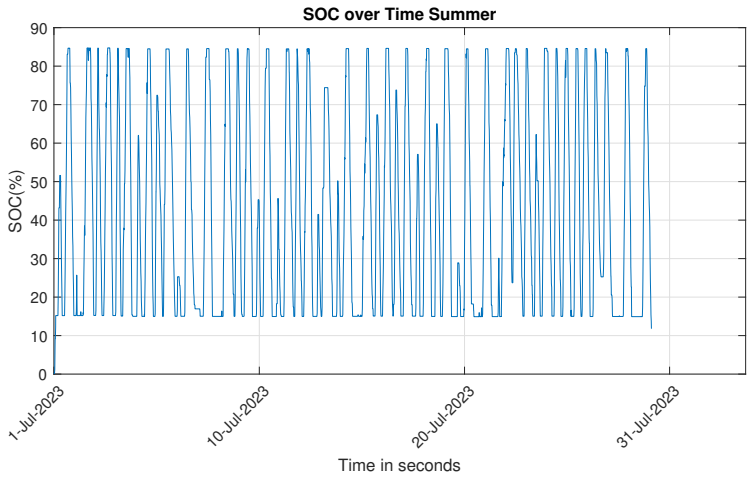

Figure 5.23: State of charge of the battery during summer

6

Conclusion

Considering current technological constraints and market conditions, how does integrating a BESS influence the techno-economic performance and viability of a UFCS connected to the grid? Is integrating a BESS into a DC UFCS beneficial? It becomes evident when the BESS performance is evaluated and compared on the critical evaluation metrics, as carried out in this thesis and concluded below.

Dynamic prices: The choice to purchase energy from the day ahead market has proven an effective measure to reduce energy costs when compared to a conventional energy contract using set tariffs. For UFCS as described in this research, the energy cost can be reduced by 36% even without the integration of a BESS. However unexpected changes in the time of peak demand and the time of peak costs make the system very vulnerable and unpredictable to changes when no battery system is present.

Grid size and Network operator cost reduction: By introducing a BESS the grid power can be substantially lowered, contributing to tackling the net congestion problem in the Netherlands, reducing the grid power up to 74%, while also offering significant financial incentives for the operator of the UFCS, while ensuring the consumer that their charge demand is met. By reducing the grid size but using it more intensively in combination with a battery the network operator costs can be significantly reduced. Both on an absolute scale by reducing the necessary power but also enabling some cases to reduce the marginal cost per kW. Leading to a cost reduction for network operator costs of 79% for the 2.5 MWh battery system.

Energy cost reduction: The battery can also play into the possible benefits that come from high price fluctuations in the day-ahead market due to mismatches in supply and demand. Charging the battery at low prices so it can be used later when prices are high using a dual simplex algorithm can reduce the cost of energy significantly. To reduce the cost of energy as much as possible it is important that both the grid and the battery are as large as possible. However, increasing the grid power leads to an increase in network operator costs. Therefore a balance needs to be found for the grid power while increasing the battery size will increase performance. The combination of a battery with dynamic prices can reduce the average cost per kWh by 49% compared to a system without a battery and set tariffs. Combining these two cost reduction methods shows that the yearly operational costs can be reduced by up to 56%. This shows that using a tailored optimization method for each of the two cost components can work very effectively.

Aging: The aging model of the battery did show a lower lifetime than expected with a maximum of 12 years. This is likely due to the fact that the battery is actively used to buy and use cheap energy to reduce energy costs,this will lead to more cycles and higher average current, significantly increasing aging due to cycling. The larger battery systems will have much smaller average currents compared to their maximum currents due to small grid sizes and limited need for high discharge power. Also due to

the larger capacity the larger batteries will have made a smaller amount of full cycles. The difference in lifetime did have a small but significant impact on the results because lifetime increased by a maximum of 20% when the larges BESS configuration was chosen.

Capital costs: For DC UFCS it is clear that the integration of a battery does not results in high capital investment costs when the reduction in costs due to power electronics on the grid side is taken into account. The investment costs on the battery side are canceled out by the lower investment costs on the grid side. However, since the lifetime of the power electronics on the grid side tends to be much higher than the lifetime of the battery system it must be noted that the investment costs for the battery have to be done at least twice. In the second investment round the costs increased significantly with increasing battery size. Nevertheless,also for existing DC UFCS the investment of an integrated BESS is highly profitable with a net cost reduction over the lifetime of the battery of 44%.

Overall profitability: When proper sizing of both the grid and battery was done, the total cost reduction of the battery over its lifetime, including payback time, can reach up to 2.5 million euros for a new DC UFCS and 1.5 million euros for an existing DC UFCS. Integrating a properly sized and deployed battery storage system into UFCS is an extremely interesting option for both investor priorities as priorities for the Dutch energy system. For this case the best option is to take a battery which is around 70% of system max power and the grid is around 30% of the system max power.

System validation: When comparing the performance of the battery in the analytical energy model to optimize the sizing and deployment with the physical model of the battery it was concluded that the actual battery would perform only 0.6% worse than the battery in the energy model. Due to minimal voltage fluctuations when the battery would be used as was determined by the optimised empirical model. It can be concluded that the battery can perform in the same manner in real life as it can in the empirical optimization model.

The integration of a BESS into a DC UFCS as described in this research is deemed highly effective capable and economically interesting. For this case the best option is to take a battery which is around 70% of system max possible power and the grid is around 30% of the system max power. It must also be noted that a grid power of 200% the max average daily power demand will allow large peak reduction while also enabling the exploitation of the day ahead market. With future charging speeds ever-increasing this case will become even more interesting. The same can be said with the increasing volatility on the day ahead market due to more and more penetration of renewable energy which will lead to higher peak and lower dales.

7

Future work and discussion

7.1. Discussion

The integration of batteries into DC Fast Charging (DCFC) stations symbolizes a pivotal advancement in EV charging infrastructure. The presented work delves into the myriad design choices and operational considerations surrounding this integration.

Central to this investigation is the DC bus system. The fixed voltage system presents a straightforward approach with inherent stability. Its standardization potential can lead to streamlined component sourcing and reduced maintenance complexities. However, the evolving landscape of EV technologies could challenge the adaptability of such a static system. In contrast, the varying voltage DC bus system offers dynamic adaptability, accommodating a wide array of EV models and evolving charging requirements. Yet, this flexibility comes at the cost of increased system intricacy and potential design challenges.

Another problem is the optimization of battery deployment. Although the prices on the energy market are known 24 hours ahead this cannot be said for the power demand. The method used in this research to model the demand gives a realistic profile of how the demand will look like for an UFCS with these characteristics, however, it is unlikely to predict the actual demand of a publicly available UFCS. Although the method is very useful in sizing the system more work has to be done to predict the energy consumption for every hour. It can however be directly used for UFCS where the demand can be calculated quite precisely. These are UFCS for trucks and logistics where it is known beforehand how many vehicles, at what time and approximately how much energy is needed for charging.

7.2. Future Work

While this study establishes a foundational understanding of battery-integrated DCFC stations, numerous avenues remain unexplored. Potential directions for future research include:

- **Advanced Control Mechanisms:** With the promise shown by varying voltage DC bus systems, there's an imperative to develop advanced control algorithms that further enhance their adaptability and performance.
- **Standardization Approaches:** Exploring means to standardize components and design protocols, aiming to facilitate easier scalability, efficient maintenance, and cost benefits in widespread deployments.
- **Economic Implications:** An in-depth analysis evaluating the financial feasibility and long-term profitability of different DC UFCS designs, taking into account efficiency metrics, operational costs, and potential revenue streams.
- **Integration with Renewable Energy Sources:** Assessing the synergy between DC UFCS and renewable sources, such as solar and wind, aiming to foster a sustainable and green charging ecosystem.

- **User-Centric Studies:** Evaluating how various DC UFCS designs impact the consumer experience in terms of charging times, interface interactions, and adaptability to diverse EV models.
- **Infrastructure Robustness:** Investigating the durability and resilience of DC UFCS setups in diverse climatic conditions and potential adverse scenarios to ensure long-term reliability and service continuity.

By delving into these areas, future research endeavors can further refine and optimize the design, operation, and user experience of battery-integrated DC UFCS, catalyzing the broader adoption of EV's and aiding the push towards a sustainable transportation future.

Bibliography

[1] URL: https://capaciteitskaart.netbeheernederland.nl/.

[2] .

[3] URL: https://ocw.tudelft.nl/wp-content/uploads/eCARS2x_Lecture_Notes_L3-3.pdf.

[4] URL: https://alenconsystems.com/whitepapers/galvanic-isolation/.

[5] URL: https://www.chademo.com/wp2016/wp-content/uploads/ChaoJi202006/ChaoJi_Presenataion_EN.pdf.

[6] URL: https://www.sciencedirect.com/topics/earth-and-planetary-sciences/nickel-cadmium-battery.

[7] URL: https://www.sciencedirect.com/topics/engineering/lead-acid-battery-systems.

[8] URL: https://energicplus.com/en/blog/how-to-maintain-your-lead-acid-battery.

[9] URL: https://search.abb.com/library/download.aspx?documentid=9akk107992a8963&documentpartid=.

[10] In: ().

[11] In: *IEEE Standard for the Design of Chargers Used in Stationary Battery Applications* (). DOI: 10.1109/ieeestd.2022.9938449.

[12] URL: https://www.keuze.nl/blog/wat-zijn-de-verschillende-soorten-energiecontracten-in-nederland#:~:text=Volgens%20cijfers%20van%20de%20Autoriteit,meest%20voorkomende%20energiecontract%20in%20Nederland..

[13] URL: https://opendata.cbs.nl/statline/#/CBS/nl/dataset/81309NED/line?ts=1696241184616&fromstatweb=true.

[14] URL: https://netztransparenz.tennet.eu/electricity-market/about-the-electricity-market/what-kind-of-markets-are-there-and-how-do-they-work/.

[15] URL: https://www.energy.gov/eere/water/articles/energy-storage-technology-and-cost-characterization-report.

[16] URL: https://www.grepow.com/blog/what-is-dod-for-lifepo4-batteries.html.

[17] URL: https://www.alibaba.com/product-detail/20KW-bidirectional-DC-DC-converter-for_1600691943802.html.

[18] URL: https://www.energy.gov/eere/vehicles/downloads/bi-directional-dc-dc-converter-0.

[19] URL: https://www.stedin.net/zakelijk/betalingen-en-facturen/tarieven.

[20] 2019. URL: https://www.toi.no/publications/charging-into-the-future-analysis-of-fast-charger-usage-article35355-29.html.

[21] 2023. URL: https://www.energievergelijk.nl/onderwerpen/netbeheerders.

[22] 2023. URL: https://www.verbouwkosten.com/warmtepomp/prijzen/.

[23] Adnan Ahmad et al. “An overview on medium voltage grid integration of ultra-fast charging stations: Current status and future trends”. In: *IEEE Open Journal of the Industrial Electronics Society* 3 (2022), pp. 420–447. DOI: 10.1109/ojies.2022.3179743.

[24] Ignas Andriunas et al. “Impact of solid-electrolyte interphase layer thickness on lithium-ion battery cell surface temperature”. In: *Journal of Power Sources* 525 (2022), p. 231126. DOI: 10.1016/j.jpowsour.2022.231126.

[25] Xuning Feng Anna Tomaszweska Zhengyu Chu. “Lithium-ion battery fast charging: A review”. In: *Elsevier Transportation* (2019). DOI: https://doi.org/10.1016/j.etran.2019.100011.

[26] Mariz B. Arias and Sungwoo Bae. “Electric vehicle charging demand forecasting model based on big data technologies”. In: *Applied Energy* 183 (2016), pp. 327–339. DOI: 10.1016/j.apenergy.2016.08.080.

[27] Ratil H. Ashique et al. “A comparative analysis of soft switching techniques in reducing the energy loss and improving the soft switching range in power converters”. In: *Electronics* 11.7 (2022), p. 1062. DOI: 10.3390/electronics11071062.

[28] I. Safak Bayram et al. “Electric Power Allocation in a network of fast charging stations”. In: *IEEE Journal on Selected Areas in Communications* 31.7 (2013), pp. 1235–1246. DOI: 10.1109/jsac.2013.130707.

[29] Adam M. Boyce et al. “Cracking predictions of lithium-ion battery electrodes by X-ray computed tomography and modelling”. In: *SSRN Electronic Journal* (2021). DOI: 10.2139/ssrn.3974815.

[30] Stephen P. Bradley, Arnoldo C. Hax, and Thomas L. Magnanti. “12”. In: *Applied mathematical programming*. Addison-Wesley, 1992.

[31] Thomas S. Bryden et al. “Electric vehicle fast charging station usage and power requirements”. In: *Energy* 152 (2018), pp. 322–332. DOI: 10.1016/j.energy.2018.03.149.

[32] Lubos Buzna et al. “Electric vehicle load forecasting: A comparison between time series and machine learning approaches”. In: *2019 1st International Conference on Energy Transition in the Mediterranean Area (SyNERGY MED)* (2019). DOI: 10.1109/synergy-med.2019.8764110.

[33] The Fast Charge. *Ev charging curves and why they are important*. 2022. URL: https://www.fastcharge.email/p/ev-charging-curves-and-why-they-are.

[34] Louis-A. Dessaint. *Experimental Validation of a Battery Dynamic Model for EV Applications*. 2009. URL: https://www.mdpi.com/2032-6653/3/2/289.

[35] Dragonfly Energy. *Why Does Energy Density Matter In Batteries?* 2022. URL: https://dragonflyenergy.com/why-does-energy-density-matter-in-batteries/.

[36] Maite Etxandi-Santolaya, Lluc Canals Casals, and Cristina Corchero. “Estimation of electric vehicle battery capacity requirements based on synthetic cycles”. In: *Transportation Research Part D: Transport and Environment* 114 (2023), p. 103545. DOI: 10.1016/j.trd.2022.103545.

[37] Maria Carmen Falvo et al. “Ev charging stations and modes: International standards”. In: *2014 International Symposium on Power Electronics, Electrical Drives, Automation and Motion* (2014). DOI: 10.1109/speedam.2014.6872107.

[38] Tao Fan et al. “Life cycle assessment of electric vehicles’ lithium-ion batteries reused for Energy Storage”. In: *Journal of Energy Storage* 71 (2023), p. 108126. DOI: 10.1016/j.est.2023.108126.

[39] Fastned. 2022. URL: https://fastnedcharging.com/hq/nl/why-fast-charging-stations-are-good-for-the-gridnl/.

[40] Fastned. 2022. URL: https://fastnedcharging.com/hq/everything-youve-always-wanted-to-know-about-fast-charging/.

[41] Erik Figenbaum. “Battery Electric Vehicle Fast Charging–evidence from the Norwegian market”. In: *World Electric Vehicle Journal* 11.2 (2020), p. 38. DOI: 10.3390/wevj11020038.

[42] Hasan Gelani et al. “Efficiency Comparison of AC and DC Distribution Networks for Modern Residential Localities”. In: *Applied Sciences* 9.3 (2019), p. 582. DOI: 10.3390/app9030582.

[43] Marc Goerigk and Anita Schöbel. “A scenario-based approach for robust linear optimization”. In: *Theory and Practice of Algorithms in (Computer) Systems* (2011), pp. 139–150. DOI: 10.1007/978-3-642-19754-3_15.

[44] Shashank Narayana Gowda et al. “Power management via integration of Battery Energy Storage Systems with electric bus charging”. In: *2022 IEEE Power amp;amp; Energy Society Innovative Smart Grid Technologies Conference (ISGT)* (2022). DOI: 10.1109/isgt50606.2022.9817511.

[45] Zhiqiang Guo et al. “Input-series-output-parallel phase-shift full-bridge derived DC–DC converters with auxiliary LC networks to achieve wide zero-voltage switching range”. In: *IEEE Transactions on Power Electronics* 29.10 (2014), pp. 5081–5086. DOI: 10.1109/tpel.2014.2309342.

[46] Chunlin He et al. *A review of surrogate-assisted evolutionary algorithms for expensive optimization problems*. 2023. DOI: 10.1016/j.eswa.2022.119495.

[47] Christopher Hecht, Jan Figgener, and Dirk Uwe Sauer. “Analysis of electric vehicle charging station usage and profitability in Germany based on empirical data”. In: *iScience* 25.12 (2022), p. 105634. DOI: 10.1016/j.isci.2022.105634.

[48] Christopher Hecht, Jan Figgener, and Dirk Uwe Sauer. “Analysis of electric vehicle charging station usage and profitability in Germany based on empirical data”. In: *iScience* 25.12 (2022), p. 105634. DOI: 10.1016/j.isci.2022.105634.

[49] Ties Van Heijden et al. “Electricity price forecasting in European Day Ahead Markets: A greedy consideration of market integration”. In: *IEEE Access* 9 (2021), pp. 119954–119966. DOI: 10.1109/access.2021.3108629.

[50] Jonas Huber et al. “pareto optimization of bidirectional half-cycle discontinuous-conduction-mode series-resonant DC/DC converter with fixed voltage transfer ratio”. In: *2013 Twenty-Eighth Annual IEEE Applied Power Electronics Conference and Exposition (APEC)* (2013). DOI: 10.1109/apec.2013.6520484.

[51] Jonas E. Huber and Johann W. Kolar. “Volume/weight/cost comparison of a 1MVA 10 kv/400 v solid-state against a conventional low-frequency distribution transformer”. In: *2014 IEEE Energy Conversion Congress and Exposition (ECCE)* (2014). DOI: 10.1109/ecce.2014.6954023.

[52] Iea. *Trends in batteries – global EV outlook 2023 – analysis*. URL: https://www.iea.org/reports/global-ev-outlook-2023/trends-in-batteries.

[53] Markku Jarvela and Seppo Valkealahti. “Comparison of AC and DC bus interconnections of energy storage systems in PV power plants with oversized PV generator”. In: *2019 IEEE 46th Photovoltaic Specialists Conference (PVSC)* (2019). DOI: 10.1109/pvsc40753.2019.8980909.

[54] Piedad Garrido Francisco J. Martinez Johann M. Marquez-Barja Julio A. Sanguesa Vicente Torres-Sanz. “A Review on Electric Vehicles: Technologies and Challenges”. In: *mdpi, Electronics and Energy* 3 (2021). DOI: https://doi.org/10.3390/smartcities4010022.

[55] Jing Kang, Changcheng Kan, and Zhongjie Lin. “Are Electric Vehicles reshaping the city? an investigation of the clustering of electric vehicle owners’ dwellings and their interaction with urban spaces”. In: *ISPRS International Journal of Geo-Information* 10.5 (2021), p. 320. DOI: 10.3390/ijgi10050320.

[56] M. Kassem et al. “Calendar aging of a graphite/lifepo4 cell”. In: *Journal of Power Sources* 208 (2012), pp. 296–305. DOI: 10.1016/j.jpowsour.2012.02.068.

[57] A.J. Keane. “Genetic algorithm optimization of multi-peak problems: Studies in convergence and robustness”. In: *Artificial Intelligence in Engineering* 9.2 (1995), pp. 75–83. DOI: 10.1016/0954-1810(95)95751-q.

[58] Abraham Alem Kebede et al. “A comprehensive review of stationary energy storage devices for large scale renewable energy sources grid integration”. In: *Renewable and Sustainable Energy Reviews* 159 (2022), p. 112213. DOI: 10.1016/j.rser.2022.112213.

[59] Peter Keil et al. “Calendar aging of lithium-ion batteries”. In: *Journal of The Electrochemical Society* 163.9 (2016). DOI: 10.1149/2.0411609jes.

[60] A. Khaligh and S. Dusmez. “Comprehensive Topological Analysis of Conductive and Inductive Charging Solutions for Plug-In Electric Vehicles”. In: *IEEE Transactions on Vehicular Technology* 61.8 (2012), pp. 3475–3489. DOI: 10.1109/tvt.2012.2213104.

[61] Yunsun Kim and Sahm Kim. “Forecasting charging demand of electric vehicles using time-series models”. In: *Energies* 14.5 (2021), p. 1487. DOI: 10.3390/en14051487.

[62] George Koolman, Marco Stecca, and Pavol Bauer. “Optimal Battery Energy Storage System Sizing for demand charge management in EV fast charging stations”. In: *2021 IEEE Transportation Electrification Conference amp;amp; Expo (ITEC)* (2021). DOI: 10.1109/itec51675.2021.9490138.

[63] Mohit Kumar Kakkar et al. “Performance comparison of genetic algorithms and particle swarm optimization for model integer programming bus timetabling problem”. In: *IOP Conference Series: Materials Science and Engineering* 332.1 (Mar. 2018), p. 012020. ISSN: 1757-899X. DOI: 10.1088/1757-899X/332/1/012020. URL: https://iopscience.iop.org/article/10.1088/1757-899X/332/1/012020https://iopscience.iop.org/article/10.1088/1757-899X/332/1/012020/meta.

[64] Alexis Laforgue et al. “Comparative investigation of the impact of fast charging at low temperature on commercial Li-ion cells”. In: *SSRN Electronic Journal* (2021). DOI: 10.2139/ssrn.3978529.

[65] Feng Leng, Cher Ming Tan, and Michael Pecht. “Effect of temperature on the aging rate of Li ion battery operating above room temperature”. In: *Scientific Reports* 5.1 (2015). DOI: 10.1038/srep12967.

[66] Kaiyuan Li and King Jet Tseng. “Energy efficiency of lithium-ion battery used as energy storage devices in micro-grid”. In: *IECON 2015 - 41st Annual Conference of the IEEE Industrial Electronics Society* (2015). DOI: 10.1109/iecon.2015.7392923.

[67] Naipeng Li et al. “A wiener-process-model-based method for remaining useful life prediction considering unit-to-unit variability”. In: *IEEE Transactions on Industrial Electronics* 66.3 (2019), pp. 2092–2101. DOI: 10.1109/tie.2018.2838078.

[68] Weilin Li, Kun He, and Yaqiang Wang. “Cost comparison of AC and DC collector grid for integration of large□scale PV Power plants”. In: *The Journal of Engineering* 2017.13 (2017), pp. 795–800. DOI: 10.1049/joe.2017.0440.

[69] Yunyan Li, Yuansheng Huang, and Meimei Zhang. “Short-Term Load Forecasting for Electric Vehicle Charging Station Based on Niche Immunity Lion Algorithm and Convolutional Neural Network”. In: *Energies* 11.5 (2018), p. 1253. DOI: 10.3390/en11051253.

[70] Kuan Lu et al. “Load forecast method of electric vehicle charging station using SVR based on GA-PSO”. In: *IOP Conference Series: Earth and Environmental Science* 69 (2017), p. 012196. DOI: 10.1088/1755-1315/69/1/012196.

[71] Yiqi Lu et al. “The Application of Improved Random Forest Algorithm on the Prediction of Electric Vehicle Charging Load”. In: *Energies* 11.11 (2018), p. 3207. DOI: 10.3390/en11113207.

[72] M. Mahesh and A.K. Panda. “High-power factor three-phase AC–DC soft-switched converter incorporating zero-voltage transition topology in modular systems for high-power industry applications”. In: *IET Power Electronics* 4.9 (2011), p. 1032. DOI: 10.1049/iet-pel.2010.0409.

[73] P. Manimekalai, R. Harikumar, and S. Raghavan. “An overview of batteries for photovoltaic (PV) systems”. In: *International Journal of Computer Applications* 82.12 (2013), pp. 28–32. DOI: 10.5120/14170-2299.

[74] Meiqin Mao, You Yue, and Liuchen Chang. “Multi-time scale forecast for schedulable capacity of Electric Vehicle fleets using big data analysis”. In: *2016 IEEE 7th International Symposium on Power Electronics for Distributed Generation Systems (PEDG)* (2016). DOI: 10.1109/pedg.2016.7527051.

[75] Matworks. *Why Does Energy Density Matter In Batteries?* 2022. URL: https://nl.mathworks.com/help/sps/powersys/ref/battery.html.

[76] Carla Menale et al. “Experimental investigation of overdischarge effects on commercial Li-Ion Cells”. In: *Energies* 15.22 (2022), p. 8440. DOI: 10.3390/en15228440.

[77] Omid Mohamad Nezami, Anvar Bahrampour, and Paria Jamshidlou. “ScienceDirect Dynamic Diversity Enhancement in Particle Swarm Optimization (DDEPSO) algorithm for preventing from premature convergence”. In: *Omid Mohamad Nezami et al. / Procedia Computer Science* 24 (2013), pp. 54–65. DOI: 10.1016/j.procs.2013.10.027. URL: www.sciencedirect.comwww.sciencedirect.com.

[78] Fazel Mohammadi and Mehrdad Saif. “A comprehensive overview of electric vehicle batteries market”. In: *e-Prime - Advances in Electrical Engineering, Electronics and Energy* 3 (2023), p. 100127. DOI: 10.1016/j.prime.2023.100127.

[79] K. Mongird et al. In: *Energy Storage Technology and Cost Characterization Report* (2019). DOI: 10.2172/1884043.

[80] Dave Murden. *What is the environmental impact of LiFePO4 batteries?* 2023. URL: https://ecotreelithium.co.uk/news/lifepo4-battery-environmentally-friendly/#:~:text=deep%2Dcycle%20applications.-,How%20Does%20LiFePO4%20Affect%20the%20Environment%3F,than%20other%20types%20of%20batteries..

[81] Noshin Omar et al. “Lithium iron phosphate based battery – Assessment of the aging parameters and development of cycle life model”. In: *Applied Energy* 113 (2014), pp. 1575–1585. DOI: 10.1016/j.apenergy.2013.09.003.

[82] Timothy Owens. *Lithium-ion battery pack costs 2022*. 2023. URL: https://www.statista.com/statistics/883118/global-lithium-ion-battery-pack-costs/.

[83] Pat. *EV charger connectors - shanghai mida EV Power Co., ltd.*. URL: https://www.evsegroup.com/ev-guide-2/.

[84] Nikolaos Ploskas and Nikolaos Samaras. “2.7 page 67”. In: *Linear programming using MATLAB®*. Springer, 2018.

[85] Md Ahsanul Rafi and Jennifer Bauman. “A comprehensive review of DC fast-charging stations with energy storage: Architectures, Power Converters, and analysis”. In: *IEEE Transactions on Transportation Electrification* 7.2 (2021), pp. 345–368. DOI: 10.1109/tte.2020.3015743.

[86] David A.J. Rand and Patrick T. Moseley. “Energy storage with lead–acid batteries”. In: *Electrochemical Energy Storage for Renewable Sources and Grid Balancing* (2015), pp. 201–222. DOI: 10.1016/b978-0-444-62616-5.00013-9.

[87] Deepak Ronanki, Apoorva Kelkar, and Sheldon S. Williamson. “Extreme fast charging technology—prospects to enhance sustainable electric transportation”. In: *Energies* 12.19 (2019), p. 3721. DOI: 10.3390/en12193721.

[88] Michael Ross et al. “COMPARISON OF AC, DC, AND AC/DC BUS CONFIGURATIONS FOR PV HYBRID SYSTEMS”. In: (Jan. 2004).

[89] L.H. Saw et al. “Electro-thermal analysis of lithium iron phosphate battery for electric vehicles”. In: *Journal of Power Sources* 249 (2014), pp. 231–238. DOI: 10.1016/j.jpowsour.2013.10.052.

[90] Michelle Selzer. *How much does a lithium-ion battery cost in 2023?* 2023. URL: https://lawnlove.com/blog/lithium-ion-battery-cost/.

[91] Hamed Shadfar, Mehrdad Ghorbani Pashakolaei, and Asghar Akbari Foroud. “Solid□State transformers: An overview of the concept, topology, and its applications in the smart grid”. In: *International Transactions on Electrical Energy Systems* 31.9 (2021). DOI: 10.1002/2050-7038.12996.

[92] Yong Shi and Xu Yang. “Wide range soft switching PWM three-level DC–DC converters suitable for industrial applications”. In: *IEEE Transactions on Power Electronics* 29.2 (2014), pp. 603–616. DOI: 10.1109/tpel.2013.2258357.

[93] S.N. Sivanandam and S.N. Deepa. “Genetic Algorithms”. In: *Introduction to Genetic Algorithms*. Springer Berlin Heidelberg, pp. 15–37. DOI: 10.1007/978-3-540-73190-0_2. URL: https://doi.org/10.1007/978-3-540-73190-0_2.

[94] Srdjan Srdic and Srdjan Lukic. “Toward extreme fast charging: Challenges and opportunities in directly connecting to medium-voltage line”. In: *IEEE Electrification Magazine* 7.1 (2019), pp. 22–31. DOI: 10.1109/mele.2018.2889547.

[95] Daniel-Ioan Stroe et al. “Suggested operation of grid-connected lithium-ion battery energy storage system for primary frequency regulation: Lifetime Perspective”. In: *2015 IEEE Energy Conversion Congress and Exposition (ECCE)* (2015). DOI: 10.1109/ecce.2015.7309813.

[96] Qiming Sun et al. “Charging load forecasting of electric vehicle charging station based on support vector regression”. In: *2016 IEEE PES Asia-Pacific Power and Energy Engineering Conference (APPEEC)* (2016). DOI: 10.1109/appeec.2016.7779794.

[97] C. A. Trauth and R. E. Woolsey. “Integer Linear Programming: A Study in Computational Efficiency”. In: *Management Science* 15.9 (May 1969), pp. 481–493. ISSN: 0025-1909. DOI: 10.1287/mnsc.15.9.481.

[98] Semen Uimonen and Matti Lehtonen. “Simulation of Electric Vehicle Charging stations load profiles in office buildings based on occupancy data”. In: *Energies* 13.21 (2020), p. 5700. DOI: 10.3390/en13215700.

[99] Battery University. *Lithium-ion safety concerns*. 2022. URL: https://batteryuniversity.com/article/lithium-ion-safety-concerns.

[100] Battery University. *What’s the best battery?* 2020. URL: https://batteryuniversity.com/article/whats-the-best-battery.

[101] Jingwen Wei, Guangzhong Dong, and Zonghai Chen. “Remaining useful life prediction and state of health diagnosis for lithium-ion batteries using particle filter and support vector regression”. In: *IEEE Transactions on Industrial Electronics* 65.7 (2018), pp. 5634–5643. DOI: 10.1109/tie.2017.2782224.

[102] Jennifer White. *LIFEPO4 BMS: The expert guide*. 2023. URL: https://blog.ecoflow.com/us/lifepo4-bms/.

[103] Chao Wu et al. “Research on Overcharge and Overdischarge Effect on Lithium-Ion Batteries”. In: *2015 IEEE Vehicle Power and Propulsion Conference (VPPC)* (2015). DOI: 10.1109/vppc.2015.7353006.

[104] Jie Yan et al. In: *EV charging load simulation and forecasting considering traffic jam and weather to support integration of renewables and EVs* (2020). DOI: 10.46855/2020.05.02.09.15.551750.

[105] Author links open overlay panelBehnam Zakeri et al. 2014. URL: https://www.sciencedirect.com/science/article/pii/S1364032114008284.

[106] Jing Zhang et al. “Study on the environmental risk assessment of lead-acid batteries”. In: *Procedia Environmental Sciences* 31 (2016), pp. 873–879. DOI: 10.1016/j.proenv.2016.02.103.

[107] Shuzhi Zhang et al. “Synchronous estimation of state of Health and remaining useful lifetime for lithium-ion battery using the incremental capacity and artificial neural networks”. In: *Journal of Energy Storage* 26 (2019), p. 100951. DOI: 10.1016/j.est.2019.100951.

[108] Wei Zhao et al. “Short-term Load Forecasting Considering Meteorological Factors and Electric Vehicles”. In: *IOP Conference Series: Materials Science and Engineering* 439 (2018), p. 032114. DOI: 10.1088/1757-899x/439/3/032114.

[109] Cong Zhu et al. “Development of a theoretically based thermal model for lithium ion battery pack”. In: *Journal of Power Sources* 223 (2013), pp. 155–164. DOI: 10.1016/j.jpowsour.2012.09.035.

[110] Juncheng Zhu et al. “Electric vehicle charging load forecasting: A comparative study of deep learning approaches”. In: *Energies* 12.14 (2019), p. 2692. DOI: 10.3390/en12142692.

[111] Juncheng Zhu et al. “Short-Term Load Forecasting for Electric Vehicle Charging Stations Based on Deep Learning Approaches”. In: *Applied Sciences* 9.9 (2019), p. 1723. DOI: 10.3390/app9091723.